RELAXATION OF QH1 (ROQH1) Functions in Sustained Photoprotective Energy Dissipation in Plants

By

Cynthia L. Amstutz

A dissertation submitted in partial satisfaction of the

requirements for the degree of

Doctor of Philosophy

in

Plant Biology

in the

Graduate Division

of the

University of California, Berkeley

Committee in charge:

Professor Krishna Niyogi
Assistant Professor Alizée Malnoë
Professor Graham Fleming
Professor Henrik Scheller

Fall 2019

Abstract

RELAXATION OF QH1 (ROQH1) Functions in Sustained Photoprotective Energy Dissipation in Plants

by

Cynthia L. Amstutz

Doctor of Philosophy in Plant Biology

University of California, Berkeley

Professor Krishna Niyogi, Co-Chair
Assistant Professor Alizée Malnoë, Co-Chair

Plants experience wide fluctuations in light intensity and must regulate light harvesting accordingly to prevent damage from excess energy. Several non-photochemical quenching (NPQ) mechanisms exist to harmlessly dissipate the excess energy and protect the photosynthetic apparatus under saturating light conditions. Each NPQ component occurs independently of each other and has different induction and relaxation kinetics involving unique molecular players. These components are outlined in Chapter 1. Under rapid light fluctuations, energy-dependent (qE) and zeaxanthin-dependent (qZ) quenching are critical and continue to be extensively studied. However, I focus here on a sustained form of antenna quenching, known as qH, that occurs under prolonged high light and abiotic stress. qH was recently identified as a distinct NPQ component independent of PsbS, ΔpH, zeaxanthin, D1 inactivation, and other qI processes. Induction of qH occurs under cold and high light stress and takes hours to days to turn off once induced. This slow relaxation rate can compete with light harvesting and limit photosynthetic efficiency. Thus, increasing the rate of qH relaxation may improve photosynthetic efficiency and crop yield. Within the last six years, three molecular players have been identified to be involved in qH. Under non-stress conditions, qH is prevented by the SUPPRESSOR OF QUENCHING1 (SOQ1) protein, which relies on a thioredoxin domain located in the thylakoid lumen. Under cold and high light, qH induction requires the plastid lipocalin protein, LCNP, which is also located in the lumen. In this dissertation, I present molecular insight into qH relaxation, which involves a previously uncharacterized protein, ROQH1.

RELAXATION OF QH1 (ROQH1) is an atypical short chain dehydrogenase/reductase that is conserved throughout the green lineage. In Chapter 2, I present the function of ROQH1 as a qH relaxation factor located in the chloroplast stroma, peripherally bound to the stroma lamellae membrane. Using various mutants and overexpressors, I show that qH does not relax in *roqh1* mutants, whereas qH does not occur in ROQH1 overexpressors. When the *soq1* and *roqh1* mutations are combined, qH can neither be prevented nor relaxed, and *soq1 roqh1* displays constitutive qH and light-limited growth. The antagonistic functions of LCNP and ROQH1 are both dosage-dependent in order to protect the photosynthetic apparatus and maintain light harvesting efficiency in plants.

The site of qH quenching is the peripheral antenna of PSII. In Chapter 3, I focus on which specific antenna component within PSII is responsible. The numerous chlorophyll fluorescence

techniques utilized in this chapter collectively support the hypothesis that at least one site of qH quenching is the LHCII trimer. In Chapter 4, I investigate the biochemical mechanism of qH relaxation through interactions between ROQH1 and LHCII. Blue-native PAGE experiments indicate that ROQH1 forms a complex with LHCII under cold and high light conditions. Since the majority of LHCII is located in the grana core and ROQH1 is located in the stroma lamella, our current working hypothesis is that strong qH quenching sites are induced by LCNP in the LHCII trimers located in the grana margins. Through connectivity to these trimers, excitation energy received by the PSII antenna within the grana core are additionally quenched. ROQH1 access to stroma-exposed LHCII is then sufficient to turn off all of qH.

Insight into qH relaxation is important as improving NPQ relaxation has been shown to be a promising way to improve photosynthetic efficiency and crop yield. To this aim, we utilized the antagonistic functions of LCNP and ROQH1 to mitigate or abolish qH in tobacco. We used CRISPR/Cas9 to disrupt both LCNP genes simultaneously, and a leaf specific promoter to overexpress ROQH1. Stable transgenic *N. tabacum* lines are currently in progress, and we plan to monitor crop performance under greenhouse and field conditions to determine whether qH modification improves photosynthetic efficiency and crop yield. Food production needs to double by 2050 to meet the growing population demand in the face of rapidly changing climates and limitations in available arable land. Therefore, continued research on photosynthetic energy conversion is vital to our future food security.

Dedication

In memory of my father, Daniel L. Amstutz, who understood the value of education. Who graduated from high school with honors, despite an attack from polio and polio-induced scoliosis his freshman year, which required corrective surgery and a full-body cast for the following two years. Who supported my graduate studies from across the country, while battling stage three pancreatic cancer and multiple rounds of chemotherapy and radiation. Thank you for supporting all my academic endeavors and providing a strong foundation for me to succeed.

Acknowledgements

First and foremost, I would like to thank Krishna Niyogi for welcoming me into his lab and being my PhD advisor. Kris provided a friendly and collaborative work environment that fostered curiosity, constructive criticism, scientific and personal growth. He supported all my future endeavors and pushed for their success. I immensely appreciated Kris for never failing to stay patient and positive throughout scientific setbacks or rabbit holes. Several times I entered his office ready to express how my experiments had failed and my project was doomed. I always left feeling completely relieved and, comically, a little overdramatic. I also must express my sincere gratitude to Kris for supporting and understanding my need to leave lab for extended periods of time during my father's failing health. During those two years, I witnessed traumatic life changes and gained responsibilities that I never expected nor could prepare for. Being part of a lab that values family and mental health was critical for me to withstand the emotional and legal burden that I experienced.

Second, I would like to thank Alizée Malnoë for providing instrumental mentorship, both scientifically and personally, during my graduate studies. I feel incredibly fortunate to have experienced my doctoral degree 'The French Way' in the Niyogi lab. My experience is incomparable to every other graduate student in the lab, as I received one-on-one technical and experimental training in a way that was comprehensive and focused, yet at the same time bubbly, loving, and inspiring. She was extremely generous to allow me to take ownership of a project that was substantially started and heavily invested in by her. She then provided guidance in almost every way possible for me and the project to succeed. Together, we have made significant strides in qH that I believe were possible due to our compatible passion and teamwork. Alizée warmly invited me into her home in Berkeley, France, and I'm sure Sweden as well. She is a nonstop social butterfly that can somehow discuss photosynthesis research from dusk till dawn while singing karoke or going dancing. I am so proud to see her succeed as a professor at Umeå University because I know she continues to be as passionate and invested in her students as she was with me. As I graduate and move forward on to the next chapter in my life, Alizée will continue to be a significant mentor and loving friend.

The work presented here would also not have been possible without several collaborators and lab mates. Rikard Fristedt performed the ROQH1 localization and salt wash experiments and Alex Schultink analyzed the whole-genome sequencing data for the ROQH1 paper. Collin Steen and Michelle Leuenberger performed all the fluorescence lifetime experiments by TCSPC. Masakazu Iwai provided significant biochemical advice and training regarding thylakoid isolation by sucrose cushion and Blue-Native PAGE experiments. He also provided critical reading of the ROQH1 manuscript and constructive feedback that made the story stronger and more complete. Masa is an incredible source of biochemical knowledge and techniques and I am grateful for the opportunity to learn from his expertise. Steven Burgess, Benjamin Haas, and Muthukumar Balasubramaniam in the laboratory of Stephen Long at the University of Illinois were also collaborators on the tobacco RIPE project. I would also like to thank Steve Ruzin and Denise Schichnes from the Biological Imaging Facility for teaching me how to use the microscopes and vibratome and Kent McDonald and Reena Zalpuri from the Transmission Electron Microscopy Facility at UC Berkeley for technical advice and assistance.

I am also grateful for Christopher Gee, who consistently provided critical discussions, memes, and moral support over the years. I admire and respect his creativity and scientific abilities as much as I love his kindness and generosity. Finally, I am grateful for my family members and

friends, Margaret, Amelia, Ryan, Sarah, Andrew, Leah, Sarah, Neem, Bailey, Snigdha, and Thien who continuously love and support me in all that I do.

This research was supported by the Division of Chemical Sciences, Geosciences, and Biosciences, Office of Basic Energy Sciences, Office of Science, US Department of Energy (Field Work Proposal 449B). This work used the Vincent J. Coates Genomics Sequencing Laboratory at UC Berkeley, supported by NIH S10 Instrumentation Grants S10RR029668 and S10RR027303. Rikard was supported by the Dutch Organization for Scientific Research (NWO) via an ECHO grant to Roberta Croce and by the U.S. Department of Energy Office of Science, Office of Biological and Environmental Research program under Award Number DE-FC02-02ER63421. Alex was supported by the National Institute of Health National Research Service Award Trainee appointment (grant no. GM007127). I was also supported by the Realizing Increased Photosynthetic Efficiency (RIPE) project funded by the Bill and Melinda Gates Foundation, Foundation for Food and Agricultural Research (FFAR), and Department for International Development (DFID).

Table of Contents

Chapter 1: Photoprotection and non-photochemical quenching of chlorophyll fluorescence---------- 1

1.1 Photoprotective strategies of plants ---------- 1
1.2 Non-photochemical quenching (NPQ) of chlorophyll fluorescence ---------- 1
1.3 NPQ mechanisms that result in thermal dissipation ---------- 3
1.4 NPQ mechanisms that do not result in thermal dissipation ---------- 4

Chapter 2: A conserved atypical short chain dehydrogenase/reductase functions as a qH relaxation factor in *Arabidopsis* ---------- 5

2.1 Abstract ---------- 5
2.2 Introduction ---------- 5
2.3 Materials and Methods ---------- 6
2.3.1 Plant material and growth conditions ---------- 6
2.3.2 Chlorophyll fluorescence video imaging suppressor screen and PAM fluorescence measurements ---------- 7
2.3.3 Genetic mapping, crosses, and overexpression ---------- 7
2.3.4 Genotyping ---------- 8
2.3.5 Protein extraction, localization, and immunoblot analysis ---------- 8
2.3.6 Pigment extraction and analysis ---------- 10
2.3.7 Microscopy ---------- 10
2.4 Results ---------- 10
2.4.1 A genetic screen uncovered mutants with constitutively quenched fluorescence ---------- 10
2.4.2 Whole-genome sequencing revealed mutations in a gene encoding an atypical short chain dehydrogenase/reductase ---------- 13
2.4.3 ROQH1 is enriched in the chloroplast stroma lamellae ---------- 19
2.4.4 Constitutive quenching is due to the combination of *soq1* and *roqh1* mutations ---------- 20
2.4.6 The constitutive quenching observed in *soq1 roqh1* is qH ---------- 28
2.4.7 Overexpression of ROQH1 prevents qH from occurring ---------- 31
2.4.8 ROQH1 is required for relaxation of qH ---------- 33
2.4.9 qH is independent of photoinhibition ---------- 37
2.5 Discussion ---------- 39
2.5.1 Constitutive qH causes a low-light acclimated phenotype ---------- 39
2.5.2 ROQH1 is annotated as an atypical short chain dehydrogenase/reductase - 40
2.5.3 ROQH1 is conserved in the green lineage and diatoms ---------- 42
2.5.4 ROQH1 functions in qH relaxation ---------- 42

Chapter 3: The site of qH quenching is the LHCII trimer ----------44

3.1 Introduction ---- 44
3.2 Materials and Methods ---- 45
3.2.1 OJIP Transient Measurements ---- 45
3.2.2 77K Fluorescence Spectroscopy ---- 45
3.2.3 TCSPC Measurements ---- 45
3.3 Results ---- 46
3.3.1 Constitutive quenching in *soq1 roqh1* requires the peripheral light-harvesting antenna of PSII ---- 46
3.3.2 The functional PSII antenna size of *soq1 roqh1* is small ---- 46
3.3.3 The site of qH quenching is the LHCII trimer ---- 47
3.4 Discussion ---- 49

Chapter 4: ROQH1 functions in a complex after cold and high light treatment ---- 50

4.1 Introduction ---- 50
4.2 Materials and Methods ---- 51
4.2.1 Thylakoid isolation by sucrose cushion ---- 51
4.2.2 Blue Native PAGE ---- 51
4.2.3 Co-Immunoprecipitation ---- 52
4.3 Results ---- 52
4.3.1 qH induction does not affect accumulation or formation of photosynthetic complexes ---- 52
4.3.2 Overexpression of ROQH1 does not alter the composition of photosynthetic complexes ---- 54
4.3.3 ROQH1 co-migrates with LHCII trimer and monomer ---- 54
4.3.4 ROQH1 does not co-immunoprecipitate with LHCII trimer proteins ---- 60
4.4 Discussion ---- 60

Chapter 5: Modifying qH to improve NPQ recovery and photosynthetic efficiency in crop plants ---- 61

5.1 Introduction ---- 61
5.2 Materials and Methods ---- 62
5.2.1 *In vitro* gRNA activity assay ---- 62
5.2.2 LCNP CRISPR construct design and assembly ---- 63
5.2.3 ROQH1 overexpression construct design and assembly ---- 64
5.2.4 *Agrobacterium fabrum* transformation ---- 64
5.2.5 Transient Expression in *Nicotiana benthamiana* and *Nicotiana tabacum* ---- 65
5.3 Results ---- 66
5.3.1 Ribonucleoprotein (RNP) digestion of *LCNP* genes *in vitro* ---- 66
5.3.2 Transient expression of *ROQH1* and disruption of *LCNP* does not alter qH kinetics in *N. benthamiana* ---- 66

5.3.3 *N. benthamiana* ROQH1 proteins lack key residues ---- 67
5.3.4 Transient expression of *ROQH1* and disruption of *LCNP* in *N. tabacum* ---- 70
5.4 Discussion ---- 71

Chapter 6: Conclusions ---- 72

References ---- 74

List of Figures

Figure 1-01. A typical PAM fluorescence trace. ... 3
Figure 2-01. Construct map of ROQH1 OE in pEG100. ... 8
Figure 2-02. Genetic screen uncovered mutants with constitutively quenched fluorescence. ... 11
Figure 2-03. Similar accumulation and formation of photosynthetic complexes between wild type and mutant #164. ... 12
Figure 2-04. ROQH1 mutations are recessive. ... 14
Figure 2-05. Causative mutation in mutant #164 is on chromosome 4. ... 15
Figure 2-06. ROQH1 is enriched in the chloroplast stroma lamellae. ... 17
Figure 2-07. ROQH1 disruption in insertional mutants ... 19
Figure 2-08. A portion of ROQH1 is strongly bound to the stroma lamellae ... 20
Figure 2-09. Constitutive quenching requires *soq1* and *roqh1* mutations alone. ... 21
Figure 2-10. Overexpression of ROQH1 prevents qH from occurring and fails to rescue the *roqh1-3* developmental phenotype. ... 22
Figure 2-11. Total chlorophyll is equal among mutants. ... 23
Figure 2-12. Constitutively quenched mutants are light-limited. ... 24
Figure 2-13. Fluorescence kinetics of *soq1 roqh1* are constitutively quenched. ... 25
Figure 2-14. Constitutively quenched mutants have thin leaves and stacked grana. ... 27
Figure 2-15. The photosynthetic flux of *soq1 roqh1-1* is limited under standard growth conditions. ... 28
Figure 2-16. Constitutive quenching requires LCNP ... 29
Figure 2-17. Accumulation of SOQ1, ROQH1, and LCNP proteins. ... 30
Figure 2-18. NPQ kinetics of *roqh1* single mutants are similar to wild type under standard conditions ... 31
Figure 2-19. Overexpression of ROQH1 prevents qH from occurring. ... 32
Figure 2-20. ROQH1 overexpression level is more than 10 times that of wild type. ... 33
Figure 2-21. ROQH1 is required for relaxation of qH. ... 34
Figure 2-22. ROQH1 is required for relaxation of qH. ... 35
Figure 2-23. Average fluorescence lifetimes before and after cold and high light. ... 36
Figure 2-24. Accumulation of SOQ1 and D1 proteins throughout qH induction and recovery. . 37
Figure 2-25. PSII efficiency and D1 protein levels are unaffected by ROQH1. ... 38

Figure 2-26. ROQH1 multiple sequence alignment..... 41
Figure 2-27. ROQH1 is required to turn off qH. 43
Figure 3-01. Constitutive quenching in *soq1 roqh1* requires the peripheral light-harvesting antenna of PSII. 46
Figure 3-02. The functional PSII antenna size of *soq1 roqh1* is small. 47
Figure 3-03. The fluorescence emission of *soq1 roqh1* is quenched at LHCII and PSII proximal antenna. 48
Figure 3-04. Chlorophyll fluorescence lifetimes are shorter across a range of wavelengths in *soq1 roqh1*. 49
Figure 4-01. Thylakoids isolated by sucrose cushion. 51
Figure 4-02. Overexpression and disruption of ROQH1 does not affect accumulation or formation of photosynthetic complexes. 53
Figure 4-03. Disruption of LCNP does not affect accumulation or formation of photosynthetic complexes. 53
Figure 4-04. Overexpression of ROQH1 does not alter the composition of photosynthetic complexes. 56
Figure 4-05. ROQH1 functions in a complex after cold and high light. 56
Figure 4-06. The ROQH1 antibody does not detect ROQH1 under native conditions. 57
Figure 4-07. SOQ1 co-migrates with multiple photosynthetic complexes. 57
Figure 4-08. ROQH1 has post-translational covalent modification(s) and SOQ1 co-migrates with photosynthetic complexes. 58
Figure 4-09. ROQH1 co-migrates with LHCII trimer and monomer. 59
Figure 4-10. ROQH1 does not co-immunoprecipitate with LHCII trimer proteins. 60
Figure 5-01. Location of gRNAs in LCNP genes in *N. tabacum*. 63
Figure 5-02. Construct map of LCNP CRISPR in pL2V_BAR15325. 64
Figure 5-03. Construct map of ROQH1 OE in pL2V_BAR15325. 65
Figure 5-04. Ribonucleoprotein digestion of LCNP genes *in vitro*. 66
Figure 5-05. The LCNP gRNAs are specific for *N. tabacum*. 67
Figure 5-06. Transient expression of ROQH1 does not alter qH in *N. benthamiana*. 68
Figure 5-07. *N. benthamiana* ROQH1 proteins lack key residues. 69
Figure 5-08. Transient expression of ROQH1 and disruption of LCNP results in photobleaching in *N. tabacum*. 70

List of Tables

Table 2-01. Sequencing and read mapping summary. 16
Table 2-02. Summary of identified mutations within mapped region. 16
Table 2-03. Average fluorescence lifetimes before and after cold and high light. 36
Table 3-01. Fluorescence lifetimes of preferentially excited chlorophyll *a* and *b*. 48

Chapter 1: Photoprotection and non-photochemical quenching of chlorophyll fluorescence

1.1 Photoprotective strategies of plants

In natural environments, photosynthetic organisms experience daily fluctuations in light intensity and quality. Light stress occurs when light energy is absorbed in excess of photosynthesis, leading to oxidative damage to the photosynthetic apparatus[1]. Thus, photosynthetic organisms have evolved a suite of photoprotective responses to prevent damage, including ways to minimize light absorption, detoxify reactive oxygen species, and dissipate excess absorbed light energy as heat[2].

To decrease light absorption, different plant species employ various strategies. Most plants contain the blue light receptor, phototropin 2, which mediates photon avoidance by chloroplast movements (for review see ref[3]). Within the chloroplast, thylakoid grana undergo vertical unstacking and decreases in diameter[4]. Under prolonged high light, light-harvesting proteins reorganize around photosystem II (PSII), chlorophyll synthesis is downregulated, and the light-harvesting antenna size decreases[5]. On an organ level, some plants can alter the leaf architecture to angle the leaves parallel to the incident sunlight. Others can develop a thicker cuticle or can accumulate salt on the leaf epidermis to increase light reflectance[2]. Under freezing temperatures, deciduous trees shed their leaves and discard the light-harvesting organ completely and produce new leaves when suitable temperatures return.

Reactive oxygen species are mainly produced in the form of singlet oxygen at PSII when excited state chlorophyll is long-lived[6]. Without a nearby quencher, excited chlorophyll enters the triplet state through intersystem crossing and reacts with molecular oxygen to form singlet oxygen[7]. Formation of this type of reactive oxygen is controlled or prevented by photoprotective carotenoids such as lutein or zeaxanthin[8]. Carotenoids de-excite singlet oxygen or triplet chlorophyll and safely return to the ground state[2]. The second most common reactive oxygen species is in the form of superoxide and is generated when photosystem I (PSI) directly reduces molecular oxygen[9]. Various enzymes and antioxidants are then used to scavenge and detoxify superoxide. Superoxide dismutase converts superoxide to hydrogen peroxide, where ascorbate is required for ascorbate peroxidase to reduce hydrogen peroxide to water and oxygen. For ascorbate to be used again, it must be re-reduced in a series of steps requiring NADPH and glutathione reductase[2].

1.2 Non-photochemical quenching (NPQ) of chlorophyll fluorescence

The harmless dissipation of excess absorbed light energy is known as non-photochemical quenching of chlorophyll fluorescence (NPQ) and is the focus of this work. When light is absorbed by photosynthetic pigments, the chlorophyll and carotenoid molecules are excited to short-lived, high-energy states. In order to return to the ground state and preferably not enter a triplet state, the absorbed energy must be emitted as fluorescence, dissipated as heat, or transferred to another component. When the energy is transferred to nearby pigments and ultimately the reaction center to drive charge separation, the energy is said to be quenched photochemically. Under conditions where light is in excess, the absorbed energy is dissipated as heat and thus said to be quenched non-photochemically. These two transfer routes occur within picoseconds, whereas fluorescence is emitted within nanoseconds. Due to the slow speed, only a small portion of energy is given off as chlorophyll fluorescence in an inversely proportional manner with photochemistry and NPQ.

The relationship between fluorescence and photosynthesis and/or NPQ provides a key tool for photosynthesis research.

The established way to assess photosynthetic performance *in vivo* in the laboratory is through pulse-amplitude modulated (PAM) fluorometry[10,11]. This noninvasive technique relies on chlorophyll *a* fluorescence, which provides information about the light reactions of photosynthesis as well as energy dissipation[12]. PAM fluorometers make use of three light sources to probe the photosynthetic chain: a weak measuring light, a moderate actinic light, and a strong saturating light. Before a PAM measurement, plant material is dark-acclimated to oxidize photosynthetic electron carriers and to relax NPQ mechanisms. Under these conditions, energy provided by the weak measuring light will be photochemically quenched by electron transfer, and the fluorescence yield will be low, known as the minimal fluorescence (F_o) (Figure 1-01). Upon illumination with a saturating pulse, electron carriers become fully reduced and electron transport through PSII is blocked. This effectively closes the reaction centers of PSII and stops photochemistry. Instead of being used, the harvested light energy is re-emitted as the maximum fluorescence (F_m) (Figure 1-01). The difference between F_m and F_o is known as the variable fluorescence (F_v), and F_v/F_m is the maximum quantum efficiency of PSII[13]. When the leaf is exposed to an actinic light in addition to these saturating pulses, the maximum fluorescence level will decrease to F_m' (Figure 1-01). This decrease is due to the induction of NPQ mechanisms that effectively quench chlorophyll fluorescence, calculated as $(F_m-F_m')/F_m'$. After turning off the actinic light, the F_m' fluorescence yield will rise as NPQ mechanisms begin to relax.

One critical assumption of PAM fluorometry is that NPQ is off at the start of a measurement. Typically, this is achieved with just 30 min of dark adaption. However, there are times when 30 min is not long enough, particularly after prolonged periods of high light stress and the induction of sustained quenching mechanisms. In these cases, longer dark-acclimation periods (such as overnight) are required, otherwise the initial F_m will be quenched by the active NPQ mechanism and appear artificially lower. The inaccurate starting F_m will result in underestimated levels of NPQ and PSII efficiency. In some cases, such as overwintering plants, an overnight dark adaption period is still not long enough, as their NPQ mechanisms stay active throughout the entire winter season[14]. Thus, NPQ is unable to be measured in these plants during this time. To get around this, researchers measure F_m twice, once before and once during winter, and designate the second F_m as F_m'. This calculation, however, is at best a rough estimation, as it incorrectly assumes that pigment and protein complex stoichiometry and abundance remains similar between freezing and non-freezing seasons.

Another assumption of PAM fluorometry that is often incorrect is that the measured NPQ is equal to heat dissipation. Genuine quenching reactions that occur by charge transfer or excitation energy transfer to a carotenoid, or chlorophyll-chlorophyll concentration quenching do result in heat dissipation when the carotenoid returns to the ground state. However, other mechanisms that decrease light absorption or transfer energy from PSII to PSI are not genuine quenching mechanisms, even though they still result in a decrease in Fm' when taking a PAM measurement. For this reason, these mechanisms are still classified as NPQ and are briefly discussed.

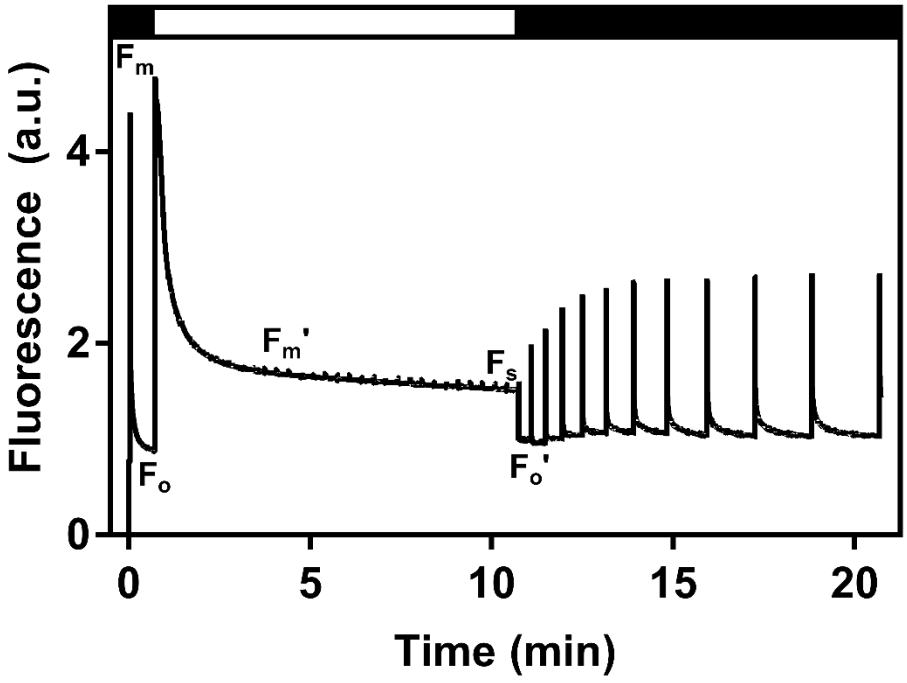

Figure 1-01. A typical PAM chlorophyll fluorescence trace. A PAM fluorescence trace from a wild-type Arabidopsis leaf with an actinic light induction for 10 min at 1,200 μmol photons m^{-2} s^{-1} (white bar) and relaxation for 10 min in the dark (black bar). F_o is the dark-acclimated minimal fluorescence yield when illuminated with the measuring light, and F_o' is the light-acclimated minimal fluorescence yield. F_m is the dark-acclimated maximum fluorescence yield when illuminated with a saturating pulse, and F_m' is the light-acclimated maximum fluorescence yield. F_s in the steady-state fluorescence level.

1.3 NPQ mechanisms that result in thermal dissipation

NPQ is comprised of several different processes, originally defined based on their relaxation kinetics and sensitivities to chemical inhibitors[15]. Currently, different NPQ processes are defined based on the molecular players involved[16], and four distinct mechanisms are known to result in thermal dissipation. Energy-dependent quenching (qE) occurs within seconds under excess light[17] and is critical for plants encountering short-term high light or fluctuating light intensities due to sun flecks, passing clouds, or canopy shading. The induction of qE occurs in excess light when there is an imbalance between the light reactions and carbon reactions of photosynthesis, producing a high ΔpH gradient across the membrane. Acidification of the thylakoid lumen results in protonation of lumen-exposed residues of photosystem II subunit S (PsbS)[18] and of violaxanthin de-epoxidase (VDE)[19,20]. Once protonated, the VDE enzyme is active and can convert violaxanthin to antheraxanthin and then to zeaxanthin, which is required alongside PsbS for quenching site formation[21–23]. While PsbS is essential for qE, it is not the site of quenching as PsbS does not bind any pigments[24], despite homology to chlorophyll *a*/*b* binding proteins and being a member of the Lhc superfamily. The quenching site of qE is still heavily debated and may be multiple locations within the PSII-LHCII supercomplex, as some find PsbS interacting with the minor antenna protein, CP29[25,26], while others have shown qE to be independent of all minor antenna complexes[27]. Zeaxanthin-dependent quenching, qZ, also relies on zeaxanthin yet it does not require PsbS or a pH gradient (ΔpH) once zeaxanthin has been produced. Instead, qZ involves

the binding of zeaxanthin to monomeric antenna proteins[28,29], and takes tens of minutes to turn on and off[30]. Previously, photoinhibitory quenching, qI, included all mechanisms that resulted in the light-induced decrease in the quantum yield of Photosystem II (PSII), namely photoinhibition due to PSII photoinactivation. Photoinhibition is mainly associated with the reaction center core protein D1 that is easily damaged by high light intensities and must be replaced *de novo*[31]. A complex system exists to migrate inactivated PSII to the grana margins, remove the damaged D1 from the otherwise functional PSII core, and replace it with a newly synthesized D1[31]. Photoinhibition occurs when the primary acceptor, Q_A, is reduced and the rate of D1 damage is faster than the rate of D1 repair[32]. This is often observed by a decrease in the F_v/F_m due to elevated F_o levels. In addition to photoinhibition, qI included all components with slow relaxation kinetics, including uncharacterized modes of sustained thermal dissipation[2,33,34]. However, qH, a sustained form of antenna quenching, was recently identified as a distinct NPQ component that is independent of PsbS, ΔpH, zeaxanthin, PSII core protein D1 inactivation and other qI processes[35,36]. Induction of qH occurs under cold and high light stress conditions and takes hours to days to turn off once induced.

Sustained quenching has been observed in nature mainly in overwintering evergreen plants that experience freezing temperatures and high light. Currently, two phases of quenching have been described in overwintering evergreens[37]. The rapid phase that relaxes within minutes upon warming is due to qE, and the slow phase that takes hours to days to relax has been attributed to either qZ and/or qI[37]. The slow phase has been classified as qZ due to the increased accumulation of xanthophyll pigments in their de-epoxidized form[37–39]. In some species, this phase is also classified as qI due to the detachment and eventual degradation of almost all D1 proteins[40]. However, due to the similar induction conditions and relaxation kinetics, it is plausible that qH is an additional sustained quenching mechanism that occurs in overwintering plants.

1.4 NPQ mechanisms that do not result in thermal dissipation

As previously stated, some NPQ mechanisms do not result in heat dissipation but rather energy distribution. Quenching due to chloroplast movement, or qM, is one such example. qM is only induced by blue or white light and is due to photon avoidance rather than a genuine quenching reaction[41]. A second component is qT, or state transitions, which relieves excess energy from PSII by balancing light absorption between PSI and PSII[42]. This is achieved when electron carriers from PSII are reduced, activating the state transition kinase, STN7, which phosphorylates light harvesting antenna proteins and initiates their migration to PSI[43,44]. When light conditions favor PSI (shade or far-red light), the TAP38 phosphatase initiates relocation back to PSII[45]. However, when both photosystems are saturated by high light intensities, the STN7 kinase is inhibited and/or degraded and qT does not contribute to NPQ[46,47]. A third mechanism that does not lead to energy dissipation is energy spillover from PSII to PSI, which has currently not been observed in plants. Energy spillover in plants is thought to be prevented by the lateral heterogeneity of the thylakoid membranes[4,48]. While PSII is located in the stacked grana, PSI is restricted to the stroma lamellae because of its bulky, stroma-exposed domains[48]. One possible location for spillover to occur is the grana margins, where both PSII and PSI may be present, yet this merits further investigation. In one red alga species where spillover was demonstrated, the two photosystems were excitonically coupled when the plastoquinone pool was reduced, and the alternative energy transfer route was favored[49]. When spillover occurred, the excitation energy lost from PSII was ultimately quenched photochemically by PSI and was therefore not a mode of heat dissipation. However, if the energy

had been dissipated by P700+ within PSI, then this would have been considered a genuine quenching reaction.

Chapter 2: A conserved atypical short chain dehydrogenase/reductase functions as a qH relaxation factor in *Arabidopsis*

Preface

Alizée Malnoë contributed extensively to this work by performing the suppressor screen that identified *soq1 roqh1-1*. She also performed the initial outcrosses and whole-genome sequencing preparations. Rikard Fristedt performed localization experiments, Alex Schultink analyzed the whole-genome sequencing data, and Collin Steen performed fluorescence lifetime experiments by TCSPC.

The majority of this chapter is based on the following submitted manuscript: Amstutz, C.L., Fristedt, R., Schultink, A., Merchant, S.S., Niyogi, K.K., and Malnoë, A. An atypical short chain dehydrogenase/reductase functions in the relaxation of sustained energy dissipation in *Arabidopsis*. In Revision *Nature Plants*

2.1 Abstract

Photosynthetic organisms experience wide fluctuations in light intensity and regulate light harvesting accordingly to prevent damage from excess energy. qH is a sustained form of energy dissipation that protects the photosynthetic apparatus under stress conditions. This photoprotective mechanism requires the plastid lipocalin, LCNP, and is prevented by SUPPRESSOR OF QUENCHING1 (SOQ1) under non-stress conditions. However, molecular insight into qH relaxation has yet to be resolved. Here, we isolated and characterized RELAXATION OF QH1 (ROQH1), an atypical short chain dehydrogenase/reductase that functions as a qH relaxation factor in *Arabidopsis*. The *ROQH1* gene belongs to the GreenCut2 inventory specific to photosynthetic organisms, and the ROQH1 protein localizes to the chloroplast stroma lamellae membrane. After a cold and high light treatment, qH does not relax in *roqh1* mutants, whereas qH does not occur in ROQH1 overexpressors. When the *soq1* and *roqh1* mutations are combined, qH can neither be prevented nor relaxed, and *soq1 roqh1* displays constitutive qH and light-limited growth. We propose that LCNP and ROQH1 perform dosage-dependent, antagonistic functions to protect the photosynthetic apparatus and maintain light harvesting efficiency in plants.

2.2 Introduction

Previously, a suppressor screen on the *Arabidopsis* (*A. thaliana*) *npq4* mutant lacking PsbS helped to uncover qH, which is negatively regulated by the SUPPRESSOR OF QUENCHING1 (SOQ1) protein[35]. SOQ1 is a multi-domain protein of 104 kD that spans the thylakoid membrane. The stroma-exposed region of SOQ1 contains a haloacid dehalogenase-like hydrolase (HAD) domain, and the lumen-exposed region contains a thioredoxin (Trx)-like and β-propeller NHL domain. The lumenal domains are required to suppress qH, whereas the stromal domain is not required[35]. To gain insight into the molecular mechanism of qH and to identify possible targets of SOQ1, a second suppressor screen was performed on *soq1 npq4*, and the peripheral antenna of PSII and the plastid lipocalin protein, LCNP, were found to be required for qH to occur[36]. LCNP is a soluble protein of 29 kD that is localized in the thylakoid lumen and upregulated during abiotic

stress such as drought and high light[50]. Lipocalin proteins can bind small hydrophobic molecules such as fatty acids, pigments, or steroids and have enzymatic activity[51]. However, the identity of the putative ligand or substrate of LCNP is unknown. Our working model is that under stress conditions, such as cold and high light, SOQ1 inhibition is relieved, and LCNP is either directly involved in quenching site formation, or indirectly through changes to the membrane environment via modification of a hydrophobic molecule. Under non-stress conditions, SOQ1 negatively regulates LCNP either directly or indirectly.

In addition to the *chlorina1* (lacking the peripheral antenna of PSII, i.e., light-harvesting complex II, LHCII) and the *lcnp* mutants, this second suppressor screen generated mutants with constitutive NPQ. We isolated and characterized these mutants, and found they were affected in an atypical short chain dehydrogenase/reductase, subsequently named RELAXATION OF QH1 (ROQH1). Interestingly, *roqh1* single mutants display wild-type dark-acclimated chlorophyll fluorescence values and only when combined to the *soq1* mutation does the *soq1 roqh1* double mutant display a low fluorescence phenotype indicative of possible constitutive NPQ. We tested whether the low, or 'quenched', fluorescence phenotype in *soq1 roqh1* is LCNP-dependent, and whether qH induction or relaxation is affected in *roqh1* single mutants. Our findings demonstrate that ROQH1 functions in the relaxation of qH.

2.3 Materials and Methods

2.3.1 Plant material and growth conditions

The wild-type and mutant *Arabidopsis thaliana* plants used in this study are of the Col-0 ecotype. Mutants *soq1 npq4 roqh1-1* (#164), *soq1 npq4 roqh1-2* (#108), *soq1 roqh1-1*, *soq1 roqh1-2*, *roqh1-1*, and *roqh1-2* were isolated in this study. The *soq1-1* mutant allele, referred to throughout as *soq1*, and *soq1-1 npq4-1* are from ref[35]. The *soq1-1 lcnp-1* mutant is from ref[36]. The *lcnp* T-DNA insertion line SALK_133049C was provided by F. Ouellet (Université du Québec à Montréal). The *chlorina1-3* mutant[52], referred to throughout as *chlorina1*, and the *roqh1* T-DNA insertion lines SALK_039706.46.80 (*roqh1-3*), SALK_061421.54.50, SALK_001123, SALK_059586, SALK_025967, and SAIL_896_F07 were obtained from the Arabidopsis Biological Resource Center. The T-DNA insertion line GABI-KAT_446A01 was obtained from the University of Bielefeld.

Arabidopsis plants were grown on agar plates containing 0.5X Murashige and Skoog medium (VWR Scientific; 95026-314) under continuous light at 100 µmol photons m^{-2} s^{-1} at 21°C for 1.5-2 weeks and then transferred to soil (Sunshine Mix 4/LA4 potting mix; Sun Gro Horticulture Distribution). Once transplanted, plants were grown under a 10/14-h light/dark photoperiod at 120-150 µmol photons m^{-2} s^{-1} (standard light) at 21°C or under an 8/16-h light dark photoperiod at 1000-1,300 µmol photons m^{-2} s^{-1} (high light) at 21°C for 4-7 weeks. For seedlings grown on agar plates, growth chamber light bulbs were cool white from General Electric (F17T8/SP41 17W). For plants grown on soil, growth chamber light bulbs were cool white (4100K) from Philips (F25T8/TL841 25W) for standard light conditions, and high-pressure sodium and metal halide lamps from Philips (C1000S52 1000W) and Sylvania (MH1000U 1000W) for high light conditions. For the cold and high-light treatment, detached leaves were placed for 5 h at 6°C and 1,600 µmol photons m^{-2} s^{-1} using a JBeamBio LED panel with cool white LEDs (BXRA-56C1100-B-00). To determine rosette dry weight in Figure 5, rosettes from 5-week-old plants were harvested and baked in aluminum foil for 8 h at 105°C and then measured for dry weight.

2.3.2 Chlorophyll fluorescence video imaging suppressor screen and PAM fluorescence measurements

Mutagenesis and chlorophyll fluorescence screening of *soq1 npq4* suppressors were performed as previously described[36]. Chlorophyll fluorescence measurements were determined at room temperature using an Imaging-PAM Maxi (Walz) or Dual-PAM-100 (Walz) fluorometer. False-colored fluorescence images and their respective F_o, F_m, and F_v/F_m values were determined using the Imaging-PAM Maxi, while NPQ induction and relaxation were determined using the Dual-PAM-100. Plant material was dark acclimated for 30 min prior to measurement unless stated otherwise. Maximum fluorescence levels after dark acclimation (F_m) and throughout an NPQ measurement (F_m') were recorded after applying a saturating pulse of light. NPQ, calculated as (F_m-F_m')/F_m', was induced for 10 min with 1,200 µmol photons m^{-2} s^{-1} and relaxed for 10 min in the dark.

2.3.3 Genetic mapping, crosses, and overexpression

Mutations in #164 were identified through whole-genome sequencing, and the causative SNP was mapped to *ROQH1* as previously described[36]. Genetic crosses were performed using standard techniques[53]. For whole-genome sequencing, #164 was backcrossed to *soq1 npq4,* and 146 seedlings with low F_m were pooled out of 709 total F2 progeny (20.6% segregation ratio). To obtain the double and single mutants, #164 and #108 were outcrossed to either *soq1* or the wild type. From the cross between #164 and *soq1*, 33 seedlings out of 140 F2 progeny were confirmed to have low F_m and both mutations (23.6% segregation ratio). From the cross between #164 and wild type, 29 seedlings out of 743 total F2 progeny were confirmed to have low F_m and both *soq1* and *roqh1-1* mutations (4% segregation ratio). From the cross between #108 and wild type, 12 seedlings out of 202 total F2 progeny were confirmed to have intermediate F_m and both *soq1* and *roqh1-2* mutations (6% segregation ratio). The double mutant, *soq1 roqh1-3* was obtained from an independent cross between *soq1* and the T-DNA insertional line SALK_039706. From this cross 103 seedlings out of 1929 total F2 progeny were confirmed to have low F_m and both *soq1* and *roqh1-3* mutations (5.3% segregation ratio). The double mutant, *soq1* SALK_001123 was obtained from an independent cross between *soq1* and the T-DNA insertional line SALK_001123. From this cross 120 seedlings out of 2323 total F2 progeny displayed intermediate F_m and contained both *soq1* and SALK_001123 mutations (5.2% segregation ratio). *ROQH1* overexpression was done by adding a C-terminal FLAG tag to *ROQH1* cDNA via round-the-horn PCR mutagenesis using the forward primer CA34 (GACCCAGCTTTCTTGTACAA) and the reverse primer CA35 (TTACTTATCATCATCATCCTTATAATCTTTGGATTCTGCAGCTTTA) and cloning ROQH1-FLAG into the pEarleyGate100 expression vector[54] under the cauliflower mosaic virus 35S promoter (Figure 2-01). *soq1 roqh1-1* and *soq1 roqh1-3* plants were transformed with this construct using the floral dip method[55], and transformants were selected on plates containing 10 µg/ml glufosinate ammonium. T1 transformants were allowed to self, and segregating T2s were screened for homozygosity on plates containing Murashige and Skoog medium with and without 10 µg/ml glufosinate ammonium. Heterozygous T2s and homozygous T3s were used in this study.

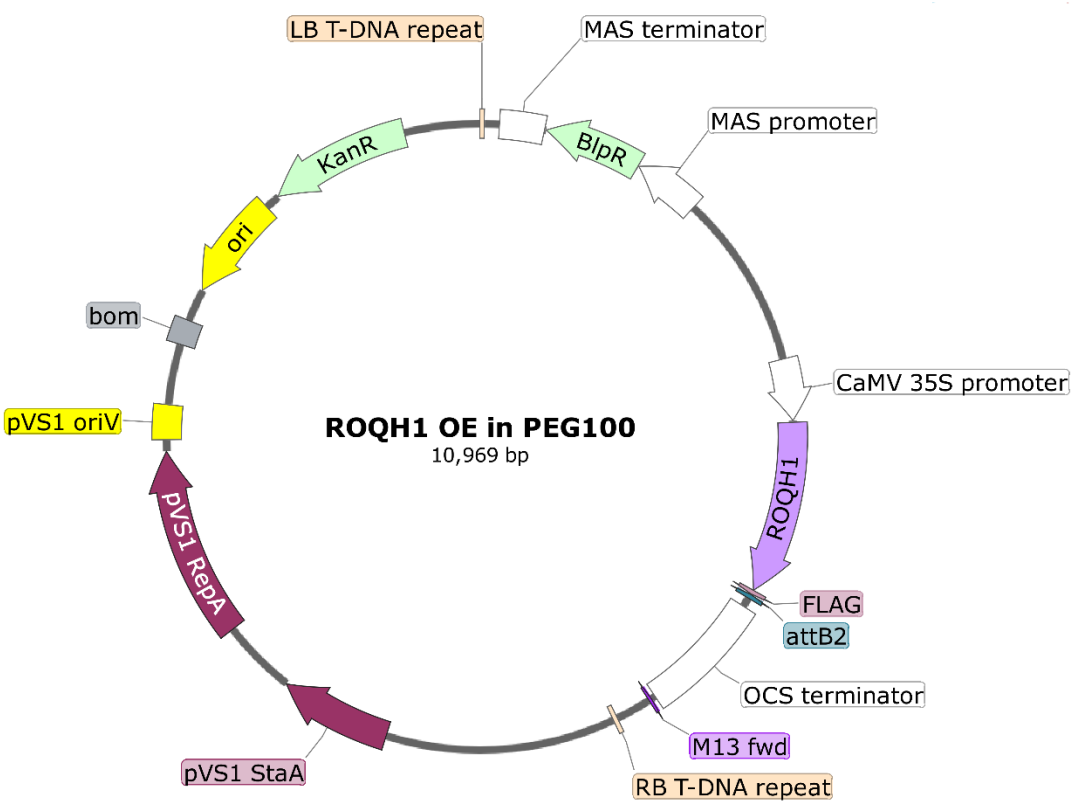

Figure 2-01. Construct map of ROQH1 OE in pEG100. ROQH1 cDNA from *Arabidopsis* is in purple. Overexpression of ROQH1 is driven by the 35S promoter and OCS terminator in white. Construct contains kanamycin resistance for bacteria and Basta resistance for plants.

2.3.4 Genotyping

Genotyping was done using the Phire Plant Direct PCR kit and protocol (ThermoFisher Scientific) with gene specific primers. Genotyping for the *soq1* mutation was done through PCR with forward primer GAAGTGGTTTCTTTTGTACAATTCTGCA and reverse primer CAATACGAATAGCGCACACG followed by digestion with the restriction enzyme, PstI. Genotyping for the *roqh1-1* SNP was done through PCR with forward primer GCTACAAAATCCCAAATCAGAA and reverse primer GTAGTGTATCCGAAATAGTGAG followed by digestion with the restriction enzyme, AciI. The digestion products were run on a 3% agarose gel at 120V. The PCR product was digested by the restriction enzyme if it was the wild-type allele and undigested if it was the mutant allele. Genotyping insertional mutants was done using the LBb1.3 border primer and gene specific primers made through the Salk Institute Genomic Analysis Laboratory T-DNA primer design tool. To genotype *roqh1-3*, forward primer TTGACCAATAACAACTGCACG and reverse primer TTTATCTTCGTCAATCACGCC were used to sequence the region containing the mutation. To genotype *lcnp-1*, LP primer AM164 (CCGCTTTGACATTTACATTACG), RP primer AM165 (TATAGCAATGTCGGCTCCAAC) and LBb1.3 primers were used[36].

2.3.5 Protein extraction, localization, and immunoblot analysis

Total proteins from whole cell extracts or isolated thylakoids were extracted, solubilized in either an SDS lysis buffer (100 mM EDTA (pH 8.0), 120 mM Tris-HCl (pH 6.8), 4% SDS, 12%

sucrose, 200 mM DTT, and 100 mM sodium carbonate for 10 min at 100°C) or LDS buffer (2% LDS, 30 mM Tris-HCl (pH 9.0), 30 mM Tris-HCl (pH 8.0), 60 mM DTT, 30% sucrose for 30 min at RT) and precipitated with methanol and chloroform. For immunoblots, samples were loaded by either equal leaf area or chlorophyll content on Any kD Mini-PROTEAN TGX Precast Protein Gels (Bio-Rad), separated by SDS-PAGE, transferred to a 0.45µm PVDF membrane (GE Healthcare), blocked with 3% nonfat dry milk, and incubated with the following antibodies. A rabbit antibody raised against a C-terminal peptide of SOQ1[36] was used at a 1:200 dilution. A rabbit polyclonal antibody raised against the C-terminal portion (starting from amino acid sequence RLLLR) of recombinant ROQH1 was used at a 1:2,500 dilution (AS12 2118). A rabbit antibody raised against recombinant LCNP protein[50] was provided by F. Ouellet (Université du Québec à Montréal) and used at a 1:2,000 dilution. An anti-FLAG antibody was obtained from Sigma-Aldrich and used at a 1:1,500 dilution. A rabbit polyclonal antibody raised against a synthetic peptide of the beta subunit of ATP synthase was obtained from Agrisera and used at 1:10,000 dilution. Antibodies used for subcellular localization and membrane salt-wash experiments were D2, Lhca1, Lhcb2, Rubisco and PsaD, all from Agrisera, Vännäs, Sweden, catalog numbers AS06 146 (1:8,000 dilution), AS06 146 (1:8,000 dilution), AS01 003 (1:8,000 dilution), AS03 037 (1:10,000 dilution) and AS09 461 (1:10,000 dilution), respectively. After incubation with an HRP-conjugated, anti-rabbit secondary antibody from GE Healthcare (1:10,000 dilution), bands were detected by chemiluminescence using SuperSignal West Femto Maximum Sensitivity Substrate (Thermo Scientific).

For subcellular localization, 40 g of four-week old *A. thaliana* leaves were homogenized in 30 mL preparation buffer (25 mM Tricine-NaOH, pH 7.8, 330 mM sorbitol, 1 mM EDTA, 10 mM KCl, 0.15% [w/v] bovine serum albumin, 4 mM sodium ascorbate, and 7 mM L-Cysteine) in a precooled Waring blender for five periods of 1 s at high speed. The homogenate was immediately filtered through four layers of Miracloth (20-µm pore size), and the pellet was collected from the filtrate by centrifugation for 3 min at 1,000 × g in the cold (4°C). The pellet was resuspended in the same buffer and centrifuged again for 5 min at 1,000 × g. Intact chloroplasts were purified on 35%/80% (v/v) Percoll step gradients and separated by centrifugation at 2,000 × g for 15 min in a swinging-bucket rotor. For fractionation into stromal and thylakoid protein fractions, 30 mL of preparation buffer was gently mixed with the chloroplasts collected from the gradient. Subsequently, the chloroplasts were recovered by centrifugation at 2,500 × g for 4 min, resuspended in 3 mL of chloroplast lysis buffer (10 mM Tricine-NaOH, pH 7.8, and 5 mM $MgCl_2$), and incubated on ice for 15 min. A Pyrex Potter-Elvehjem tissue grinder (homogenizer) was used to mediate complete lysis of the chloroplasts. The thylakoid membranes were collected by centrifugation for 5 min at 8,000 × g, resuspended in buffer (100 mM sorbitol, 25 mM Tricine-NaOH, pH 7.8, 5 mM $MgCl_2$, and 10 mM KCl), and purified on a sucrose gradient (40%–80%) by centrifugation at 30,000 × g for 1 h. The soluble stromal proteins were collected from the supernatant of the chloroplast lysis. The stromal fraction was centrifuged at 8,000g for 4 min to remove any membrane particles and concentrated in a SpeedVac. For subfractionation thylakoids membranes were solubilized for 15 min on ice in the presence of 1% digitonin. The reaction was quenched by addition of 10-fold volume of ice-cold resuspension buffer. After centrifugation at 1,000 × g for 3 min at 4°C, the supernatant was collected, and grana membranes were obtained by centrifugation at 10,000 g for 30 min at 4°C. The supernatant was centrifuged at 40,000 × g for 30 min at 4 °C to collect the grana margins and then to pellet the stroma lamellae membranes, the supernatant was centrifuged at 145,000 × g for 1 h at 4°C.

For salt washing of thylakoid membranes and further immunolocalization of ROQH1, isolated thylakoid membranes described previously were vortexed for 1 min and then sonicated for 15 min on ice in the presence of 1M NaCl, 0.1M Na_2CO_3 or 0.1M $CaCl_2$ in buffer (100 mM sorbitol, 25 mM Tricine-NaOH, pH 7.8, 5 mM $MgCl_2$, and 10 mM KCl) before centrifugation to separate soluble and membrane fractions. 3 µg chlorophyll from supernatant and pellets was loaded on the SDS-PAGE gel. For control, thylakoids without any treatment of salt were used.

2.3.6 Pigment extraction and analysis

Whole plants or detached leaves were sampled under standard light (120-150 µmol photons m^{-2} s^{-1}) or treated with high light (1,000 µmol photons m^{-2} s^{-1}) for 30 min prior to pigment analysis. Three samples from different individuals were weighed and pigment analysis was normalized by fresh weight and total chlorophyll. For the cold and high light treatment, three samples from different individuals of each genotype were taken at indicated time points (0, 5, and 28 h) and zeaxanthin levels were normalized by total chlorophyll. Chlorophylls and carotenoids were extracted and quantified by HPLC analysis as previously described[56].

2.3.7 Microscopy

For transmission electron microscopy, leaves were subjected to high pressure freezing, freeze-substitution in osmium tetroxide, and infiltration with epoxy resin[57]. Chloroplast ultrastructure was imaged on a Tecnai 12 and all grana on 10 representative chloroplast images of each genotype were quantified using ImageJ.

For light microscopy, leaves were embedded in 7% agarose and sectioned into 80-100 µm thick sections using a 752/M vibroslice tissue cutter from Campden Instruments Limited[58]. Sections were stained with 0.02% toluidine blue O for 30 s and imaged on a Zeiss AxioImager with a QImaging MicroPublisher color camera. For quantification of leaf and vein thickness, 10 representative images of each genotype were measured using ImageJ. Leaf thickness was measured approximately 150 µm away from the mid-vein where a lateral vein or trichome was not present, and the mid-vein was measured from the adaxial surface to the abaxial surface.

2.4 Results

2.4.1 A genetic screen uncovered mutants with constitutively quenched fluorescence

Previously, a genetic screen was performed by chlorophyll fluorescence video imaging on mutagenized *soq1 npq4 Arabidopsis* plants, lacking both SOQ1 and PsbS, to identify molecular players involved in qH[36]. Through this approach, the *chlorina1-4* and *-5* and *lcnp-2* and *-3* mutations were isolated, demonstrating the requirement of LHCII and LCNP for qH to occur (see ref[36]). In addition, two mutants were isolated with altered maximum chlorophyll fluorescence yield in the dark (F_m) (Figure 2-02A). Mutant #164 showed severely decreased dark-acclimated minimal fluorescence (F_o) and F_m, and mutant #108 showed mildly decreased F_o and F_m (Figure 2-02A). The fluorescence yield of #164 and #108 remained low throughout a high light and dark treatment (Figure 2-02B) indicating that the mutants were quenched constitutively. Thus, the NPQ levels of #164 and #108 could not be accurately measured through standard pulse-amplitude modulated fluorometry techniques (Figure 2-02C). The low fluorescence yield was not due to a lack of chlorophyll, as the total chlorophyll level determined by HPLC analysis of #164 and #108 was

slightly higher and unchanged, respectively, compared to the parental strain, *soq1 npq4* (Figure 2-02D). In addition, there were no major differences between wild type and #164 in the accumulation of photosynthetic proteins and complexes (Figure 2-03). We hypothesized that the low F_m may be due to a constitutively active NPQ mechanism. However, #164 and #108 lacked PsbS and accumulated wild-type levels of zeaxanthin under standard growth conditions and after a high light treatment (Figure 2-02E). Thus, fluorescence quenching was not attributable to constitutive qE or qZ. Instead, we hypothesized that the quenched F_o and F_m may be the result of constitutive qH.

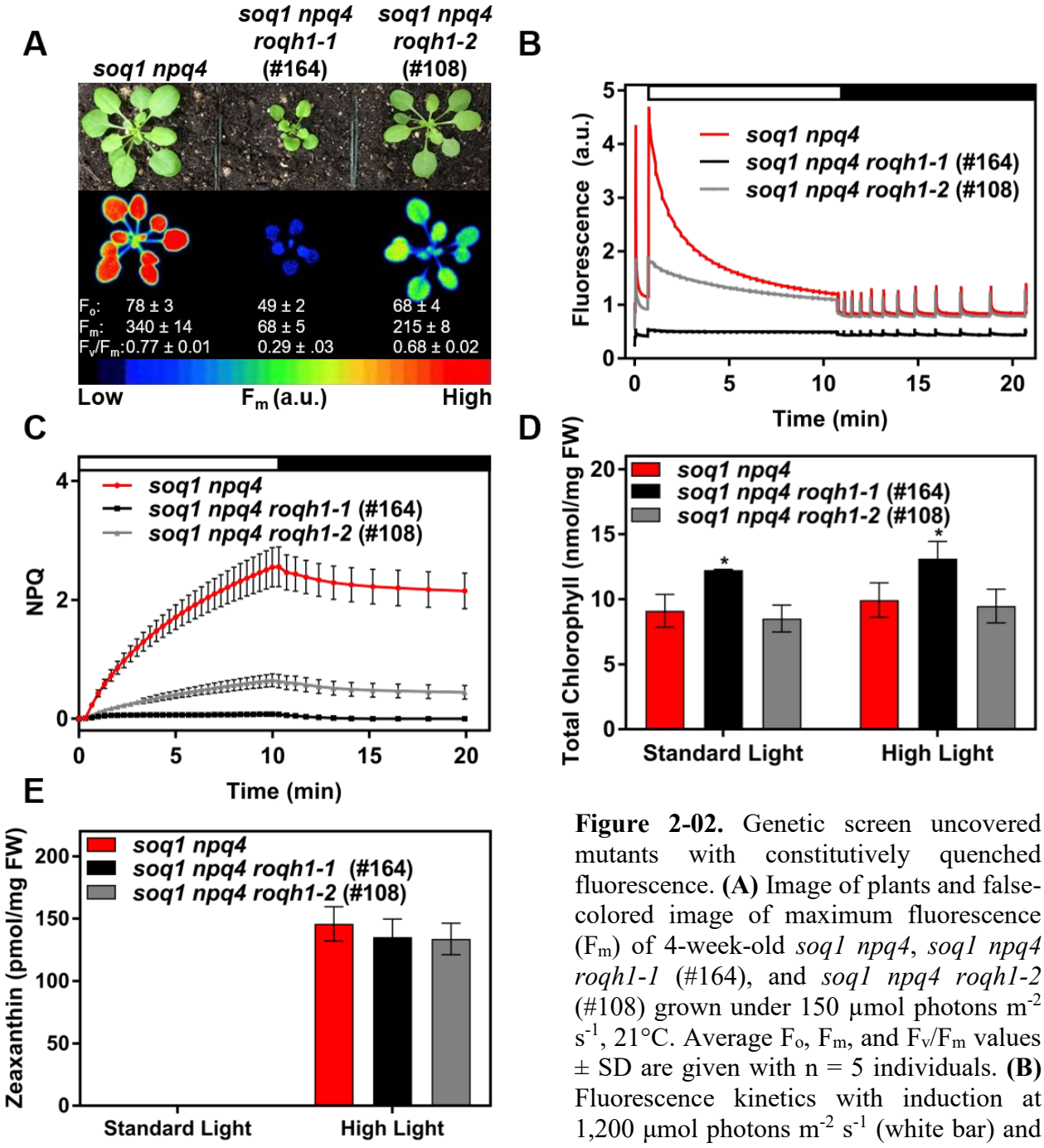

Figure 2-02. Genetic screen uncovered mutants with constitutively quenched fluorescence. **(A)** Image of plants and false-colored image of maximum fluorescence (F_m) of 4-week-old *soq1 npq4*, *soq1 npq4 roqh1-1* (#164), and *soq1 npq4 roqh1-2* (#108) grown under 150 µmol photons m^{-2} s^{-1}, 21°C. Average F_o, F_m, and F_v/F_m values ± SD are given with n = 5 individuals. **(B)** Fluorescence kinetics with induction at 1,200 µmol photons m^{-2} s^{-1} (white bar) and relaxation in the dark (black bar). Data

represent means, n = 3 individuals, error bars not shown. **(C)** NPQ kinetics with induction and relaxation as indicated in (B). **(D)** Total chlorophyll and **(E)** zeaxanthin levels determined by HPLC analysis of 4-week-old plants under standard light conditions (150 µmol photons m^{-2} s^{-1}) and after a 30-min high light treatment (1,000 µmol photons m^{-2} s^{-1}) to induce zeaxanthin accumulation. Under standard light conditions, zeaxanthin accumulation is below detection limit of 0.15pmol. Tukey's multiple comparison test shows a significant increase in chlorophyll levels of *soq1 npq4 roqh1-1* (#164) compared to *soq1 npq4* and *soq1 npq4 roqh1-2* (#108). Data represent means ± SD, n = 3 individuals, * = p-value <0.05.

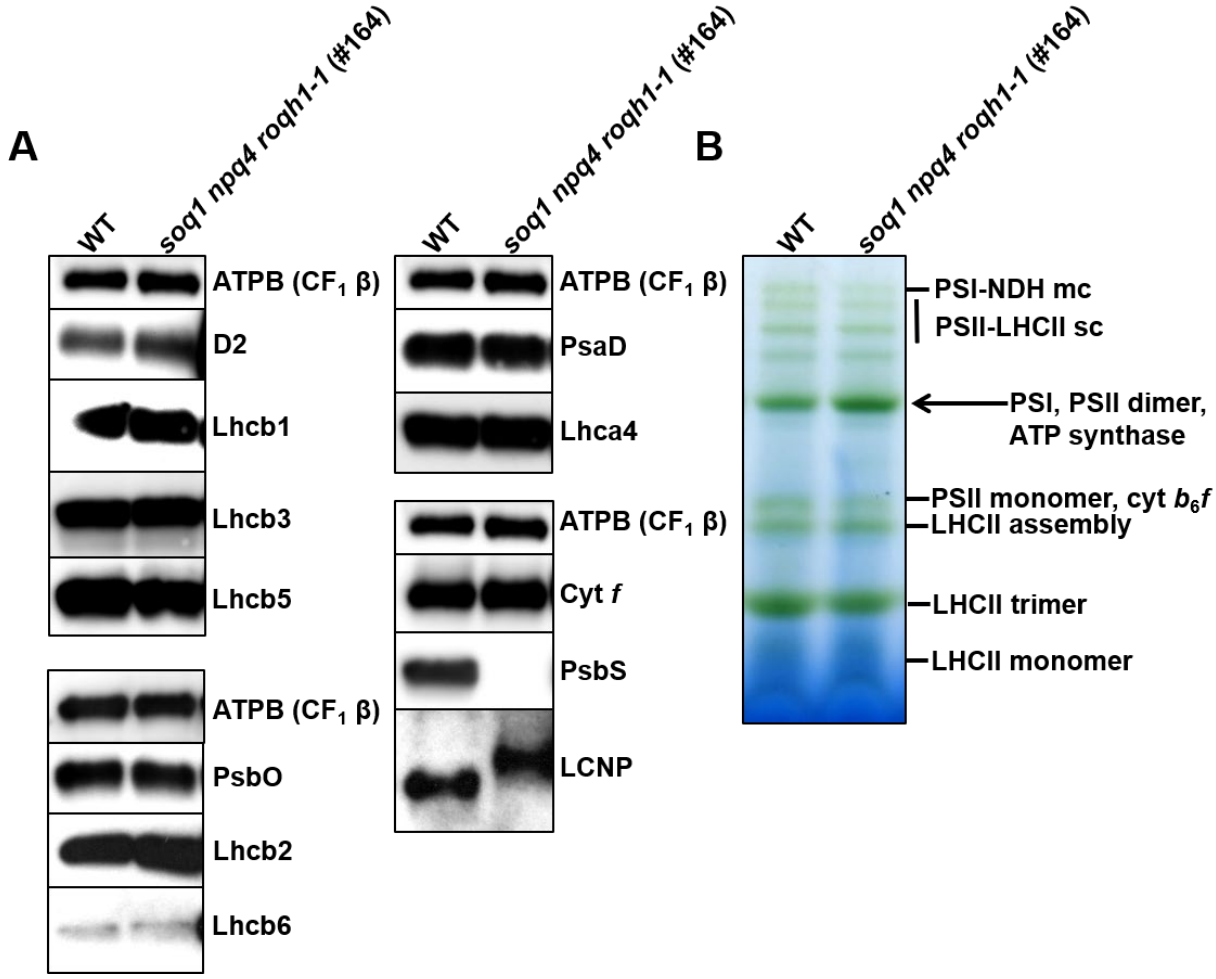

Figure 2-03. Similar accumulation and formation of photosynthetic complexes between wild type and mutant #164. **(A)** Immunoblot analysis of major photosynthetic proteins. Proteins were harvested from 4-week-old plants grown under 100 µmol photons m^{-2} s^{-1}, separated by SDS-PAGE, and analyzed by immunodetection with indicated antibodies. Samples were loaded by same leaf area and ATPB is shown as a loading control. **(B)** Isolated thylakoids from 4-week-old plants grown under 100 µmol photons m^{-2} s^{-1} were solubilized in 1.5% β-DM at 1µg/µl chlorophyll for 10 min on ice. Samples were loaded by equal chlorophyll (5µg) and separated by BN-PAGE. Identity of complexes were inferred from ref[59].

2.4.2 Whole-genome sequencing revealed mutations in a gene encoding an atypical short chain dehydrogenase/reductase

To identify the mutation responsible for the low fluorescence phenotype, a mapping-by-sequencing approach was used. Mutant #164 was backcrossed to *soq1 npq4*, and all progeny from the F1 generation displayed fluorescence and NPQ values similar to *soq1 npq4* (Figure 2-02), indicating that the causative gene contained a recessive mutation. From the segregating F2 population, 20.6% of seedlings displayed low F_m. The seedlings with low F_m were pooled and compared to the parental strain through whole-genome sequencing. Single nucleotide polymorphism analysis (Figure 2-05) revealed non-synonymous point mutations in seven nuclear genes on chromosome 4 that were enriched in the low F_m pool but absent in the parental strain (Tables 2-01 and 2-02). The list of candidate genes potentially responsible for the low F_m phenotype was narrowed down using TargetP[60] to genes encoding chloroplast-targeted proteins (because a protein involved in NPQ is most likely chloroplast localized). Among the two remaining candidates, only At4g31530 was also disrupted in the mutant #108, strongly suggesting that mutations in this gene caused the low fluorescence phenotype of #108 and #164.

At4g31530 encodes a 29-kD atypical short chain dehydrogenase/reductase protein, subsequently named RELAXATION OF QH1 (ROQH1). The ROQH1 protein is predicted to contain a Rossmann-fold with an NAD(P)-binding motif (GXXGXXG) and a partial catalytic tetrad (D-S-VXXXK) (Figure 2-06A). #164 and #108 contained allelic mutations in *ROQH1*, named *roqh1-1* and *roqh1-2*, respectively. G-to-A point mutations were found in the first exon (*roqh1-1*) and sixth exon (*roqh1-2*) causing the following amino acid changes: Gly81Asp within the NAD(P)-binding motif in *roqh1-1* and Gly211Glu within the partial catalytic tetrad in *roqh1-2* (Figure 2-06A). In addition to *roqh1-1* and *roqh1-2*, we obtained seven insertional mutants potentially affecting At4g31530 expression. Through PCR and immunoblot analysis, we confirmed that three insertional lines were disrupted in the *ROQH1* gene and in ROQH1 protein accumulation (Figure 2-07). We proceeded with SALK_039706, subsequently named *roqh1*-3, which contained a T-DNA insertion in the second exon of *ROQH1*. To determine the effect of the *roqh1-1*, *roqh1-2*, and *roqh1-3* mutations on ROQH1 protein abundance, protein accumulation was investigated in the different mutant alleles. Both *roqh1-1* and *roqh1-2* showed decreased ROQH1 levels, accumulating approximately 50% in *roqh1-1* and 25% in *roqh1-2* in comparison to wild type (Figure 2-06B). The insertional mutant, *roqh1-3*, showed complete disruption of protein accumulation and is therefore a null allele (Figure 2-06B).

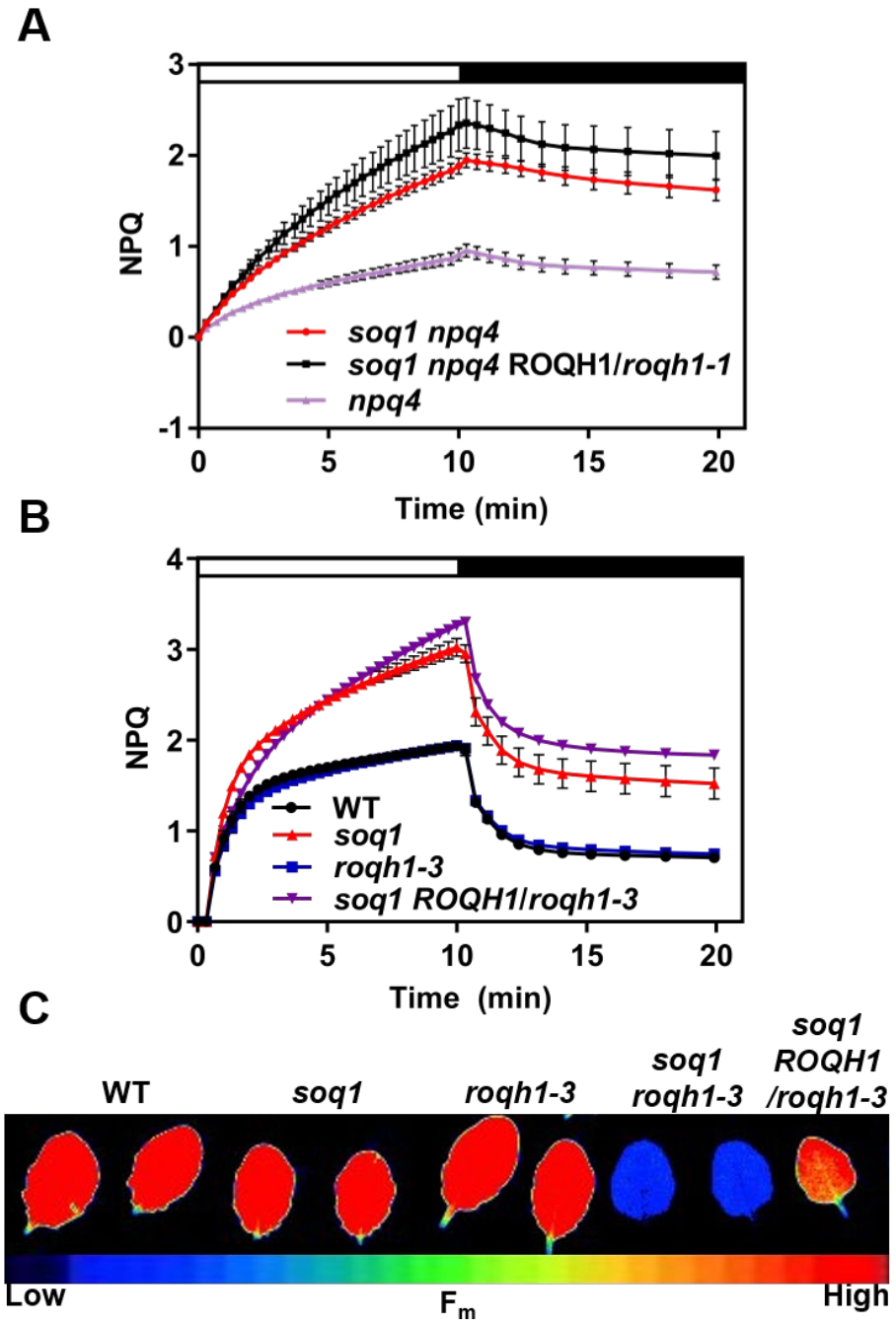

Figure 2-04. ROQH1 mutations are recessive. **(A)** NPQ kinetics of *npq4*, *soq1 npq4*, and F1 from cross *soq1 npq4* x #164 (*soq1 npq4 roqh1-1*). Data represent means ± SD, n=3. Growth at 120 µmol photons m^{-2} s^{-1}, induction of NPQ at 1,200 µmol photons m^{-2} s^{-1} (white bar) and relaxation in the dark (black bar). **(B)** NPQ kinetics of wild type, *soq1, roqh1-3*, and F1 from cross *soq1* x *roqh1-3*. Data represent means ± SD, n=3 (n=1 for F1). Growth at 120 µmolphotons m^{-2} s^{-1}, induction of NPQ at 1,200 µmol photons m^{-2} s^{-1} (white bar) and relaxation in the dark (black bar). The difference in NPQ induction and relaxation between wild type and *soq1* is due to qH. **(C)** False-colored images of maximum fluorescence (Fm) of detached leaves of wild type, *soq1*, *roqh1-3*, *soq1 roqh1-3*, and F1 from cross *soq1* x *roqh1-3*.

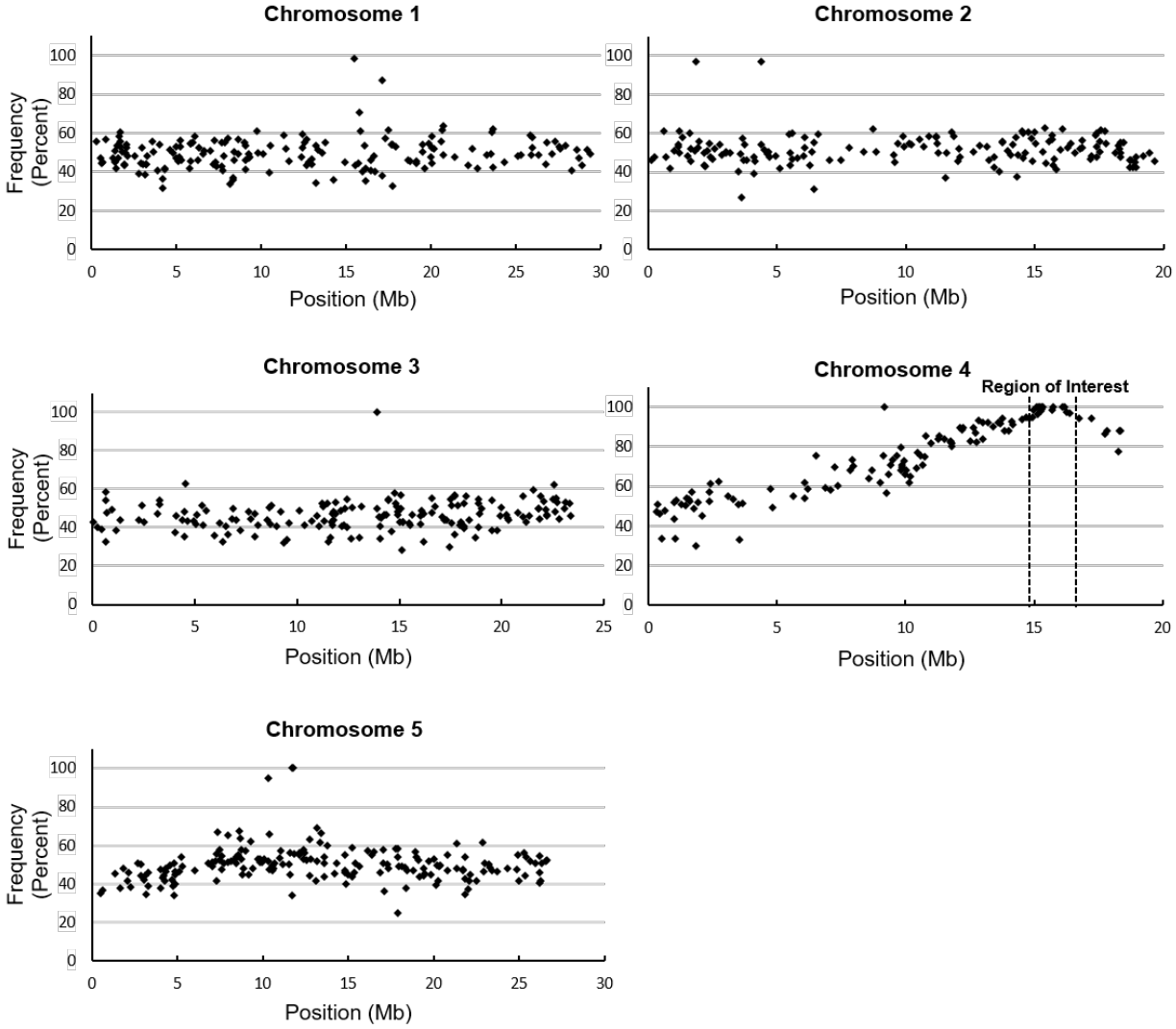

Figure 2-05. Causative mutation in mutant #164 is on chromosome 4. Detected single nucleotide polymorphisms (SNPs) from the pooled mutant F2 individuals with same NPQ phenotype as #164 (*soq1 npq4 roqh1-1*), from *soq1 npq4* x #164 cross. Identified SNPs were filtered for quality and to remove SNPs present in the parental line (*soq1 npq4*). The remaining SNPs were plotted with the allele frequency on the Y axis and position on each chromosome on the X axis. A region enriched for SNPs showing tight linkage to the mutant phenotype was identified on chromosome 4.

	Total Reads	Mapped Reads	Average Coverage
soq1 npq4	132,003,442	115,078,143	95.77
#164 (*soq1 npq4 roqh1-1*)	141,679,042	128,262,382	106.97

Table 2-01. Sequencing and read mapping summary. The samples were multiplexed and run with two unrelated samples in two lanes on an Illumina HiSeq2000/2500 to obtain 100 bp paired-end reads. The reads were mapped to the Col-0 reference sequence from TAIR. #164 (*soq1 npq4 roqh1-1*) are pooled F2 individuals with same NPQ phenotype as mutant #164 from the cross *soq1 npq4* x #164.

Chromosome	Position	Nucleotide change	AGI	AA change	Gene mutated in #108 (*soq1 npq4 roqh1-2*)?
Chr4	15,164,562	G->A	At4g31200	R3Stop	No
Chr4	15,202,747	G->A	At4g31330	D106N	No
Chr4	15,266,122	G->A	At4g31480	A660T	No
Chr4	15,282,522	G->A	At4g31530	G81D	Yes
Chr4	15,286,604	G->A	At4g31540	L67F	No
Chr4	16,103,193	C->T	At4g33470	D317N	No
Chr4	16,382,123	C->T	At4g34220	V602M	No

Table 2-02. Summary of identified mutations within mapped region. Seven mutations predicted to result in amino acid changes were identified within the mapped region on chromosome 4 for mutant #164 (*soq1 npq4 roqh1-1*). Only one of these genes, At4g31530 encoding for ROQH1 was also disrupted in the allelic mutant #108 (*soq1 npq4 roqh1-2*).

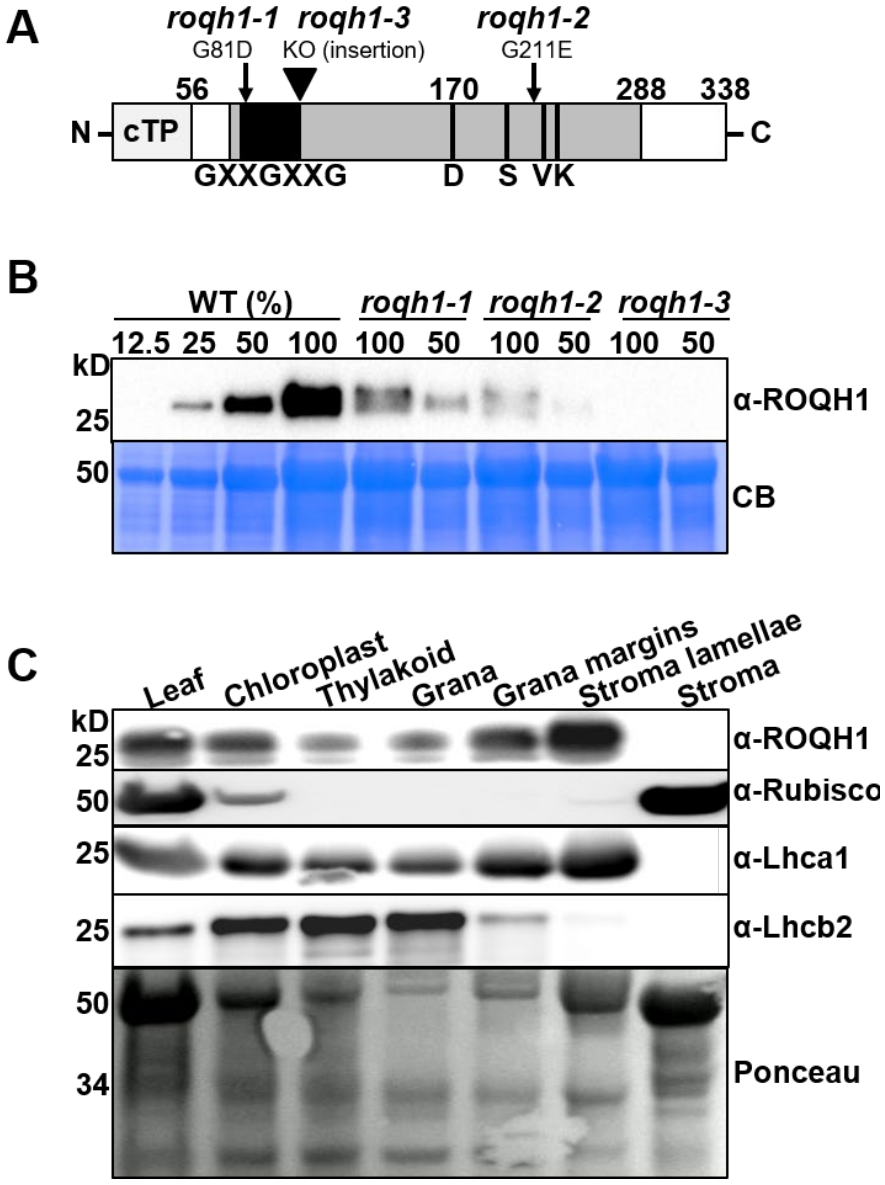

Figure 2-06. ROQH1 is enriched in the chloroplast stroma lamellae. **(A)** Schematic representation of ROQH1 protein with positions of mutations. Predicted chloroplast transit peptide (cTP; light grey) suggesting a mature size of 29 kD, Rossmann-fold (grey), NAD(P)-binding motif (GXXGXXG; black), and partial catalytic tetrad of residues (D-S-VXXXK; black lines). Numbers indicate amino acid positions and arrows indicate mutations. ROQH1-G81D (*roqh1-1*) and ROQH1-G211E (*roqh1-2*) from suppressor mutants #164 and #108, respectively; KO, knock-out mutant allele from T-DNA insertion (*roqh1-3*). **(B)** and **(C)** Proteins were separated by SDS-PAGE and analyzed by immunodetection with antibodies against ROQH1, Rubisco, Lhca1, Lhcb2, D2, or PsaD. Coomassie blue (CB) or Ponceau are shown as loading controls. Molecular masses (kD) are indicated according to the migration of Precision Plus Protein Standards markers from Bio-Rad. **(B)** Total leaf extract from plants grown under 150 µmol photons m^{-2} s^{-1}, 21°C. Samples were loaded by equal total chlorophyll content (2.5 µg). The appearance of two bands in *roqh1-1* (100) and *roqh1-2* (100) are most likely due to protein shadowing by the LHC proteins, as only one band is present in the diluted (50) sample. **(C)** Total leaf extract (Leaf) from plants grown under 120 µmol photons m^{-2} s^{-1}, 21°C were fractionated into chloroplasts, thylakoids, grana (appressed membranes), grana margins, stroma, and stroma lamellae (non-appressed membranes). Samples were loaded by equal total chlorophyll content (3 µg).

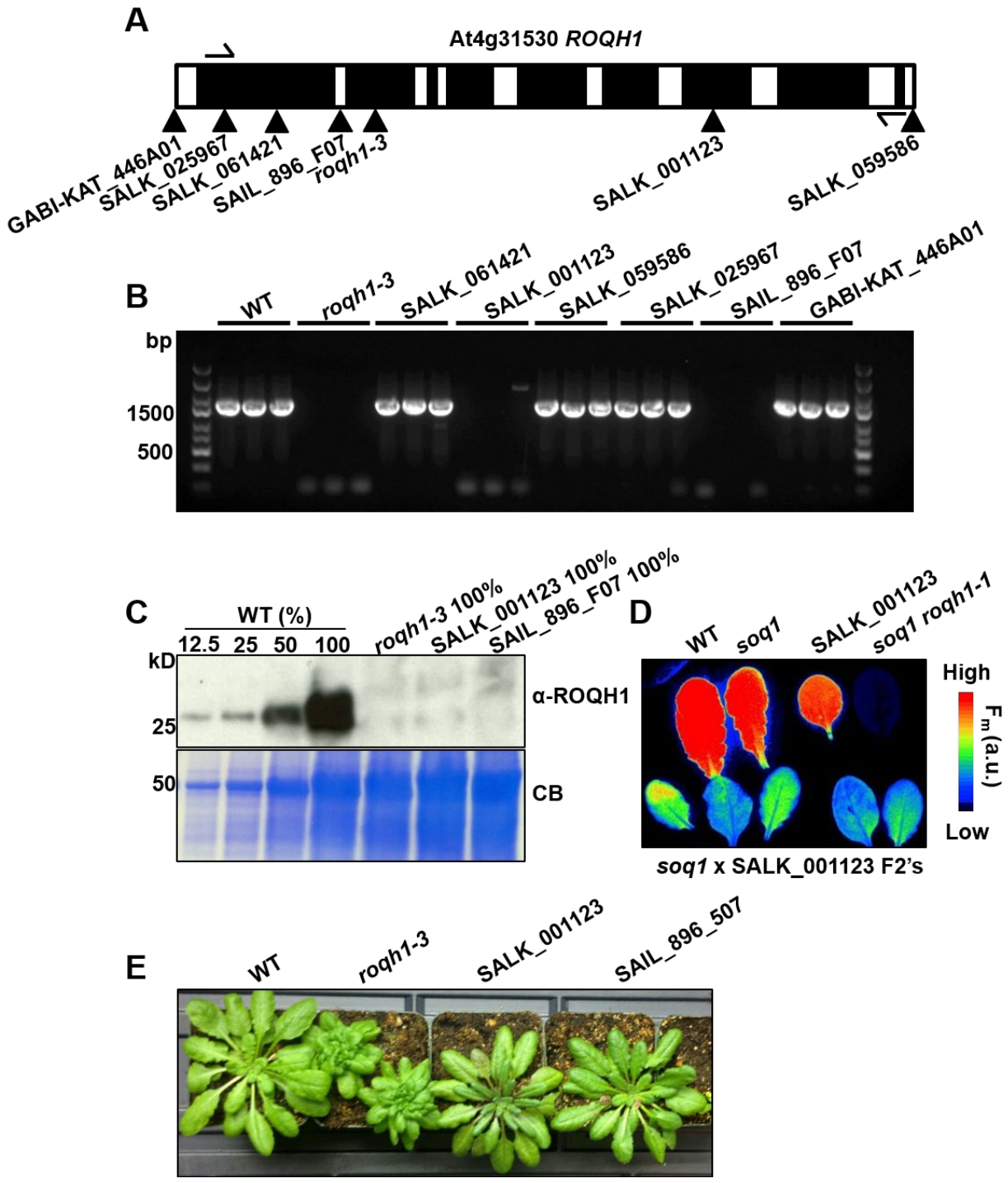

Figure 2-07. ROQH1 disruption in insertional mutants**. (A)** Schematic of *ROQH1* gene. Black boxes represent exons and white boxes represent introns, 5', and 3' UTR. Arrows indicate putative locations of insertions and half arrows indicate location of primers CA113F (GCTACAAAATCCCAAATCAGAA) and CA65R (ATTGCTGTGGATCACTTCCTG) used to amplify *ROQH1* in (B). White arrows indicate insertions that were not found by PCR in (B). **(B)** *ROQH1* gene amplified by PCR in wild type and insertional mutants using primers CA113F and CA65R and separated on a 2% agarose gel. PCR failed to amplify *ROQH1* in mutants *roqh1-3*

(SALK_039706), SALK_001123, and SAIL_896_F07. **(C)** Isolated whole cells from 6-week-old plants, grown under 150 μmol photons m^{-2} s^{-1}. Samples from wild type and insertional mutants *roqh1-3* (SALK_039706), SALK_001123, and SAIL_896_F07 were loaded by equal total chlorophyll content (100% = 2.5 μg total chlorophyll), separated by SDS-PAGE, and analyzed by immunodetection with an antibody against ROQH1. Coomassie blue (CB) is shown as a loading control. Molecular masses (kD) are indicated according to the migration of Precision Plus Protein Standards from Bio-Rad. SALK_039706 (*roqh1-3*), SALK_001123, and SAIL_896_F07 are disrupted in ROQH1 protein accumulation and accumulate less than 12.5% of wild type-levels. **(D)** False-colored image of leaves from wild type, *soq1*, SALK_001123, *soq1 roqh1-1*, and *soq1* SALK_001123. The fluorescence level of soq1 SALK_001123 is intermediate between wild type and *soq1 roqh1-1*. (E) Images of wild type, r*oqh1-3*, SALK_001123, and SAIL_896_F07. Growth of SALK_001123, and SAIL_896_F07 is comparable to wild type.

2.4.3 ROQH1 is enriched in the chloroplast stroma lamellae

A previous proteomics study of chloroplast membranes identified ROQH1 in the stroma lamellae within the chloroplast[61]. Subcellular localization of ROQH1 was confirmed by isolating and fractionating wild-type chloroplasts into thylakoid sub-compartments, including grana core, margins, stroma lamellae, and the soluble stroma fraction. Immunoblot analysis identified the majority of ROQH1 in the stroma lamellae fraction (Figure 2-06C), consistent with the previous report[61]. According to protein topology prediction tools, Aramemnon and Protter[62,63], ROQH1 is predicted to contain either one or no transmembrane domains. To discern whether ROQH1 is an intrinsic or peripherally bound protein, we tested the strength of ROQH1 association to the stroma lamellae by subjecting isolated thylakoids to various salt treatments. After treatments with NaCl, Na_2CO_3, and $CaCl_2$, ROQH1 was present in both the pellet and the supernatant fractions, indicating that a portion of ROQH1 is loosely associated to the stroma lamellae while a portion remains strongly bound (Figure 2-08).

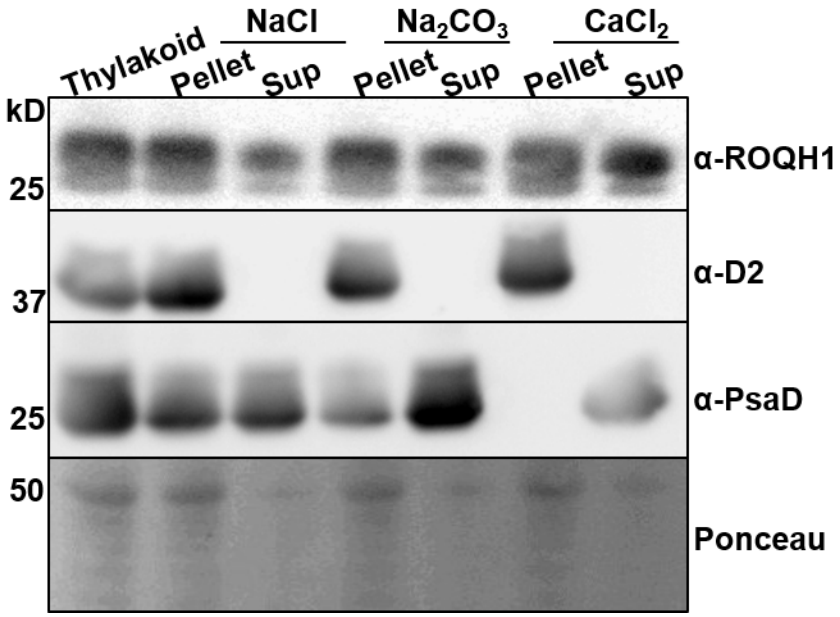

Figure 2-08. A portion of ROQH1 is strongly bound to the stroma lamellae. Isolated thylakoids from wild type were subjected to salt washes with NaCl, Na_2CO_3, and $CaCl_2$. The initial thylakoids, pellets, and supernatants (Sup) were loaded by equal total chlorophyll content (3 μg). Proteins were separated by SDS-PAGE and analyzed by immunodetection with antibodies against ROQH1, D2, and PsaD. Ponceau is shown as a loading control. Molecular masses (kD) are indicated according to the migration of Precision Plus Protein Standards markers from Bio-Rad.

2.4.4 Constitutive quenching is due to the combination of *soq1* and *roqh1* mutations

As ROQH1 had not been previously characterized, we investigated the phenotype of the *roqh1* single mutants. By crossing #164 and #108 to the wild type, the *roqh1-1* and *roqh1-2* mutations were isolated from the *soq1* and *npq4* mutations. When grown under standard growth conditions, all single *roqh1* mutants displayed wild-type chlorophyll fluorescence levels, and *roqh1-1* and *roqh1-2* were indistinguishable from the wild type (Figure 2-09). The null allele, *roqh1-3*, had a developmental phenotype and overproduced leaves with short petioles (Figure 2-09). However, complementation of *roqh1-3* with *ROQH1* showed that this phenotype was independent of the *roqh1* mutation, as complemented lines retained the developmental phenotype (Figure 2-10A-C). It is likely that the *roqh1-3* growth phenotype is due to a mutation in a nearby gene and linked to the T-DNA insertion (approximately 2000 seedlings were examined for petiole length from the cross *soq1* x *roqh1-3*, and no *roqh1-3* mutant could be found without the short petiole phenotype). HPLC analysis of leaves showed that the pigment composition of all single mutants did not differ from the wild type (Figure 2-11C, Figure 2-12A).

In addition to the *soq1* and *roqh1* mutations, #164 and #108 also lacked PsbS due to the *npq4* mutation. To determine which mutations were necessary for constitutive quenching, we outcrossed #164 and #108 to the wild type. Of the segregating F2 populations, 4% and 6% of seedlings displayed low F_m, indicating that two mutations were necessary for the phenotype. To determine if the *npq4* mutation was required, we separated *soq1 roqh1-1* and *soq1 roqh1-2* from *npq4*. The F_o and F_m values of *soq1 roqh1-1* and *soq1 roqh1-2* remained as low as the original

soq1 npq4 roqh1-1 and *soq1 npq4 roqh1-2* mutants (Figure 2-09 and Figure 2-13). For independent confirmation, we crossed *soq1* with the null allele, *roqh1-3*. Of the segregating F2 population, 5.3% of seedlings displayed low F_m, consistent with two mutations being required. The homozygous double mutant, *soq1 roqh1-3* displayed decreased F_o and F_m values similar to *soq1 roqh1-1*, further confirming that this phenotype required both *soq1* and *roqh1* mutations and was independent of *npq4* (Figure 2-09). In addition, the *soq1/soq1 ROQH1*/*roqh1-3* heterozygote displayed normal fluorescence and NPQ (Figure 2-03), indicating that *roqh1-3* was also a recessive mutation.

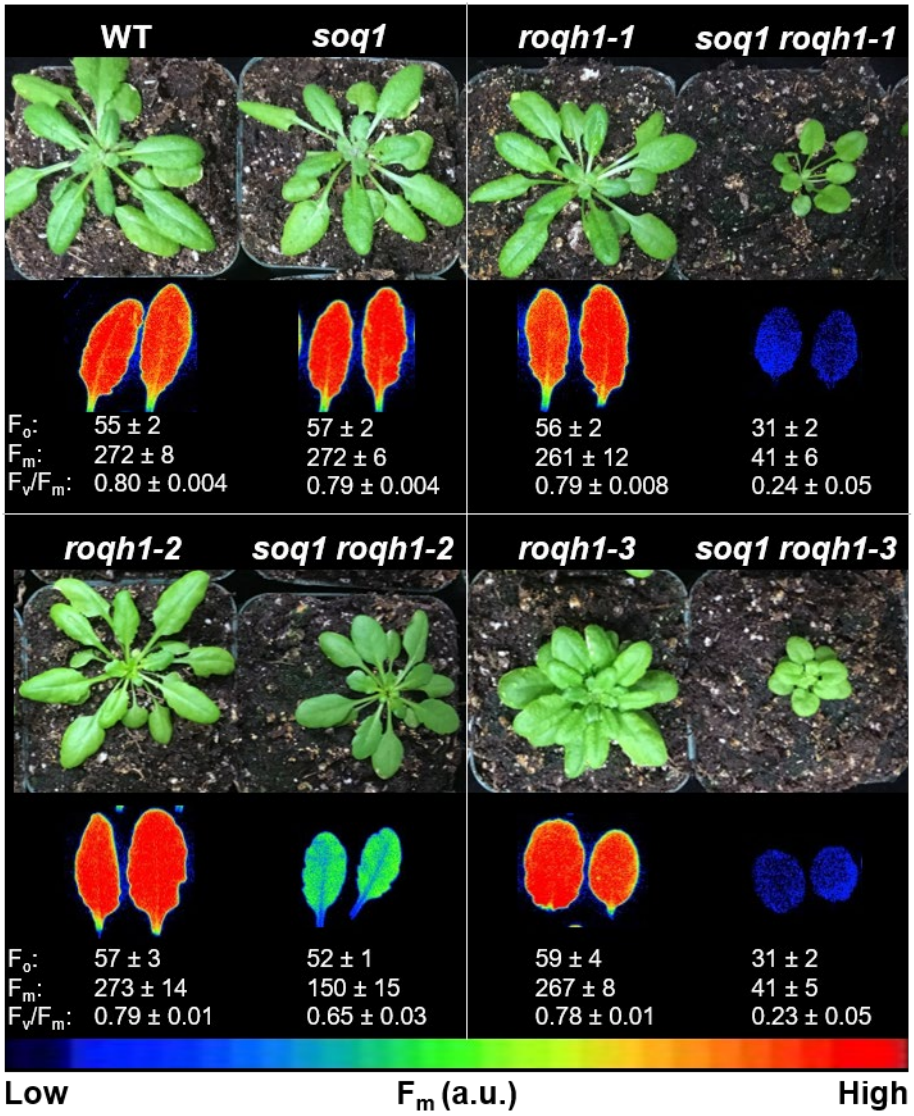

Figure 2-09. Constitutive quenching requires *soq1* and *roqh1* mutations alone. Images of plants and false-colored images of maximum fluorescence (F_m) of detached leaves from 5-week-old plants grown under 150 µmol photons m^{-2} s^{-1}, 21°C. Average F_o, F_m, and F_v/F_m values ± SD are given with n = 5 individuals for each genotype.

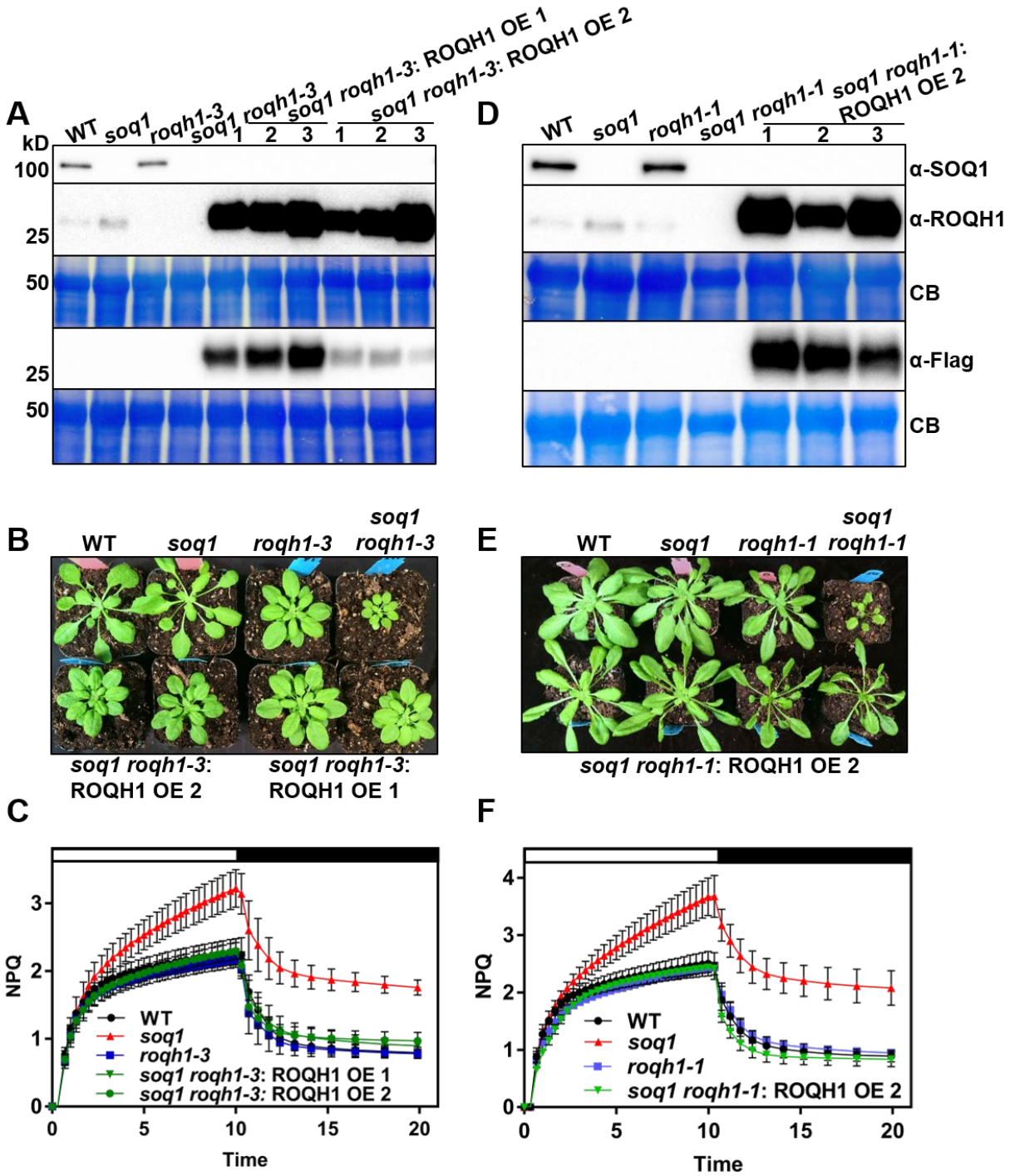

Figure 2-10. Overexpression of ROQH1 prevents qH from occurring and fails to rescue the *roqh1-3* developmental phenotype. Plants of *soq1 roqh1-3*: ROQH1 OE 1 corresponds to T2 individuals from independent line 1, plants of *soq1 roqh1-3*: ROQH1 OE 2 corresponds to T2 individuals from independent line 2, and plants of *soq1 roqh1-1*: ROQH1 OE 2 corresponds to T2 individuals from independent line 2. **(A)** and **(D)** Isolated whole cells from 4-6-week-old plants grown under 120 µmol photons m^{-2} s^{-1}. Samples were loaded by same leaf area, separated by SDS-PAGE, and analyzed by immunodetection with antibodies against SOQ1, ROQH1, and Flag. Coomassie blue (CB) is shown as loading control. Molecular masses (kD) are indicated according to the migration

of Precision Plus Protein Standards markers from Bio-Rad. **(B)** and **(E)** Images of 4-6-week-old plants grown under 120 µmol photons m^{-2} s^{-1} **(C)** and **(F)** NPQ kinetics with induction at 1,200 µmol photons m^{-2} s^{-1} (white bar) and relaxation in the dark (black bar). Data represent means ± SD, n=3. The difference in NPQ induction and relaxation between wild type and *soq1* is due to qH.

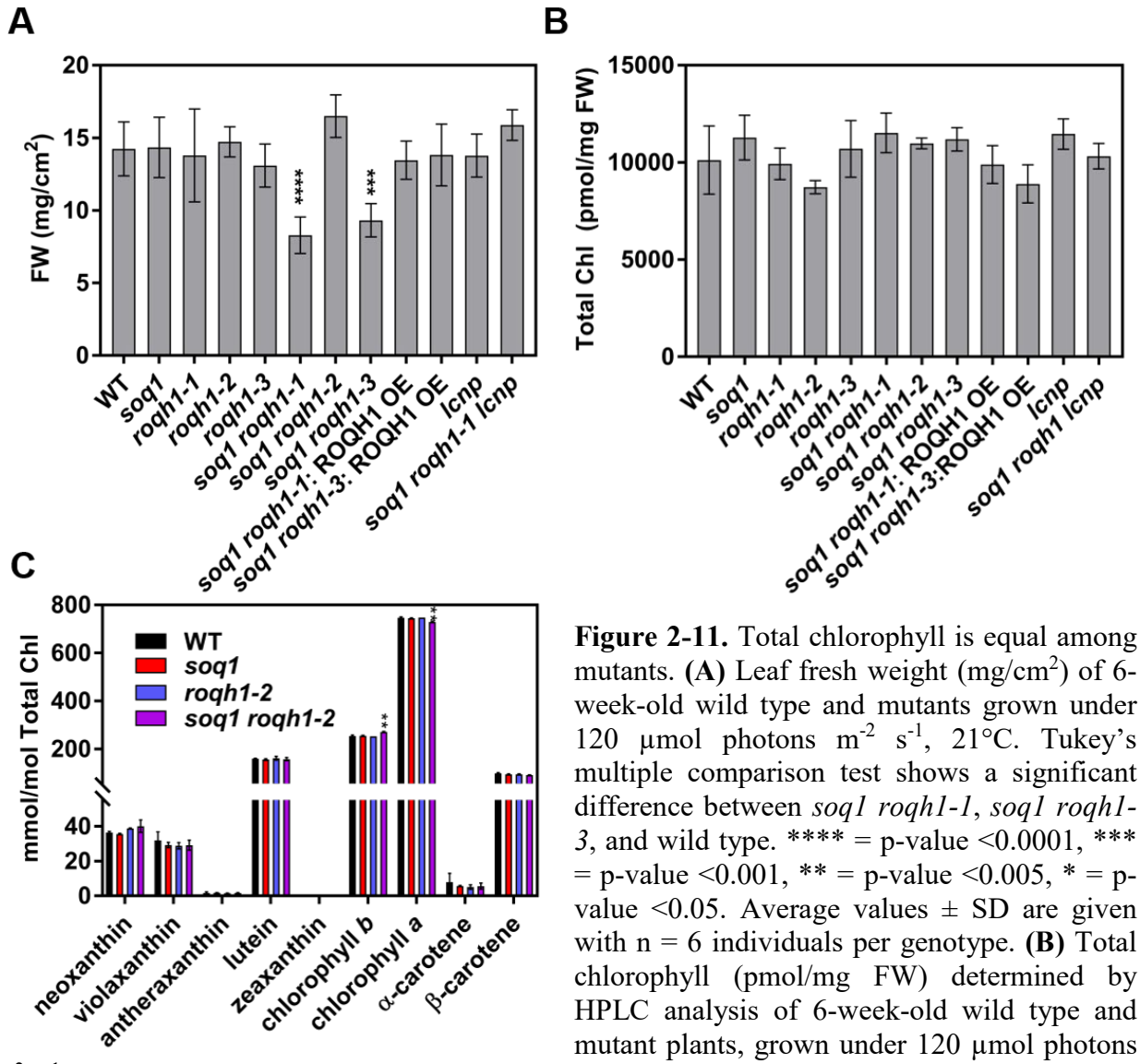

Figure 2-11. Total chlorophyll is equal among mutants. **(A)** Leaf fresh weight (mg/cm^2) of 6-week-old wild type and mutants grown under 120 µmol photons m^{-2} s^{-1}, 21°C. Tukey's multiple comparison test shows a significant difference between *soq1 roqh1-1*, *soq1 roqh1-3*, and wild type. **** = p-value <0.0001, *** = p-value <0.001, ** = p-value <0.005, * = p-value <0.05. Average values ± SD are given with n = 6 individuals per genotype. **(B)** Total chlorophyll (pmol/mg FW) determined by HPLC analysis of 6-week-old wild type and mutant plants, grown under 120 µmol photons m^{-2} s^{-1}, 21°C. Tukey's multiple comparison test shows no significant difference among wild type and mutants. Average values ± SD are given with n = 3 individuals per genotype. **(C)** Pigment composition determined by HPLC analysis of 6-week-old plants, grown under 120 µmol photons m^{-2} s^{-1}, 21°C. Tukey's multiple comparison test shows a significant increase in chlorophyll *b* and a significant decrease in chlorophyll *a* in *soq1 roqh1-2* compared to wild type. **** = p-value <0.0001, *** = p-value <0.001, ** = p-value <0.005, * = p-value <0.05. Average values ± SD are given with n = 3 individuals per genotype.

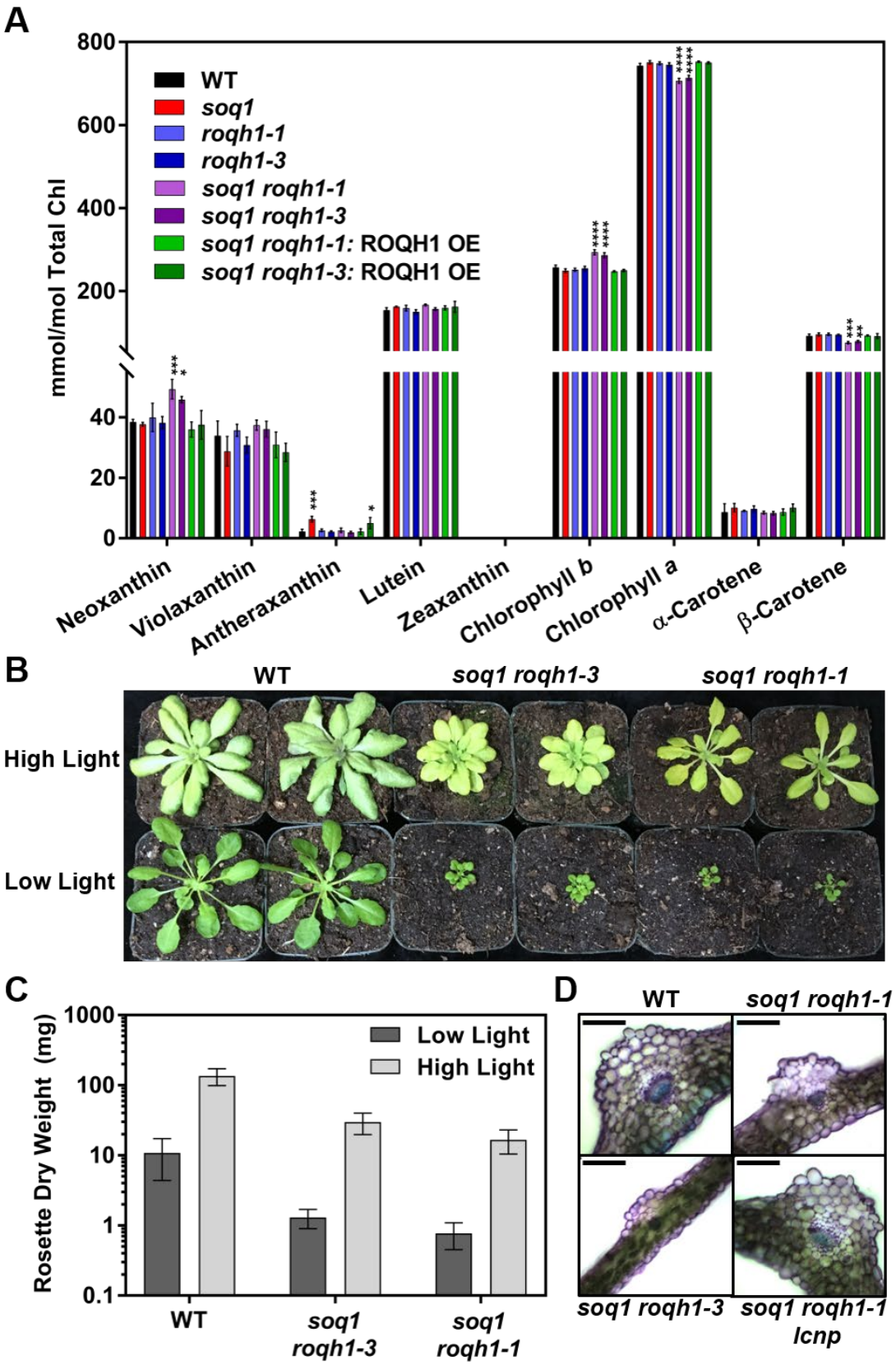

Figure 2-12. Constitutively quenched mutants are light-limited. **(A)** Pigment composition determined by HPLC analysis of 6-week-old plants, grown under standard light conditions (120

µmol photons m^{-2} s^{-1}, 21°C). Under standard light conditions, zeaxanthin accumulation is below detection limit of 0.15pmol. Tukey's multiple comparison test shows a significant increase in neoxanthin and chlorophyll *b* and a significant decrease in chlorophyll *a* and β-carotene in *soq1 roqh1-1* and *soq1 roqh1-3* compared to wild type. **** = p-value <0.0001, *** = p-value <0.001, ** = p-value <0.005, * = p-value <0.05. Average values ± SD are given with n = 3 individuals per genotype. **(B)** Images of 5-week-old plants grown under low (100 µmol photons m^{-2} s^{-1}) or high (1,300 µmol photons m^{-2} s^{-1}) light. **(C)** Rosette dry weight harvested from plants indicated in (B). Average values ± SD are given with n = 8-12 individuals. Note the log scale Y-axis. **(D)** Microscopy images of leaf cross-sections at the mid-vein. Plants are 6-7 weeks old grown under 150 µmol photons m^{-2} s^{-1}, 21°C. Scale bar represents 100 µm.

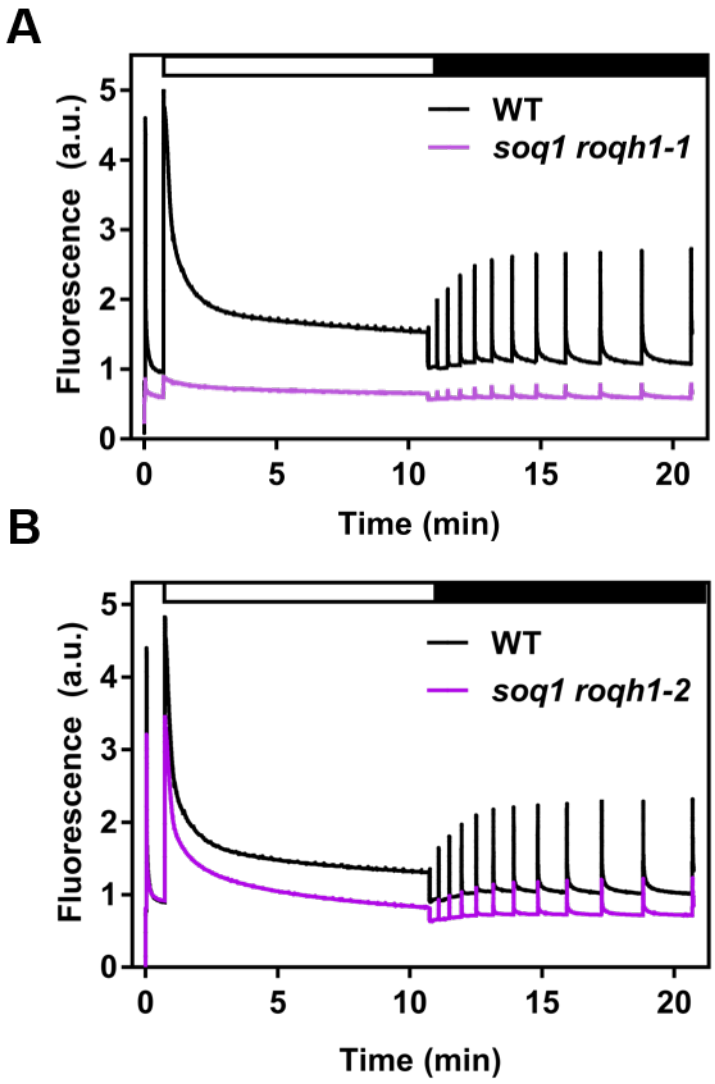

Figure 2-13. Fluorescence kinetics of *soq1 roqh1* are constitutively quenched. Fluorescence kinetics with induction at 1,200 µmol photons m^{-2} s^{-1} (white bar) and relaxation in the dark (black bar). Data represent means, n = 3 individuals, error bars not shown. **(A)** Fluorescence kinetics of wild type and *soq1 roqh1-1*. **(B)** Fluorescence kinetics of wild type and *soq1 roqh1-2*

2.4.5 Constitutively quenched mutants grow slowly and contain an altered pigment composition

Compared to the single *soq1* and *roqh1* mutants, *soq1 roqh1-1* and *soq1 roqh1-3* showed severely decreased F_o, F_m, and photoautotrophic growth (Figure 2-09). Leaf thickness was also decreased by 70 μm compared to the wild type (Figure 2-12A and Figure 2-14A, B). As a result, the leaves of the double mutants had lower fresh weight per area than wild type (Figure 2-11A). Accordingly, pigment analysis was normalized to fresh weight rather than leaf area, and *soq1 roqh1-1* and *soq1 roqh1-3* showed equal total chlorophyll per mg of fresh weight compared to wild type (Figure 2-11B). However, the pigment composition relative to total chlorophyll was altered, and both mutants contained significantly higher amounts of chlorophyll *b* and neoxanthin, and lower amounts of chlorophyll *a* and β-carotene (Figure 2-12A). The growth and carotenoid composition of the milder allele, *soq1 roqh1-2*, was unaltered, yet the chlorophyll *a*/*b* ratio was mildly decreased (Figure 2-09 and Figure 2-11C).

The constitutive quenching phenotype led us to question whether growth in the double mutants was limited by light. Under increased light intensity, growth of *soq1 roqh1-1* and *soq1 roqh1-3* improved as shown by an increase in dry rosette weight compared to standard light conditions (Figure 2-12B, C). While the fluorescence was still constitutively quenched under high light, it appeared that the photon flux through the photosystems was increased. Consistent with this hypothesis was the abundance of PSI subunits in *soq1 roqh1-1*. Under standard growth conditions, *soq1 roqh1-1* accumulated approximately 50% less PsaA and PsaD compared to the wild type. Yet under high light, the accumulation of PsaA and PsaD returned to wild-type levels (Figure 2-15). This suggested that under standard conditions, constitutive quenching results in downregulation of PSI in order to balance the low photon flux through the photosystems. For further confirmation, of light limitation, the thylakoid ultrastructure of *soq1 roqh1-1* was determined using transmission electron microscopy. The thylakoid membranes of *soq1 roqh1-1* appeared to be more stacked and in larger grana compared to wild type (Figure 2-14C, D) suggesting a light-limited thylakoid architecture.

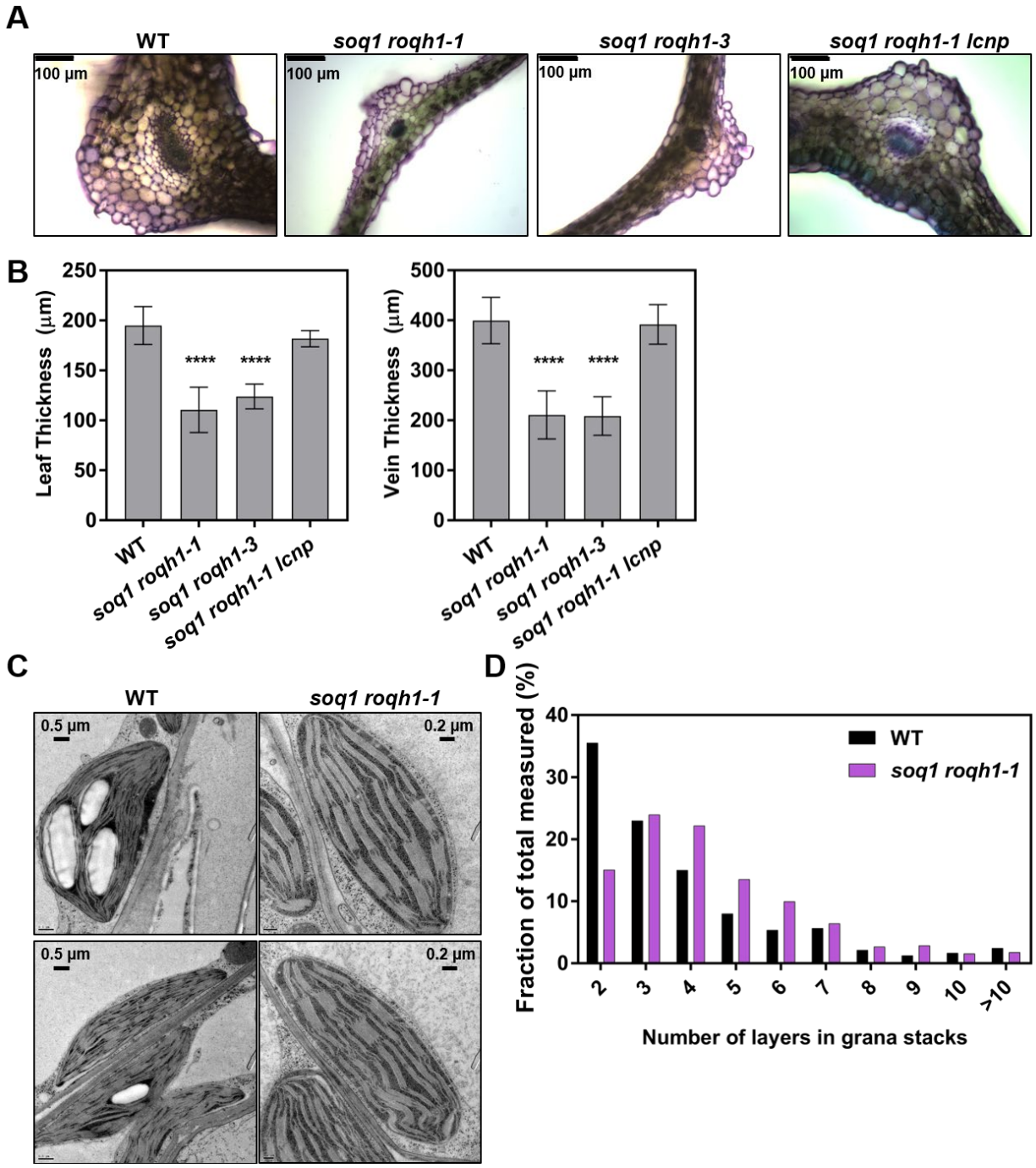

Figure 2-14. Constitutively quenched mutants have thin leaves and stacked grana. **(A)** Light microscopy images of leaf cross-sections at the mid-vein from wild type, *soq1 roqh1-1*, *soq1 roqh1-3*, and *soq1 roqh1-1 lcnp*. Plants are 6-7 weeks old, grown under 150 µmol photons m^{-2} s^{-1}, 21°C. **(B)** Quantification of leaf and mid-vein thickness. Tukey's multiple comparison test shows a significant decrease in leaf and mid-vein thickness in *soq1 roqh1-1* and *soq1 roqh1-3* compared to wild type. **** = p-value <0.0001. Data represent means ± SD, n=10 representative images. **(C)** Transmission electron microscopy images of chloroplasts from 4.5-week-old wild type and

soq1 roqh1-1 plants grown under 130 µmol photons m^{-2} s^{-1}, 21°C. **(D)** Frequency distribution of layers in grana stacks from 10 representative chloroplast images.

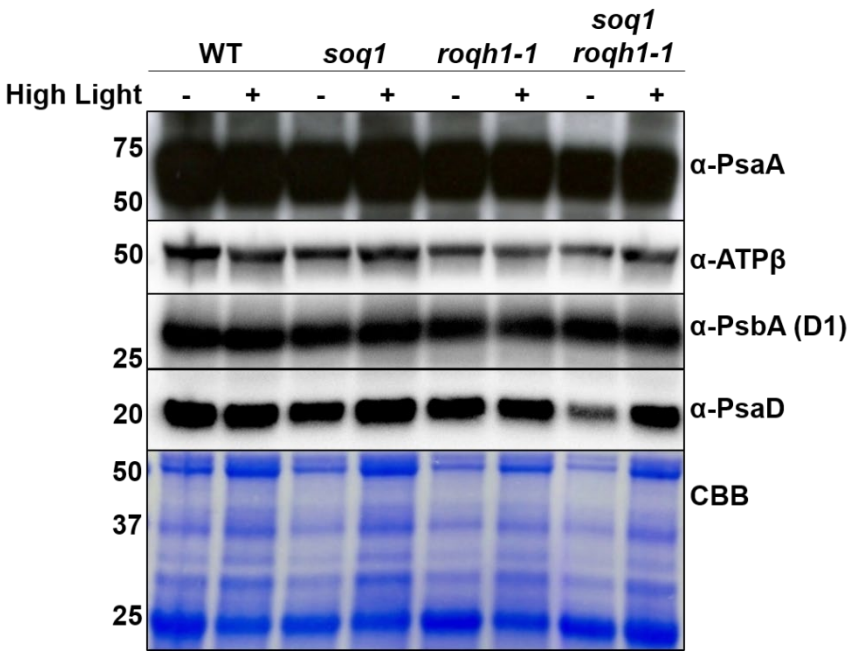

Figure 2-15. The photosynthetic flux of *soq1 roqh1-1* is limited under standard growth conditions. Thylakoids isolated from plants grown under standard (130 µmol photons m^{-2} s^{-1}) or high light (1,300 µmol photons m^{-2} s^{-1}) were loaded based on equal total protein and separated by SDS-PAGE and immunoblotted for PSI and PSII components.

2.4.6 The constitutive quenching observed in *soq1 roqh1* is qH

To determine if the constitutive quenching in *soq1 roqh1* was qH, we tested whether LCNP was required for the constitutive quenching to occur, as LCNP is required for qH[36]. To this aim, the LCNP knockout mutant (*lcnp*) was combined with *soq1 roqh1-1*. Indeed, the fluorescence values, F_o and F_m, of the triple mutant *soq1 roqh1-1 lcnp* returned to wild-type levels (Figure 2-16A). In addition, *soq1 roqh1-1 lcnp* recovered wild type growth, pigment composition, and leaf thickness, confirming that these phenotypes were a consequence of quenching and not the *soq1* and *roqh1* mutations themselves (Figure 2-14A, B and Figure 2-16B). Furthermore, the *soq1 roqh1-1 LCNP/lcnp* heterozygote recovered an intermediate F_m phenotype (Figure 2-16A and Figure 2-17). This is consistent with the previously reported observation that qH is dependent on LCNP dosage[36]. Altogether, these results demonstrate that the constitutive quenching observed in *soq1 roqh1-1* is qH.

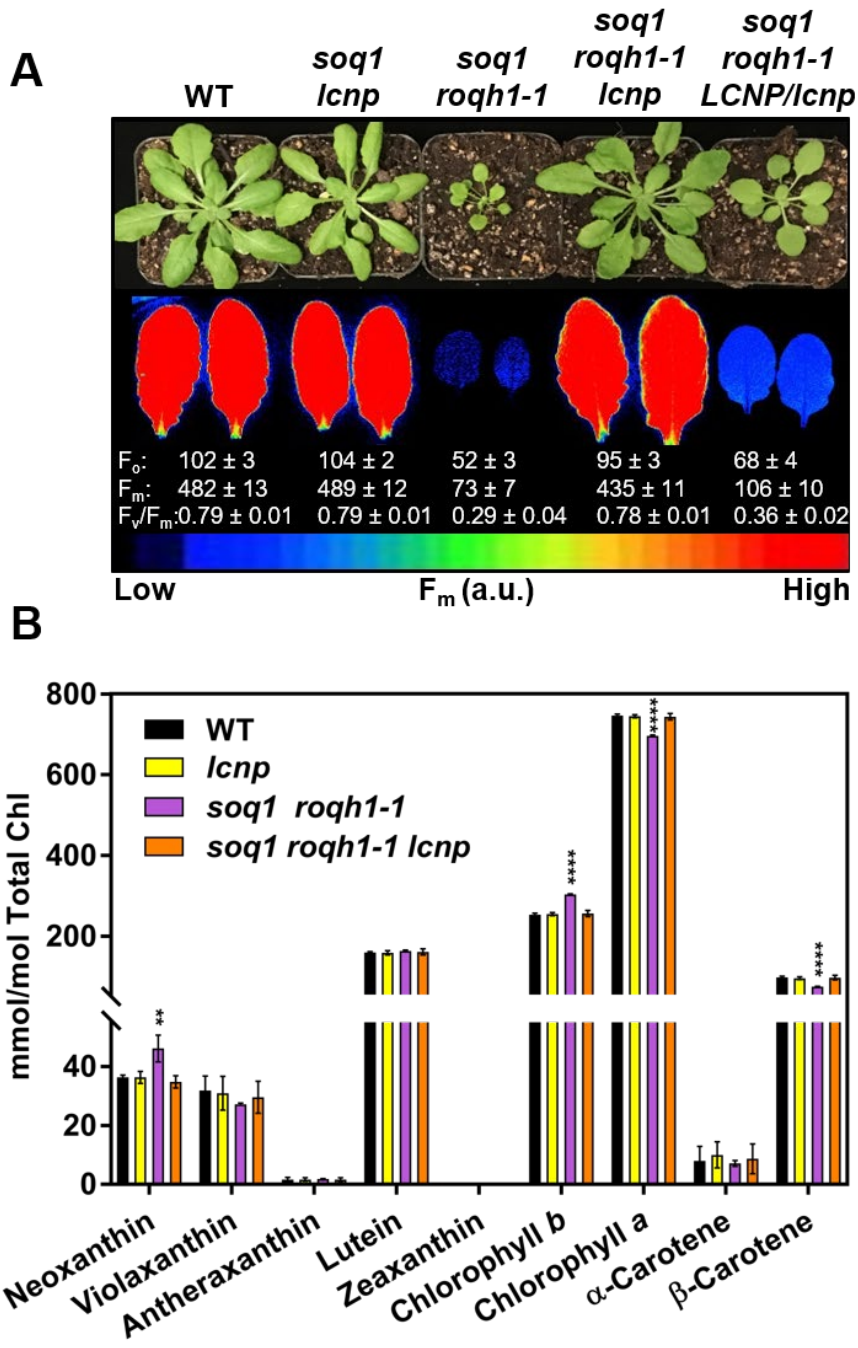

Figure 2-16. Constitutive quenching requires LCNP **(A)** Images of plants and false-colored images of maximum fluorescence (F_m) of detached leaves from 6-week-old plants grown under standard growth conditions (120 µmol photons m^{-2} s^{-1}, 21°C). Average F_o, F_m, and F_v/F_m values ± SD are given with n = 3 individuals for each genotype. **(B)** Pigment composition determined by HPLC analysis of 6-week-old plants grown under standard growth conditions (120 µmol photons m^{-2} s^{-1}, 21°C). Under standard light conditions, zeaxanthin accumulation is below detection limit of 0.15pmol. Tukey's multiple comparison test shows a significant increase in neoxanthin and chlorophyll *b* and a significant decrease in chlorophyll *a* and β-carotene in *soq1 roqh1-1* but not in *soq1 roqh1-1 lcnp*. **** = p-value <0.0001, *** = p-value <0.001, ** = p-value <0.005, * = p-value <0.05. Average values ± SD are given with n = 3 individuals per genotype.

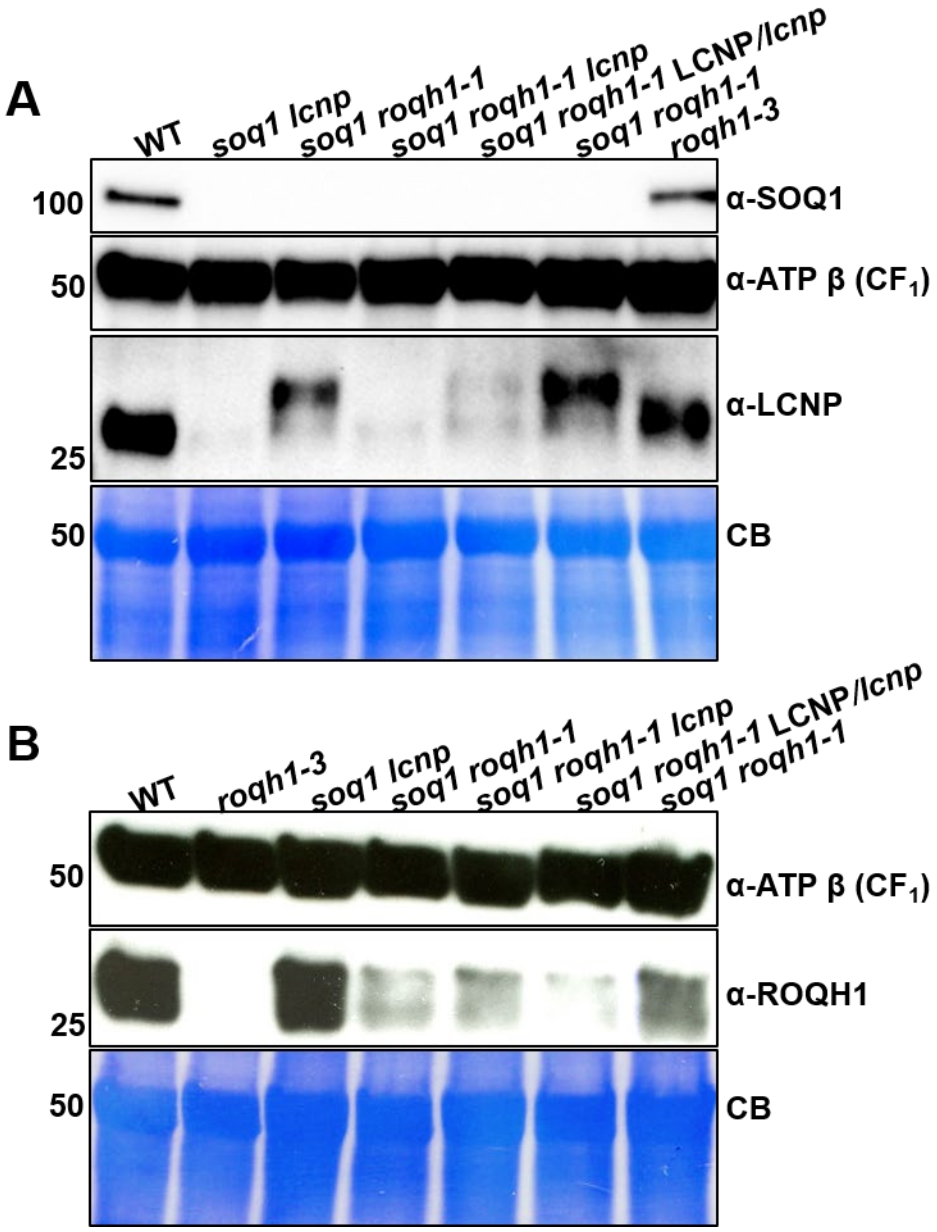

Figure 2-17. Accumulation of SOQ1, ROQH1, and LCNP proteins. Isolated whole cells from 6.5-week-old plants grown under 120 µmol photons m^{-2} s^{-1}. Samples were loaded by equal total chlorophyll content (3 µg), separated by SDS-PAGE, and analyzed by immunodetection with the following antibodies: SOQ1, LCNP, and ATP β in **(A)**, ROQH1 and ATP β in **(B)**. Coomassie blue (CB) and ATP β are shown as loading controls. Molecular masses (kD) are indicated according to the migration of Precision Plus Protein Standards markers from Bio-Rad. LCNP migrates slower and displays a band shift in a *soq1* mutant background consistent with ref[36]. LCNP protein accumulation in the *soq1 roqh1-1* LCNP/*lcnp* heterozygote is less than wild type, consistent with the intermediate F_m observed in Figure 2-14B and the hypothesis that qH is LCNP dosage-dependent[36].

2.4.7 Overexpression of ROQH1 prevents qH from occurring

While *roqh1* has no discernible NPQ phenotype compared to wild type under standard growth conditions (Figure 2-18), the constitutive quenching in *soq1 roqh1* implies that ROQH1 is required to prevent or relax quenching. However, qH can be induced by a 10-min high light treatment in the *soq1* mutant grown under standard conditions (Figure 2-18), which indicates either that qH can occur in the presence of ROQH1 and/or that the ROQH1 protein level is insufficient to prevent or relax quenching in this condition. The NPQ phenotype of *soq1* led us to question whether the function of ROQH1 is dosage-dependent. To test the dosage effect of ROQH1, we overexpressed (OE) ROQH1-FLAG in the *soq1 roqh1-1* mutant background and obtained lines with increased expression by a factor of >10 times that of wild type (Figure 2-19A and Figure 2-20). Overexpression of ROQH1 returned growth of *soq1 roqh1-1* to wild-type levels (Figure 2-19B). Surprisingly, overexpression restored NPQ to wild-type levels and not to *soq1* levels (Figure 2-19C), suggesting that ROQH1 overexpression prevents qH from occurring. To ensure that the NPQ phenotype was not due to any interaction between wild-type ROQH1 and the residual ROQH1-Gly81Asp protein that accumulated in *soq1 roqh1-1*, we overexpressed ROQH1-FLAG in the *soq1 roqh1-3* mutant background (Figure 2-10). The NPQ phenotype of *soq1 roqh1-3*: ROQH1 OE also reached wild-type levels (Figure 2-10C), confirming that overexpression of *ROQH1* prevents qH from occurring.

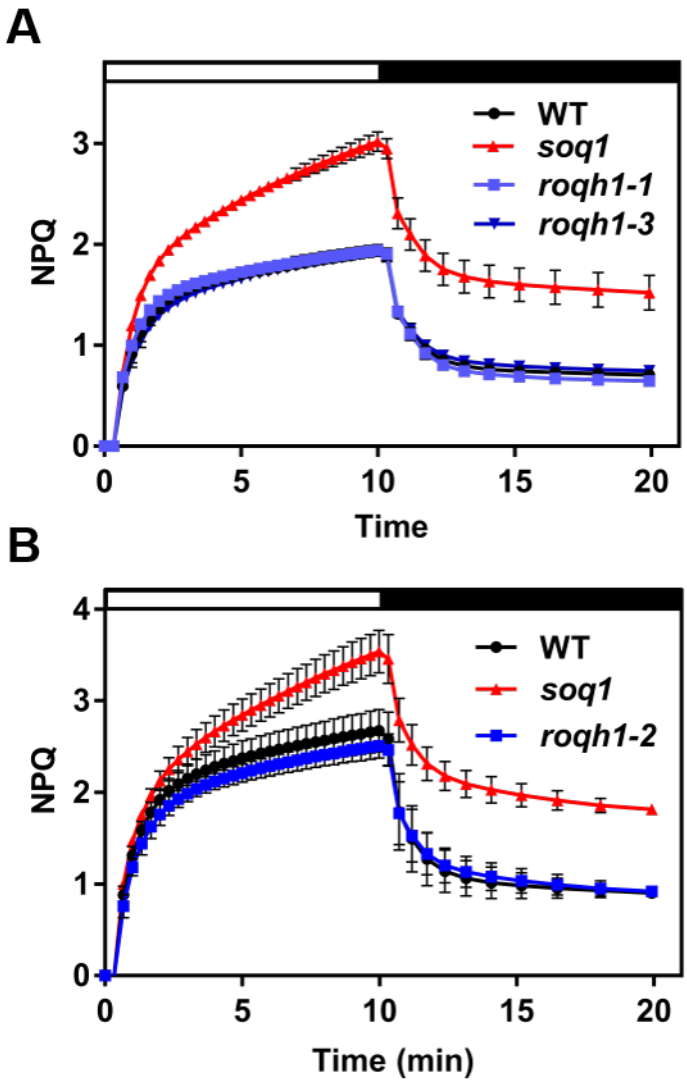

Figure 2-18. NPQ kinetics of *roqh1* single mutants are similar to wild type under standard conditions. Induction at 1,200 µmol photons m^{-2} s^{-1} (white bar) and relaxation in the dark (black bar). Data represent means ± SD, n=3. **(A)** NPQ kinetics of wild type, *soq1*, *roqh1-1*, and *roqh1-3*. **(B)** NPQ kinetics of wild type, *soq1*, and *roqh1-2*.

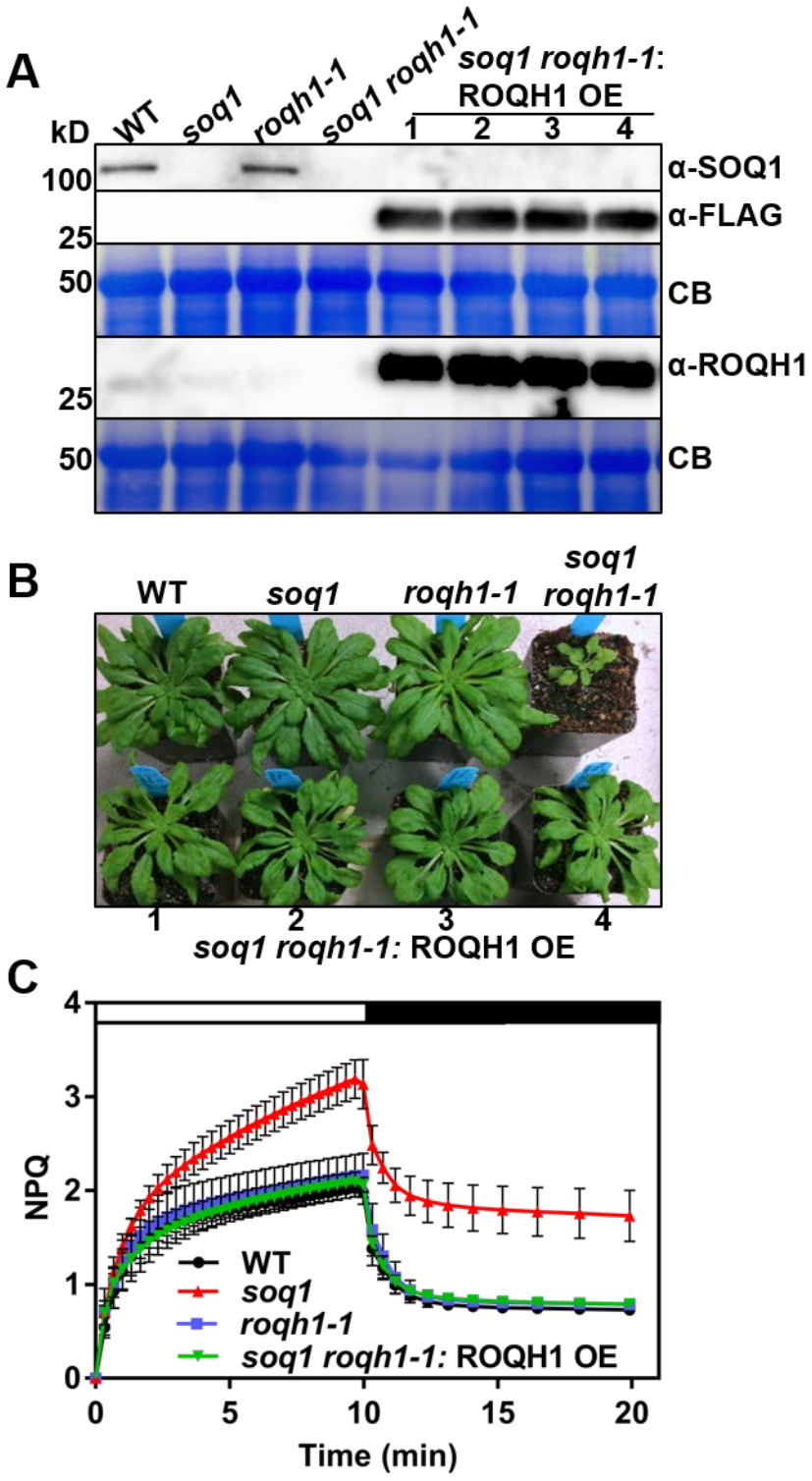

Figure 2-19. Overexpression of ROQH1 prevents qH from occurring. Plants 1-4 of *soq1 roqh1-1:* ROQH1 OE corresponds to T2 individuals from independent line 1. Additional independent lines can be found in Supplemental Figure 6. **(A)** Isolated whole cells from 6.5-week-old plants grown under 120 µmol photons m^{-2} s^{-1}. Samples were loaded by same leaf area, separated by SDS-PAGE, and analyzed by immunodetection with antibodies against ROQH1, SOQ1 and FLAG. Coomassie blue (CB) is shown as loading control. Molecular masses (kD) are indicated according to the migration of Precision Plus Protein Standards markers from Bio-Rad. Wild type ROQH1 signal is weak to prevent overexposure of *soq1 roqh1-1*: ROQH1 OE. **(B)** Images of 7-week-old plants grown under 120 µmol photons m^{-2} s^{-1}. **(C)** NPQ kinetics of wild type, *soq1*, *roqh1-1* and *soq1 roqh1-1:* ROQH1 OE. Induction at 1,200 µmol photons m^{-2} s^{-1} (white bar) and relaxation in the dark (black bar). Data represent means ± SD, n = 3. The difference in NPQ induction and relaxation between wild type and *soq1* is due to qH.

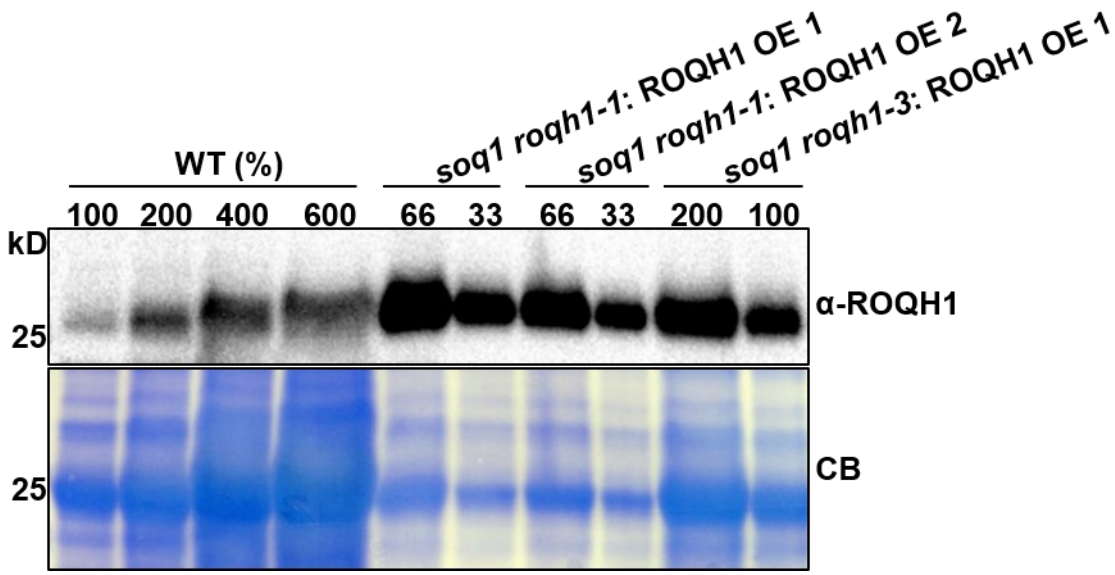

Figure 2-20. ROQH1 overexpression level is more than 10 times that of wild type. Plants of *soq1 roqh1-1*: ROQH1 OE 1 corresponds to individuals from T2-T1-4, plants of *soq1 roqh1-1*: ROQH1 OE 2 corresponds to individuals from T2-T1-2, and plants of *soq1 roqh1-3*: ROQH1 OE 1 corresponds to T2-T1-3. Isolated thylakoids from 6-week-old plants grown under 150 µmol photons m^{-2} s^{-1}. Samples were loaded by total chlorophyll content (100% = 3 µg total chlorophyll), separated by SDS-PAGE, and analyzed by immunodetection with an antibody against ROQH1. Coomassie blue (CB) is shown as a loading control. Molecular masses (kD) are indicated according to the migration of Precision Plus Protein Standards markers from Bio-Rad. Expression level of ROQH1 in *soq1 roqh1-1*: ROQH1 OE 1, *soq1 roqh1-1*: ROQH1 OE 2, and *soq1 roqh1-3*: ROQH1 OE 1 is more than 10 times that of wild type.

2.4.8 ROQH1 is required for relaxation of qH

Induction of qH in wild type has been observed under cold and high light conditions[36]. Although *roqh1* displayed wild-type NPQ kinetics under standard growth conditions (Figure 2-18), we hypothesized that *roqh1* may be affected in qH induction and/or relaxation under stress conditions. To test qH kinetics in *roqh1*, NPQ induction was monitored as a quenching of F_m during a cold and high light treatment of 6°C and 1,600 µmol photons m^{-2} s^{-1} (Figure 2-21 and 2-22). After 5 h of cold and high light, SOQ1 protein levels had decreased (Figure 2-23) and *soq1, roqh1-1*, and *roqh1-3* displayed elevated NPQ levels of 11, 6, and 8, respectively. In contrast, *soq1 roqh1-1*: ROQH1 OE and *soq1 roqh1-1 lcnp* displayed decreased NPQ levels of 3.5 and 3, respectively, compared to wild type (Figure 2-21B). This altered NPQ was similarly observed through fluorescence lifetime measurements of leaves before and after cold and high light (Figure 2-23 and Table 2-03). Before cold and high light, the dark-adapted fluorescence lifetimes were similar among genotypes with the exception that *soq1 roqh1 lcnp* was slightly shorter (Figure 2-23A). After cold and high light, the average fluorescence lifetimes of *soq1* and *roqh1* were shorter than wild type while the lifetimes of *soq1 roqh1-1*: ROQH1 OE and *soq1 roqh1-1 lcnp* were longer than wild type (Figure 2-23A). The shorter lifetime indicated that a quenching site was present and closer than the energy transfer route to the PSII reaction center. From the average fluorescence lifetimes, NPQτ was calculated (Figure 23B) and each genotype displayed values similarly found by fluorescence yield measurements in Figure 2-21. The additional NPQ observed in the *soq1* and

roqh1 mutants was attributed to qH rather than qI or qZ as D1 protein levels and zeaxanthin accumulation were comparable to wild type throughout the time course (Figure 2-20C, Figure 2-24, and Figure 2-25). After quenching was induced by cold and high light, NPQ relaxation was monitored throughout recovery under standard growth conditions. After 28 h of recovery, NPQ in *soq1* had relaxed to nearly wild-type levels, while the *roqh1* mutants remained quenched, as indicated by their lower F_m and higher NPQ values (Figure 2-21A, B). Notably, zeaxanthin levels were similarly close to zero in all lines after recovery (Figure 2-21C). The impaired qH relaxation in the *roqh1* mutants indicated that ROQH1 is required for relaxing qH.

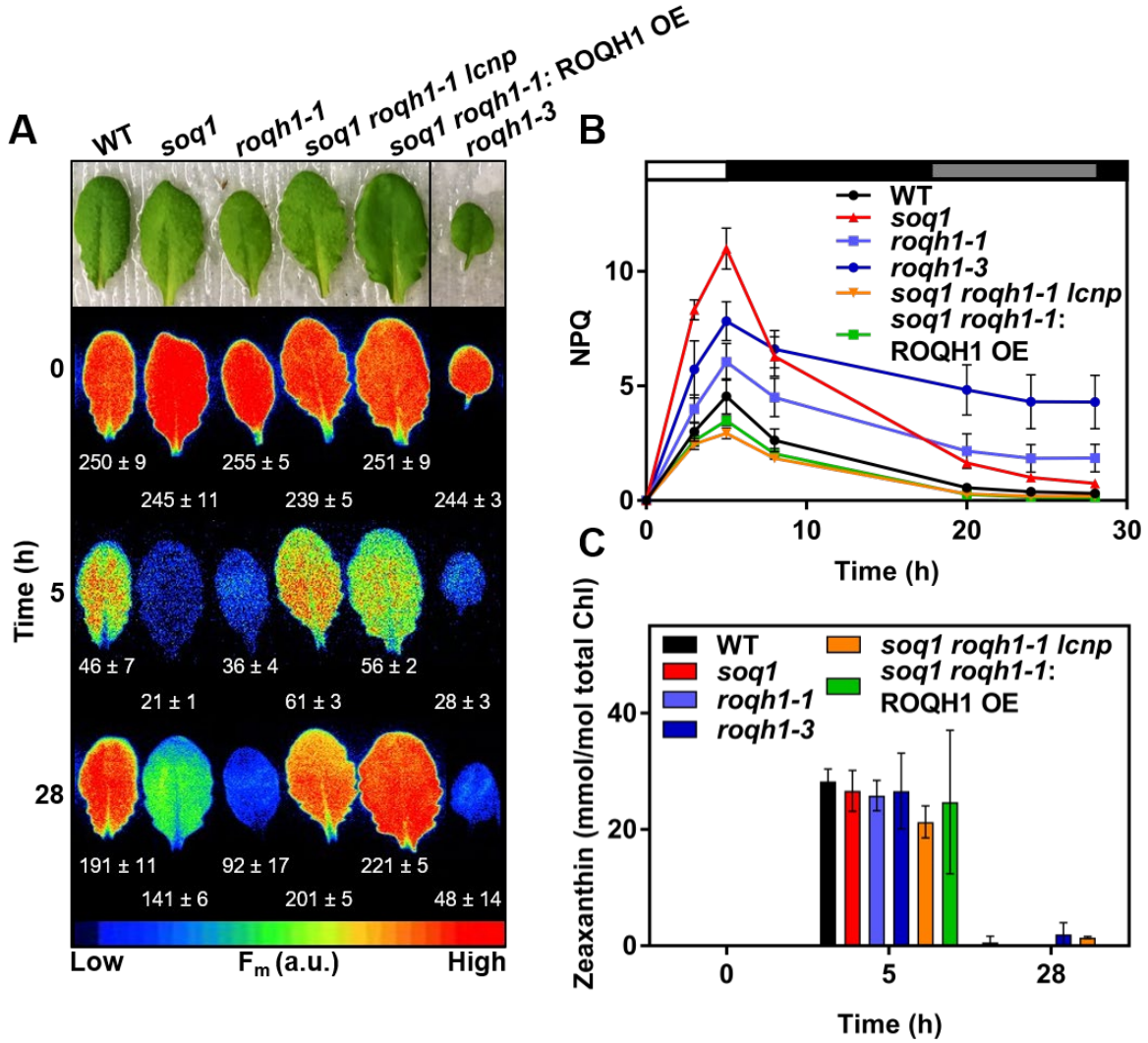

Figure 2-21. ROQH1 is required for relaxation of qH. Detached leaves from 5-week-old plants grown under standard light conditions (150 µmol photons m^{-2} s^{-1}, 21°C) were subjected to a cold and high light treatment (white bar) of 6°C and 1,600 µmol photons m^{-2} s^{-1} for 5 h, and a recovery treatment of 150 µmol photons m^{-2} s^{-1} and a 10 h/14 h day/night cycle at 21°C (black, night period and grey, day period bars) for 28 h. **(A)** Images of detached leaves and false-colored images of maximum fluorescence (F_m) of detached leaves before the cold and high light treatment (Time 0), after the cold and high light treatment (Time 5) and after a recovery period (Time 28). Leaves were dark-adapted for 10 minutes before fluorescence measurement to relax qE. Additional leaves between *soq1 roqh1-1:* ROQH1 OE and *roqh1-3* were cropped out for simplicity, and an

uncropped image can be found in Figure 2-20. Average F_m values ± SD are given with n = 4-8 individuals from two independent experiments performed within two days of each other using same batch of plants never exposed to treatment. **(B)** NPQ kinetics calculated as (F_m Time 0 - F_m')/F_m' throughout the cold, high light and recovery treatment indicated in (A). Data represent means ± SD, n = 4-8 individuals. The difference in NPQ induction and relaxation between wild type and *soq1 roqh1 lcnp*, and between wild type and *soq1* is due to qH. **(C)** Zeaxanthin levels before the cold and high light treatment (Time 0), after the cold and high light treatment (Time 5) and after a recovery period (Time 28). Tukey's multiple comparison test shows no significant difference in zeaxanthin levels among wild type and mutants before or after treatments. Data represent means ± SD, n = 3 individuals.

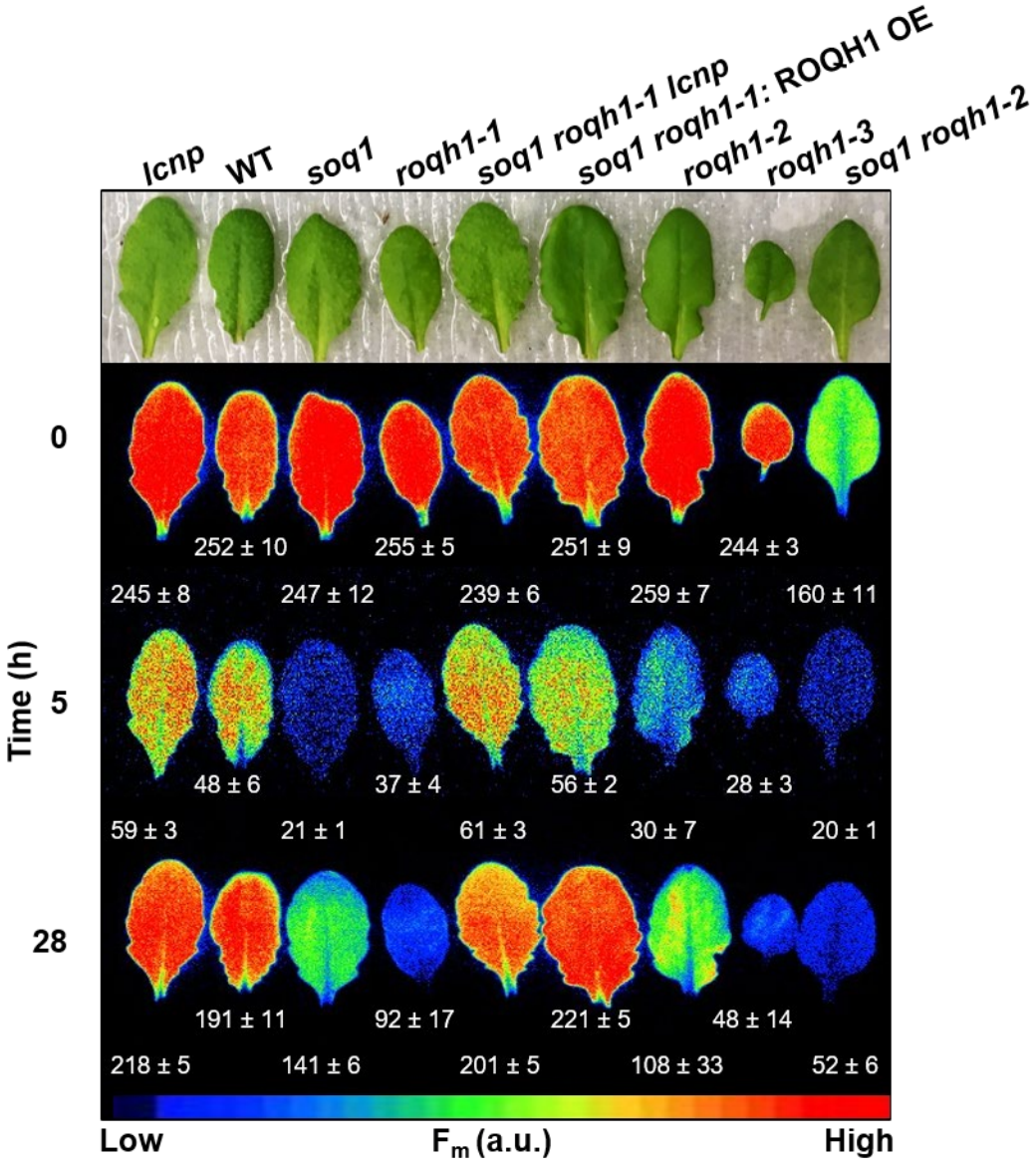

Figure 2-22. ROQH1 is required for relaxation of qH. Uncropped images of detached leaves and false-colored images of maximum fluorescence (F_m) of detached leaves from 5-week-old plants grown under 150 µmol photons m^{-2} s^{-1} and 21°C, subjected to a cold and high light treatment of 6°C and 1,600 µmol photons m^{-2} s^{-1} for 5 h, and a recovery treatment of 150 µmol photons m^{-2} s^{-1} and a 10 h/14 h day/night cycle at 21°C for 28 h. Leaves were dark-adapted for 10 min before

fluorescence measurement to relax qE. Average F_m values ± SD are given with n=6 (for *roqh1-3*, n=4) individuals from two independent experiments performed within two days of each other using same batch of plants never exposed to treatment.

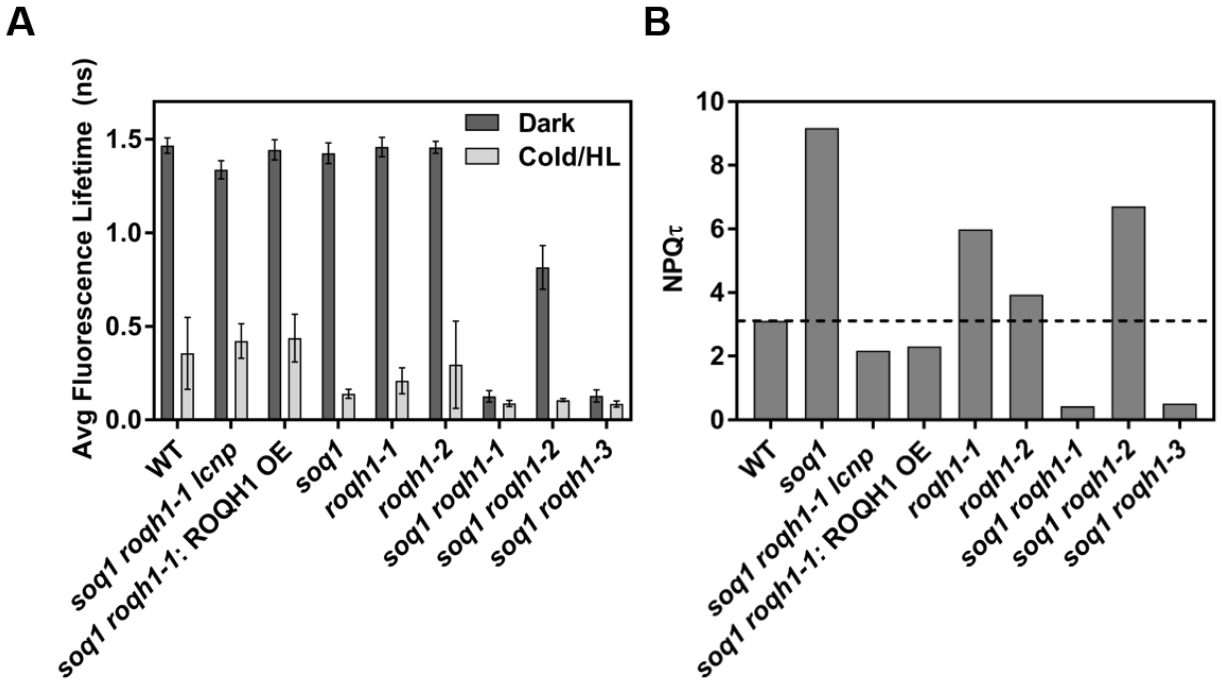

Figure 2-23. Average fluorescence lifetimes before and after cold and high light. **(A)** Average fluorescence lifetimes determined by time-correlated single photon counting (TCSPC) before and after a 6 h cold and high light treatment (6°C and 1,600 µmol photons m^{-2} s^{-1}). Plants were dark adapted for 10 min prior to measurement on individual leaves. Data represents mean ± SD, n = 20-24. **(B)** NPQτ calculated as $\tau_{dark} - \tau_{cold/HL} / \tau_{cold/HL}$.

Genotype	Avg Dark Lifetime (ns) ± SD	Avg Cold HL Lifetime (ns) ± SD	Calculated NPQτ
WT	1.465 ± 0.041	0.356 ± 0.192	3.11
roqh1-1	1.458 ± 0.052	0.209 ± 0.069	5.99
roqh1-2	1.456 ± 0.032	0.295 ± 0.233	3.94
roqh1-3	N/A (bolted)	N/A (bolted)	N/A (bolted)
ROQH1 OE	1.443 ± 0.054	0.437 ± 0.127	2.30
soq1	1.424 ± 0.055	0.140 ± 0.024	9.17
soq1 roqh1-1	0.126 ± 0.031	0.088 ± 0.016	0.43
soq1 roqh1-2	0.815 ± 0.117	0.106 ± 0.008	6.71
soq1 roqh1-3	0.128 ± 0.033	0.085 ± 0.016	0.51
soq1 roqh1 lcnp	1.336 ± 0.049	0.422 ± 0.092	2.17

Table 2-03. Average fluorescence lifetimes before and after cold and high light. Average fluorescence lifetimes and calculated NPQτ determined by TCSPC.

2.4.9 qH is independent of photoinhibition

The qH component is induced under cold and high light conditions which similarly induce photoinhibitory quenching. To confirm that qH is independent of photoinhibtion we investigated D1 protein abundance in wild type, *soq1*, *roqh1-1*, and *lcnp* throughout qH induction and relaxation. After a cold and high light treatment, the D1 protein level did not differ between wild type and the mutants (Figure 2-23). Protein levels remained similar after a relaxation period with the exception that the *soq1* mutant had slightly elevated D1 levels and *roqh1-1* had slightly decreased D1 levels (Figure 2-23). To further confirm that qH was independent of photoinhibition, we examined D1 protein levels in the presence and absence of the translation inhibitor lincomycin. Leaves from wild type, *soq1*, *roqh1-1*, *roqh1-3*, *soq1 roqh1-1*, and *soq1 roqh1-3* were floated on either water or 1 mM lincomycin overnight and then subjected to 90 min of high light at 1,000 µmol photons m^{-2} s^{-1}, followed by a recovery treatment of 4 h at 25 µmol photons m^{-2} s^{-1}. Throughout the treatment, the efficiency of PSII (F_v/F_m) of *roqh1* single mutants did not differ from the wild type with or without lincomycin (Figure 2-24A, B). The F_v/F_m of *soq1* decreased further and recovered slower than wild type after the light treatment, however, this decrease in F_v/F_m was due to a decrease in F_m and not an increase in F_o as usually observed in other photoinhibition mutants. In addition, this difference was independent of lincomycin treatment, and therefore D1 turnover (Figure 2-24B). The constitutive qH and dark-adapted F_m in the double mutants was so severe that the F_v/F_m neared the detection limit of the instrument during a high light treatment and was difficult to monitor and distinguish from background signal (Figure 2-24C, D). We then examined D1 protein levels before and after the high light treatment as well as after the recovery treatment in the presence and absence of lincomycin. We observed that *soq1* D1 protein levels remained slightly elevated after high light and similar to wild type after recovery (Figure 2-24E). While D1 levels in *roqh1-1* decreased slightly after recovery, the D1 levels of *roqh1-3* remained unchanged compared to wild type at each timepoint. Despite the low F_v/F_m values in *soq1 roqh1*, the D1 protein levels of *soq1 roqh1* were higher than wild-type at all timepoints, (Figure 2-25E) confirming that constitutive qH is not due to the lack of D1.

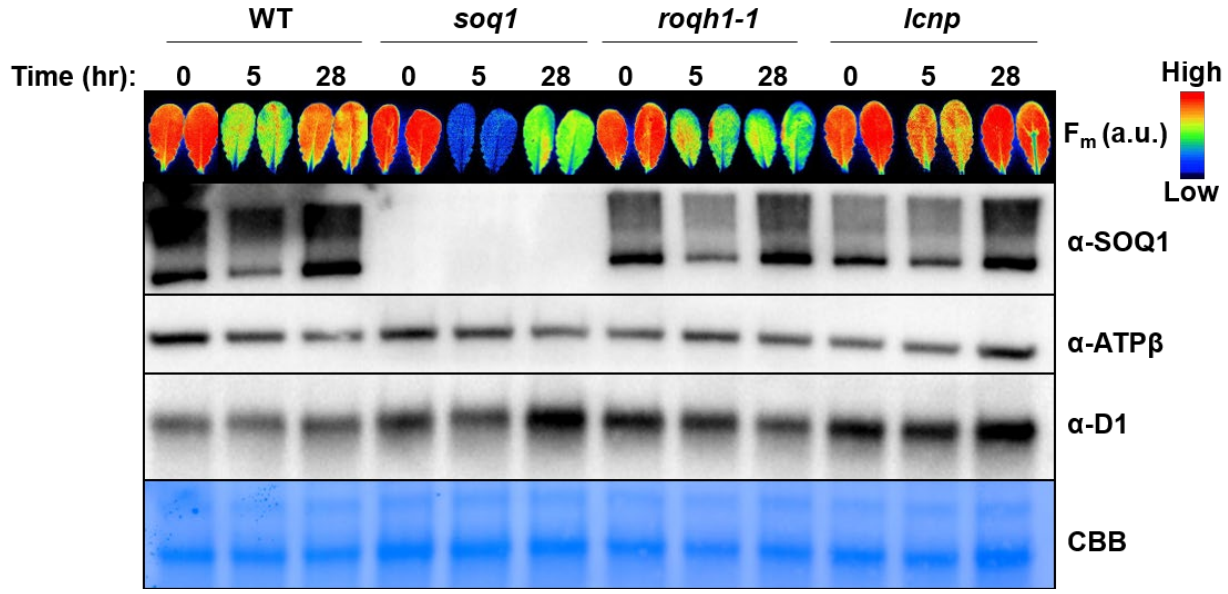

Figure 2-24. Accumulation of SOQ1 and D1 proteins throughout qH induction and recovery. SOQ1 and D1 protein levels before and after a 5 h cold and high light treatment and after a recovery treatment in wild type, *soq1*, *roqh1-1,* and *lcnp*. Proteins were extracted from isolated thylakoids

at similar chlorophyll concentrations, precipitated with methanol and chloroform, and separated by SDS-PAGE. ATPβ and CBB are shown as loading controls.

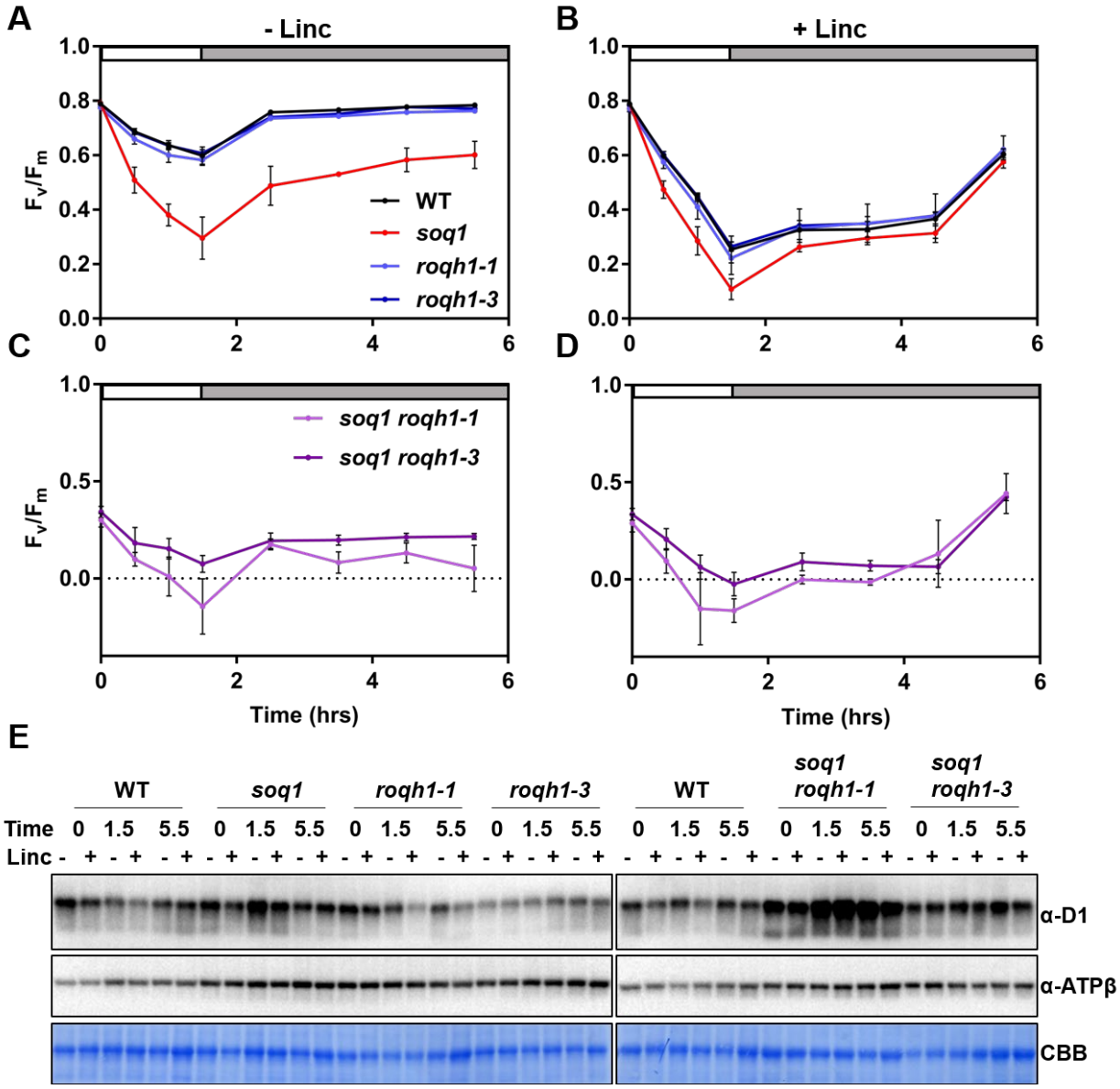

Figure 2-25. PSII efficiency and D1 protein levels are unaffected by ROQH1. Efficiency of PSII (F_v/F_m) was monitored throughout a high light treatment of 1,000 µmol photons m^{-2} s^{-1}, 21°C and a recovery treatment of 25 µmol photons m^{-2} s^{-1}, 21°C. Average F_v/F_m values ± SD are given with n = 4-12 individuals. After 90 min of high light, the F_v/F_m of *soq1 roqh1-1* neared the detection limit of the instrument and we could not obtain accurate values. (A) and (C) Leaves were floated on water and subjected to high light for 1.5 h. (B) and (D) Leaves were floated on 1 mM lincomycin and subjected to high light for 1.5 h (E) D1 protein levels before and after a 1.5 hr high light and 4 hr recovery treatment. Proteins were extracted from thylakoids isolated from leaves floating on water or 1mM lincomycin, precipitated with methanol and chloroform, and separated by SDS-PAGE. ATPβ and CBB are shown as loading controls.

2.5 Discussion

2.5.1 Constitutive qH causes a low-light acclimated phenotype

Both *soq1 roqh1-1* and *soq1 roqh1-3* (collectively termed here as *soq1 roqh1*) are constitutively quenched (Figure 2-09) and display features typically found in shade and low-light-acclimated plants, including thinner leaves, a lower chlorophyll *a*/*b* ratio, and more thylakoid stacking compared to wild type (Figure 2-12 and Figure 2-14). Under standard growth conditions, leaves and vasculature from *soq1 roqh1* are respectively 70 µm and 150 µm thinner than wild type due to a decrease in cell size and number (Figure 2-14A, B). This observation is consistent with shade and low-light-acclimated plants, where photosynthetically inactive leaf material such as the cell wall, epidermis, and vascular tissue is limited to maximize photosynthetically active tissue to total plant mass[64,65]. Compared to the wild type, *soq1 roqh1* contains more antenna-associated pigments (chlorophyll *b* and neoxanthin) and fewer photosystem-associated pigments (chlorophyll *a* and *β*-carotene) per mole of total chlorophyll (Figure 2-12A), indicating that *soq1 roqh1* may have more antenna complexes associated with fewer reaction centers[66]. An increase in antenna size could allow for an increased light-harvesting capacity and has been observed in wild-type *Arabidopsis* under limiting light conditions[67,68]. In addition, the thylakoid architecture of *soq1 roqh1-1* is highly stacked with limited stroma lamellae membrane (Figure 2-14B, C). Grana stacking also increases the functional antenna size by forming semi-crystalline arrays of PSII-LHCII supercomplexes[69,70]. This organization enables excitation energy to flow between membranes until an open PSII reaction center is found[48]. Similar adjustments to grana organization and structure have been observed in shade obligate species and *Arabidopsis* plants transferred from high to low light intensities[70,71]. Taken together, these similarities between *soq1 roqh1* and low-light-acclimated plants suggest that under standard growth conditions, the *soq1 roqh1* mutants are light limited. This is confirmed under higher light intensities, where the growth of *soq1 roqh1* improves in comparison to low light (Figure 2-12B, C). The possibility remains that enlarged grana are a direct consequence of the *soq1 roqh1* mutations, which might promote energy dissipation through PSII-PSI spillover, and this merits future investigation.

Light intensity and quality are perceived in higher plants by phytochromes, cryptochromes, phototropins, and UV RESISTANCE LOCUS 8 (UVR8)[72]. These photoreceptors, particularly PhyB and Cry1, elicit signaling networks to control the shade avoidance syndrome and low light acclimation in germinating and growing seedlings[72,73]. However, once the chloroplast and photosynthetic apparatus is fully developed, chloroplast redox signals act above cytosolic photoreceptors to control acclimation[74,75]. This notion is shown through photoreceptor mutants that retain their ability to acclimate to various light intensities[76]. Thus, it is reasonable to assume that the light-limited phenotype observed in *soq1 roqh1* is due to redox signals from photosynthetic starvation, rather than a defect in light perception or signaling. Photosynthetic starvation occurs because the constitutive qH in *soq1 roqh1* dissipates the majority of light energy absorbed, leaving little for photochemistry. This hypothesis finds confirmation through *soq1 roqh1-1 lcnp*, which lacks qH and recovers normal growth, pigment composition, and leaf thickness (Figure 2-14A, B and Figure 2-16) A similar response has been observed in the *Arabidopsis* mutants lacking either all minor light-harvesting complexes (NoM)[77] or the chloroplast NADPH thioredoxin reductase C (NTRC)[78]. Both NoM and *ntrc* display moderate light starvation phenotypes, either due to reduced excitation trapping in PSII[77] or enhanced qE[78]. In the case of NoM, the mutant over-accumulates major LHCIIs as a compensation mechanism, similar to how *soq1 roqh1* over-accumulates chlorophyll *b* and neoxanthin. In the case of the *ntrc* mutant, when combined with mutation

affecting PsbS (*ntrc npq4*), qE is eliminated and the double mutant shows improved growth[78], similar to *soq1 roqh1-1 lcnp*. The *ntrc* mutant further demonstrates the physiological consequences of overprotection by enhanced NPQ.

2.5.2 ROQH1 is annotated as an atypical short chain dehydrogenase/reductase

Short chain dehydrogenases/reductases (SDR)s form a large NAD(P)H-dependent oxidoreductase protein superfamily. Members of this superfamily are found in all domains of life and perform diverse functions in lipid, amino acid, carbohydrate, steroid, and xenobiotic metabolism as well as in redox sensing[79,80]. SDRs are grouped by their conserved Rossmann-fold consisting of a central β-sheet with two or three α-helices flanking each side[80]. Within the Rossmann-fold, classical SDRs contain a dinucleotide binding motif (TGXXX[AG]XG) and a tetrad of catalytically active residues (D-S-YXXXK), yet sequence conservation is otherwise quite low[80,81]. In fact, atypical SDRs are the least conserved SDR family and may contain sequence modifications to these domains[82]. Such is the case with ROQH1, which contains a cofactor binding motif similar to the extended SDR subfamily ([ST]GGXGXXG)[80] and a valine instead of a tyrosine in the predicted catalytic tetrad (D-S-VXXXK) (Figure 2-06A and Figure 2-25). Typically, enzymatic function relies on the tyrosine to donate or remove protons to or from the substrate[80], thus ROQH1 and other atypical SDRs are currently not known to have catalytic activity[82]. Of the 178 SDRs in *Arabidopsis*, 8 are classified as atypical[81]. Among these eight are the chloroplast stem loop-binding proteins 41a (CSP41a), CSP41b, high chlorophyll fluorescence173 (HCF173) and HCF244, all of which participate in RNA metabolism in the chloroplast[83,84]. In fungi, atypical SDRs also function as transcriptional regulators and/or redox sensors, as in the case of NmrA in *Aspergillus nidulans*[85]. NmrA preferentially binds oxidized dinucleotide cofactors to negatively regulate nitrogen metabolite repression[85,86]. These examples highlight the diverse roles of atypical SDRs, even though catalytic activity may be absent.

Point mutations within the Rossmann fold of ROQH1 affect its stability and/or degradation as well as its function to varying degrees. The ROQH1-Gly81Asp (*roqh1-1*) and ROQH1-Gly211Glu (*roqh1-2*) respectively accumulate 50% almost fully non-functional and 25% functional protein (Figures 2-06, Figure 2-09, and Figure 2-21). Indeed, mutation to the putative NAD(P)H binding motif (GGTGGVG to GDTGGVG) in *roqh1-1* results in a low fluorescence phenotype similar to the null allele, *roqh1-3*, when combined with the *soq1* mutation (Figure 2-09). This result suggests that ROQH1-Gly81Asp is non-functional, however after a 5 h cold and high light treatment, NPQ is slightly higher in *roqh1-3* compared to *roqh1-1* (Figure 2-21). This result indicates that the Gly81Asp mutation does not fully impair ROQH1 function. The point mutation in *roqh1-2* disrupts a well conserved glycine residue (Figure 2-26) that precedes the valine in the D-S-VXXXK motif (Figure 2-06A) and results in an intermediate lower F_m when combined with *soq1* (Figure 2-09). Low levels of ROQH1 protein are sufficient to partially turn off qH (the *soq1* SALK_001123 mutant displays an intermediate F_m phenotype, Figure 2-07). Furthermore, the wild-type NPQ phenotype of *soq1 roqh1:* ROQH1 OE lines revealed that ROQH1 function is dosage dependent at high concentrations (Figure 2-10 and Figure 2-19). The milder fluorescence phenotype, together with the dosage dependence of ROQH1 for relaxation of qH, suggests that the Gly211Glu mutation does not impair ROQH1 function and that the *soq1 roqh1-2* phenotype is due to decreased protein levels rather than modified function.

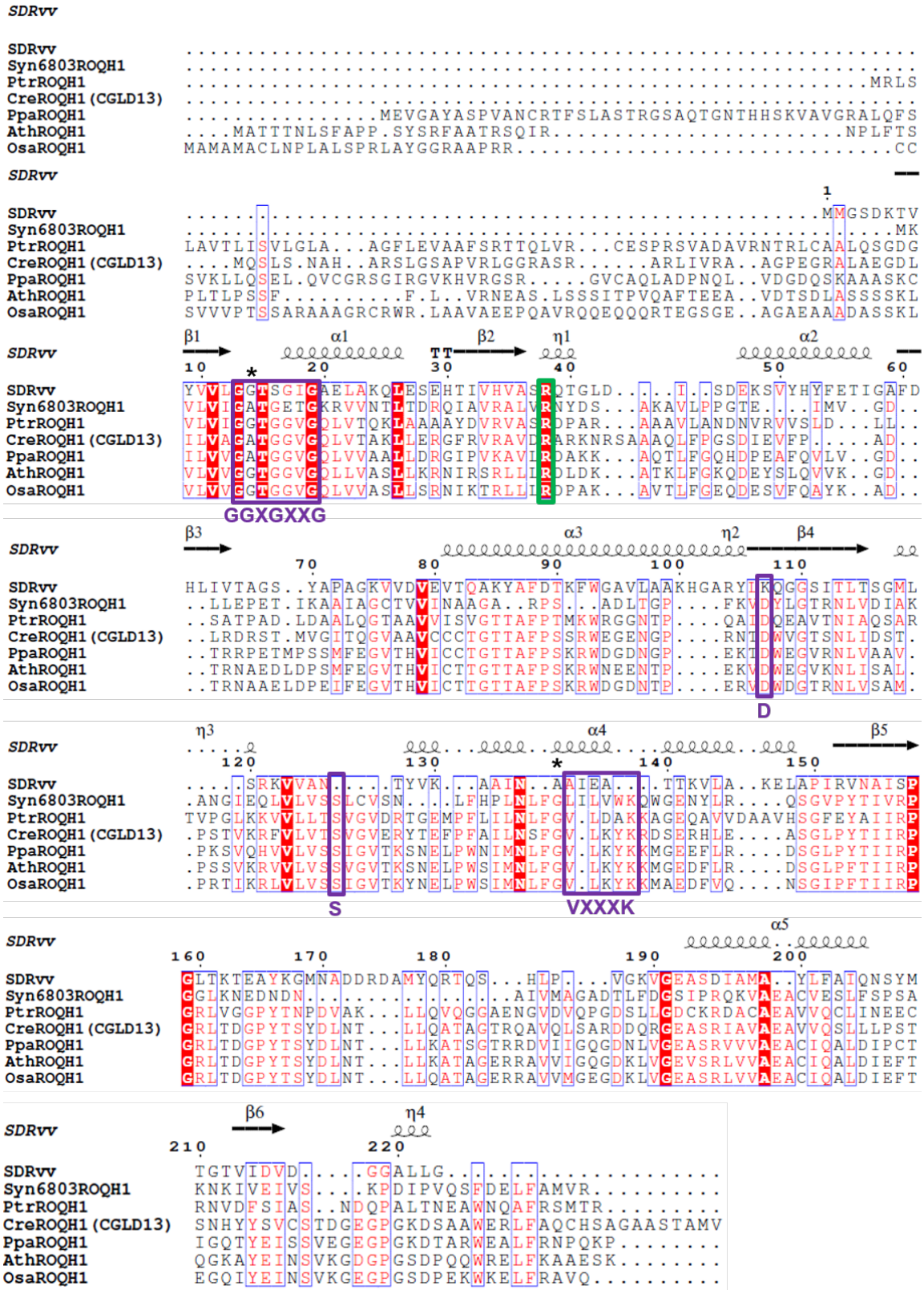

Figure 2-26. ROQH1 multiple sequence alignment. Multiple sequence alignment of ROQH1 homologues from *Oryza sativa* (Osa, Os03g23980), *Arabidopsis thaliana* (Ath, At4g31530), *Physcomitrella patens* (Ppa, Pp3c18_4890V3), *Chlamydomonas reinhardtii* (Cre,

Cre03.g181250), *Phaeodactylum tricornutum* (Ptr, Phatr1.50631), *Synechocystis* sp. PCC 6803 (Syn6803, sll1218), and an atypical SDR from *Vibrio vulnificus* (SDRvv, VVA1599). The amino acid sequences were aligned using Clustal Omega (https://www.ebi.ac.uk/Tools/msa/clustalo/) and secondary structures were defined from the PDB coordinate for the crystal structure of NADPH-complexed SDRvv (3UCF)[82] using ESPRIPT (http://espript.ibcp.fr/). The conserved Gly-rich cofactor-binding motif (GGXGXXG) and partial catalytic tetrad (D-S-VXXXK) is outlined in purple. The conserved arginine involved in cofactor preference is outlined in green. The *roqh1*-1 and *roqh1-2* point mutations are indicated by black asterisks (*).

2.5.3 ROQH1 is conserved in the green lineage and diatoms

ROQH1 is specific to plastid-containing organisms and is a member of the GreenCut2 inventory (named CGLD13 in *Chlamydomonas reinhardtii*)[87,88]. Among ROQH1 homologs, the predicted cofactor preference for $NADP^+$ over NAD^+ remains conserved. The cofactor preference is predicted by charged residues at the C-terminal end of the β_2-strand[89], and the conserved arginine residue in the β_2-strand of ROQH1 indicates a conserved preference for $NADP^+$ (Figure 2-26). In *Synechocystis* sp. PCC *6803*, the closest *ROQH1* gene homolog is *sll1218,* annotated as "hypothetical protein YCF39". *slr0399* encodes YCF39, a PSII assembly factor homolog of HCF244 in *Arabidopsis*[90,91]. YCF39 forms a complex with terminal chlorophyll synthase G (ChlG) and high-light-inducible proteins, HliC and HliD, to provide safe delivery of chlorophyll to nascent PSII[91]. During PSII assembly, energy is dissipated from chlorophyll *a* via direct energy transfer to *β*-carotene within HliD[92,93]. It is proposed that YCF39 influences the binding pocket of β-carotene within HliD, allowing this quenching reaction to occur[92]. Perhaps ROQH1 functions through a similar mechanism as YCF39, but to promote relaxation of quenching in *Arabidopsis*.

The *SOQ1* and *LCNP* genes are conserved among all land plants, yet they do not belong to the GreenCut2 inventory. In the case of *SOQ1*, this may be due to its multi-domain protein structure. *SOQ1* homologs have been identified in *Chlamydomonas* and *Synechocystis* sp. PCC *6803*, but as two separate proteins that contain either the HAD domain or the NHL and Trx-like domains. In *Arabidopsis*, it was previously shown that alternative splicing occurs, producing truncated transcripts with only the HAD domain 70% of the time instead of the full-length protein[94]. This supports the hypothesis that the multi-domain structure of SOQ1 in *Arabidopsis* is a recent protein fusion event and the HAD domain functions independently of the other domains[95]. Within the lipocalin superfamily, members show high structural similarity but poor sequence conservation[96], thus *LCNP* gene homologs remain difficult to identify. Therefore, further investigation is required to determine whether qH is broadly conserved across the green lineage or restricted to land plants.

2.5.4 ROQH1 functions in qH relaxation

The low F_o and F_m values in dark-acclimated *soq1 roqh1* are due to constitutive qH, as quenching requires the LCNP protein[36]. The triple mutant, *soq1 roqh1-1 lcnp*, indeed rescues fluorescence values to a similar level as *soq1 lcnp* (Figure 2-16). The combined effects of the *soq1* and *roqh1* mutations indicate that SOQ1 and ROQH1 have independent functions in qH. This notion becomes clear after a cold and high light treatment, where *soq1* and *roqh1* exhibit different qH induction and relaxation kinetics (Figure 2-21). Under cold and high light, *roqh1* displays elevated levels of qH but to a lesser extent than *soq1*. Once returned to standard growth conditions, the additional qH relaxes normally in *soq1* but fails to do so in *roqh1*. This inhibited relaxation explains the additional NPQ induced in *roqh1*. These results demonstrate that SOQ1 functions in

inhibiting qH induction while ROQH1 functions in promoting qH relaxation (see working model, Figure 2-27). Interestingly, by overexpressing *ROQH1* in a *soq1 roqh1* background, the NPQ induction and relaxation kinetics under standard conditions resemble those of wild type rather than *soq1* (Figure 2-10 and Figure 2-19). We hypothesize that the high levels of ROQH1 in the *soq1 roqh1*: ROQH1 OE lines may have inhibited qH by relaxing quenching sites faster than they are produced, even in the absence of SOQ1. Consistent with this hypothesis is the low NPQ in *soq1 roqh1-1*: ROQH1 OE under cold and high light compared to wild type (Figure 2-21). These results suggest that the functions of ROQH1 and LCNP are antagonistic and dosage dependent (Figure 2-27). This concept is analogous to the photoprotective NPQ mechanism in cyanobacteria involving the orange carotenoid protein (OCP) and the fluorescence recovery protein (FRP) (for review see ref[97]). In this photoprotective cycle, quenching is induced by OCP upon photoconversion from the inactive orange form to the active red form[98]. Under low irradiance, FRP is required for OCP inactivation and removal from the phycobilisome[99,100]. Without this recovery factor, quenching in the *frp* mutant fails to relax, similarly to *roqh1*, while FRP overexpression minimizes quenching[99], similarly to ROQH1 overexpression. However, FRP-mediated fluorescence recovery is achieved through a direct interaction between OCP and FRP[99,101], and in the case of qH, ROQH1 and LCNP are physically separated by a thylakoid membrane. Thus, any antagonistic interaction between ROQH1 and LCNP is probably indirect. Future experiments to determine the exact interacting partners and/or substrates of ROQH1, SOQ1 and LCNP will provide further insights into the overall quenching mechanism and its regulation.

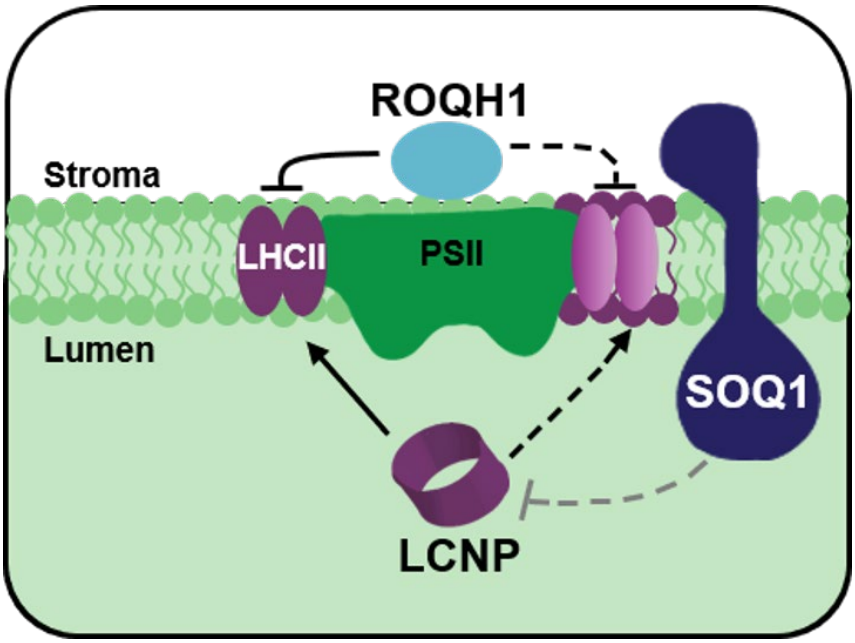

Figure 2-27. ROQH1 is required to turn off qH. Under non-stress conditions, SOQ1 inhibits LCNP activity. Under stress conditions, such as cold and high light, SOQ1 inhibition is relieved (grey dashed line) and LCNP is active. Quenching sites indicated by purple color are produced in the peripheral antenna directly mediated by LCNP (solid arrow) or indirectly (dashed arrow) through LCNP modification of LHCII hydrophobic environment. ROQH1 recycle these quenching sites back to light harvesting sites either directly by acting at the antenna (solid line) or indirectly through modification of LHCII hydrophobic environment (dashed line). Adapted from ref[16].

Chapter 3: The site of qH quenching is the LHCII trimer

Preface

Alizée Malnoë and Michelle Leuenberger contributed to work in this chapter. Alizée Malnoë aided in the OJIP transient measurements, and Michelle Leuenberger performed the TCSPC measurements.

3.1 Introduction

The possible quenching sites that result in thermal dissipation in plants (presented in Chapter 1.3) are within the PSII core or the peripheral light-harvesting antenna. The PSII core is composed of the P680 reaction center and the proximal light-harvesting antenna proteins, CP43 and CP47[49,102]. These contain chlorophyll *a* molecules that accept and transfer energy from the peripheral antenna to the reaction center[102]. The peripheral antenna system associated with PSII is composed of a variety of complexes made up of light-harvesting proteins that bind chlorophyll and carotenoid pigments[103,104]. The complexes are divided into major and minor components. The major antenna complex is composed of three Lhcb proteins, Lhcb1, 2, 3 or LHCII, that form hetero- and homo-trimers and associate with varying degrees to PSII[49,104]. The minor antenna complex consists of three monomeric Lhcb proteins, Lhcb 4, 5, and 6 or CP29, 26, and 24, respectively. The pigments associated with both the major and minor antenna complex include the chlorophylls *a* and *b*, and carotenoids lutein, violaxanthin (and zeaxanthin), and neoxanthin[48,104].

The focus of this chapter is to investigate the site of qH quenching using various fluorescence techniques including pulse amplitude-modulated (PAM) fluorometry (presented in Chapter 1.2), OJIP fluorescence transients, low temperature (77K) spectroscopy, and time-resolved fluorescence spectroscopy using time-correlated single photon counting (TCSPC). While PAM fluorometry can assess the maximum chlorophyll fluorescence (F_m) of a dark-adapted leaf, the OJIP transients can examine the fast kinetics and intermediate phases during the fluorescence rise to F_m, which occur under 2 s within PSII[105]. The first phase of the OJIP transient is from the origin, similarly called F_o, to the J peak. It occurs within 2 ms and is due to the reduction of the Q_A site of plastoquinone, the primary electron acceptor in PSII[105]. The second intermediate phase is the I peak and occurs within 30 ms due to the reduction of the Q_B site of PSII[106]. While the I to P phase is still under debate, the final peak P corresponds to a fully reduced plastoquinone pool and closed PSII reaction centers. In the presence of DCMU, the J and I peaks are no longer present as the inhibitor competitively binds to the Q_B site of PSII and artificially closes the reaction center[105]. In this chapter, the OJIP transient of *soq1 roqh1* is explored to determine whether PSII reaction centers are closed in the mutant.

PAM fluorometry and OJIP transients can provide in-depth details of energy and electron transfer within PSII, yet they cannot provide insight into PSI. This is because under *in vivo* conditions, only 10% of the total chlorophyll fluorescence emissions comes from PSI, and this cannot be distinguished from overlapping PSII-associated fluorescence due to intramolecular vibrations and reabsorption[107]. Therefore, 77K spectroscopy is a useful technique that provides fluorescence information from PSII and PSI. At 77K, electron transfer and intramolecular vibrations are inhibited, allowing distinguishable fluorescence emissions from both photosystems. Here, 77K is used to determine which specific component within PSII-LHCII is the site of qH quenching. Similarly, TCSPC measurements at different emission and excitation wavelengths were used to determine the fluorescence lifetimes of chlorophylls associated with different photosynthetic complexes. The shorter the lifetime, the closer the chlorophyll molecule is to a

quencher, whether that be the reaction center or a NPQ site. Paired together, these two techniques reveal that the LHCII trimer is the site of quenching in *soq1 roqh1*.

3.2 Materials and Methods

3.2.1 OJIP Transient Measurements

OJIP measurements were performed using a Joliot Type Spectrophotometer using the following script: "4(5ms D) 300µs E 10(30µs D) 10(60µs D) {100µs, 30, 0.255s D} 100µs F" where D is the detector and E is the saturating actinic light on and F is saturating actinic light off. The actinic light was set to 3,600 µmol photons m^{-2} s^{-1} and leaves were dark adapted for 5 min before running the script. Leaves were infiltrated with 1 mM hydroxylamine to prevent charge recombination and 20 µM 3-(3,4-dichlorophenyl)-1,1-dimethylurea (DCMU) to block electron transfer from the Q_A site to the Q_B site of PSII.

3.2.2 77K Fluorescence Spectroscopy

Low temperature fluorescence was performed using the Fluoromax instrument and FluorEssence software from Horiba Scientific. Samples were prepared by either cutting whole leaf tissue into 0.8 x 1.3 cm rectangles or isolating intact chloroplasts and placing them into a capillary tube at a concentration of 20 µg/mL total chlorophyll. For whole leaf tissue under standard conditions, leaves were treated with far red light for 2 h to induce state 1, where all LHCII antenna complexes are associated with PSII. For isolated chloroplasts, 1 µM of recombinant GFP was added as an internal control according to ref[108]. Capillary tubes were slowly frozen in liquid nitrogen and placed in a dewar containing liquid nitrogen on the Fluoromax platform. Excitation wavelength was 435 nm with a slit width of 2 nm and the emission spectrum was recorded between 600-800 nm with a slit width of 2 nm and an integration time of 0.3 ms. For data analysis, the lowest baseline fluorescence was subtracted from each value, and each replicate was averaged and normalized to either 730 nm or the GFP signal at 513 nm.

3.2.3 TCSPC Measurements

TCSPC measurements were performed by Michelle Leuenberger, as described here and in ref[109]. Each sample set was made up of 10 whole leaves from each respective genotype. Before TCSPC snapshot experiments, plants were dark-acclimated for 30 min, and no plant was dark-acclimated more than once during any 1.5-h period. Leaves were removed from dark-acclimated plants immediately before TCSPC experiments and placed in a home-built holder. A 532-nm Coherent Verdi G10 diode laser pumped an ultrafast Ti:Sapph Coherent Mira 900f oscillator with the birefringence adjusted, such that the center wavelength was either at 840 nm or 896 nm with an FWHM of ~9 nm. The 840- or 896-nm output pulses from the Mira were then frequency doubled to 420 nm or 447 nm respectively, using a beta barium borate crystal to excite the Soret band of chlorophyll *a* or chlorophyll *b*. The portion of the beam that reached the sample was incident on the leaf at a 70° angle to the adaxial side of the leaf. The average power of the laser at the sample was 1.75 mW, corresponding to about 1,800 µmol photons m^{-2} s^{-1} of light at 420 nm and about 1,900 µmol photons m^{-2} s^{-1} at 447 nm with a pulse energy of 19.8 pJ. A monochromator (HORIBA Jobin-Yvon; H-20) set to transmit $\lambda \pm 8$ nm was placed before the MCP PMT detector

(Hamamatsu R3809U MCPPMT), and the detection wavelength was cycled from 680-760 nm, taking ten snapshots at each wavelength.

3.3 Results

3.3.1 Constitutive quenching in *soq1 roqh1* requires the peripheral light-harvesting antenna of PSII

Previous work has indicated that qH occurs in the peripheral light-harvesting antenna of PSII[36]. To confirm that the constitutive quenching in *soq1 roqh1* also occurs in the peripheral antenna and not the PSII core, we crossed *soq1 roqh1-1* to *chlorina1*, a mutant lacking chlorophyll *b*[110]. Without chlorophyll *b*, the light-harvesting antenna proteins fail to organize into functional LHCII trimers or monomers within PSII-LHCII[52]. Constitutive quenching was abolished in the triple mutant *soq1 roqh1-1 chlorina1* indicated by the similar F_o and F_m values compared with *soq1 chlorina1* (Figure 3-01). This result suggests that the site of quenching in *soq1 roqh1-1* is the peripheral antenna of PSII, consistent with previous research on the site of qH quenching.

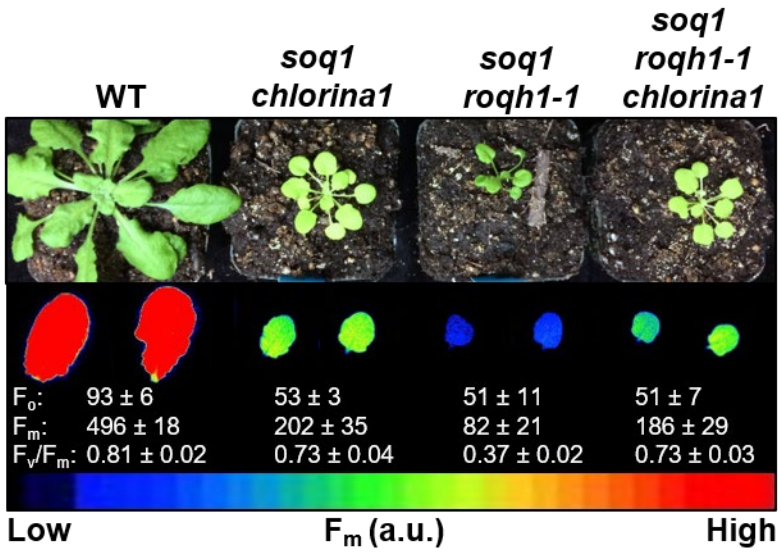

Figure 3-01. Constitutive quenching in *soq1 roqh1* requires the peripheral light-harvesting antenna of PSII. Images of plants and false-colored images of maximum fluorescence (F_m) of detached leaves from 6-week-old plants grown under standard growth conditions (120 µmol photons m^{-2} s^{-1}, 21°C). Average F_o, F_m, and F_v/F_m values ± SD are given with n = 3 individuals for each genotype.

3.3.2 The functional PSII antenna size of *soq1 roqh1* is small

To confirm that the low fluorescence in *soq1 roqh1* was due to quenching in the peripheral antenna and not the inability to close PSII reaction centers, we measured the OJIP transient fluorescence rise in the presence and absence of 3-(3,4-dichlorophenyl)-1,1-dimethylurea (DCMU). DCMU competitively binds to the Q_B site of PSII, blocking electron transfer from PSII to plastoquinone and artificially closing PSII. In the absence of DCMU, the fluorescence of *soq1 roqh1* was low throughout the saturating light pulse and when normalized to wild type appeared to be missing the J and/or I peaks corresponding to the reduction of the Q_A and Q_B plastoquinone-binding sites[105] (Figure 3-02A, B). In the presence of 20 µM DCMU, *soq1 roqh1* remained low, indicating that the fluorescence was quenched regardless of PSII reaction centers being in an open or closed state (Figure 3-02C). When the OJIP transient of *soq1 roqh1* was normalized to the wild

type, the fluorescence rise in the presence of DCMU was slow to reach saturation (Figure 3-02D), indicating that the functional antenna size of *soq1 roqh1* was small[111]. As total chlorophyll is equal between wild type and *soq1 roqh1* (Figure 2-10B), most likely this is not due to a decreased amount of light-harvesting antenna complexes. Instead, this may be due to most complexes being in a quenched state and not a light-harvesting state.

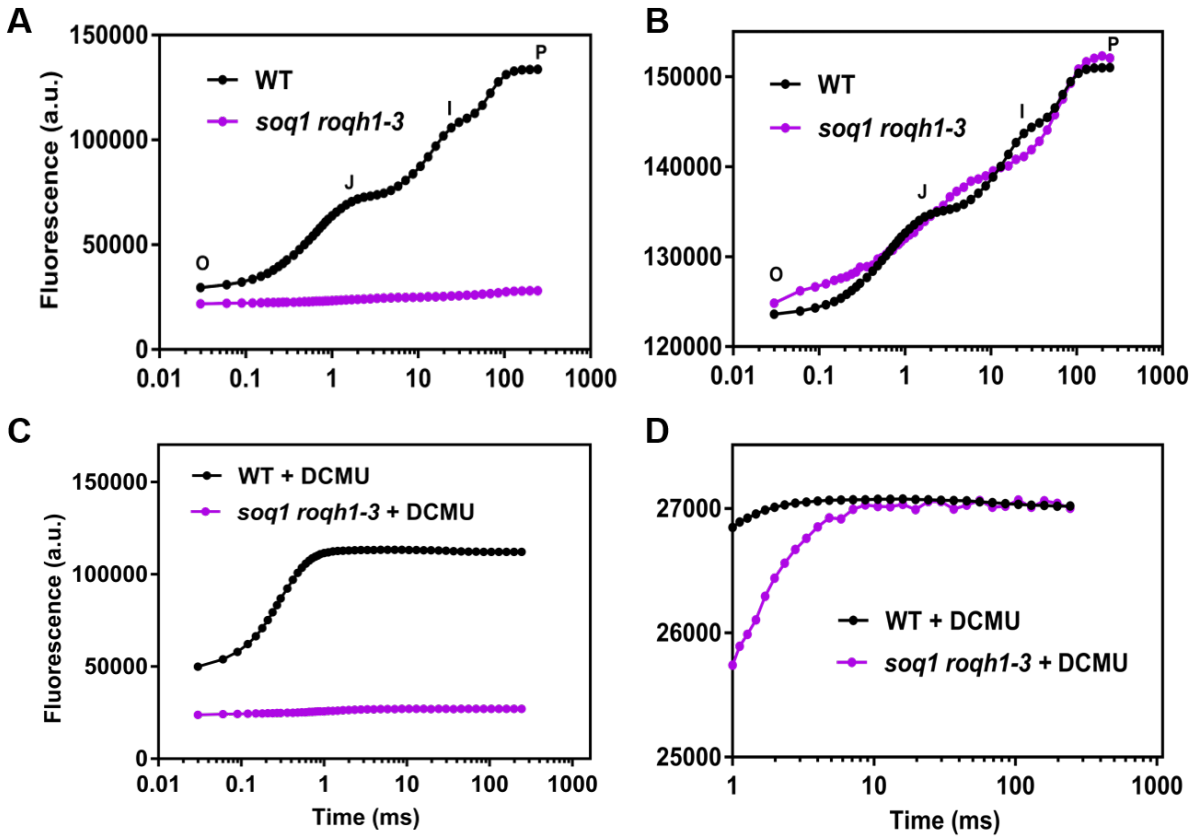

Figure 3-02. The functional PSII antenna size of *soq1 roqh1* is small. OJIP transient fluorescence rise in **(A)** the absence of DCMU. **(B)** The data in (A) normalized to wild type F_o (O) and F_m (P). **(C)** The OJIP transient fluorescence rise in the presence of DCMU. **(D)** The data in (C) normalized to wild type F_o (O) and F_m (P). Leaves were dark adapted for 5 min and infiltrated with 1mM hydroxylamine and 20 µM DCMU. Saturating actinic pulse was at 3,600 µmol photons m^{-2} s^{-1}.

3.3.3 The site of qH quenching is the LHCII trimer

To determine the specific quenching location within the peripheral light-harvesting antenna, 77K fluorescence spectroscopy was performed to distinguish PSI-, PSII-, and LHCII-associated fluorescence emission. Under standard growth conditions, *soq1 roqh1-1* lacked the fluorescence shoulder and peak associated with LHCII at 680 nm and PSII proximal antenna at 685 nm (Figure 3-03)[107]. Ultrafast time-resolved fluorescence spectroscopy through time-correlated single photon counting (TCSPC) was performed by Michelle Leuenberger to determine the chlorophyll fluorescence lifetime over a range of different wavelengths (known as decay associated spectra), which correspond to chlorophylls associated with different photosynthetic complexes[112]. When chlorophyll *a* was preferentially excited at 420 nm, the lifetime of *soq1 roqh1-1* was below 200 ps at every measured wavelength (Figure 3-04A). However, normalizing

the lifetimes of wild type and *soq1 roqh1-1* to their respective maxima revealed that the shortest lifetime in *soq1 roq1-1* was between 660-690 nm (Figure 3-04B), the emission region associated with LHCII. To confirm that LHCII trimer was the quenching site, Michelle examined the fluorescence lifetime at 680 nm when preferentially exciting PSII-associated chlorophyll *a* at 420 nm in comparison to preferentially exciting LHCII-associated chlorophyll *b* at 447 nm. In wild type, the lifetime of excited chlorophyll *b* was longer than excited chlorophyll *a*, due to the longer distance the excitation must travel from LHCII to the reaction center (Table 3-01). This resulted in a lifetime difference of 210 ps in wild type. However, in *soq1 roqh1-1*, there was no significant difference between the lifetime of excited chlorophyll *a* compared to excited chlorophyll *b* (Table 3-01), suggesting that LHCII was the site of quenching, as the excitation did not need to travel to the reaction center to be quenched.

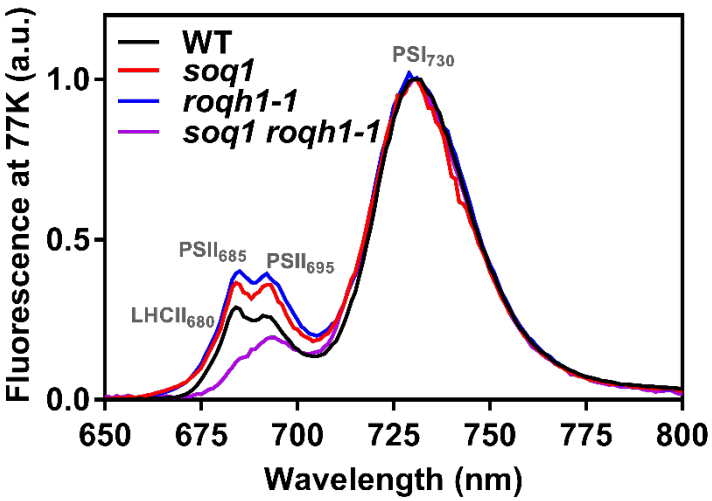

Figure 3-03. The fluorescence emission of *soq1 roqh1* is quenched at LHCII and PSII proximal antenna. Chlorophyll fluorescence emission spectra at 77K of whole leaf tissue from wild type, *soq1*, *roqh1-1*, and *soq1 roqh1-1*, treated with far red light to induce state 1 and ensure all LHCII antenna complexes are associated with PSII, and normalized to PSI emission at 730 nm. Emission components inferred from ref[107]

Excitation wavelength	$WT_{680\ nm}$	$soq1\ roqh1\text{-}1_{680\ nm}$
420 nm	τ_{avg} = 1.05 ± 0.06 ns	τ_{avg} = 0.137 ± 0.033 ns
447 nm	τ_{avg} = 1.26 ± 0.12 ns	τ_{avg} = 0.132 ± 0.021 ns
Measured difference in τ_{avg}	0.210 ± 0.134 ns	0.005 ± 0.039 ns

Table 3-01. Fluorescence lifetimes of preferentially excited chlorophyll *a* and *b*. Measured average fluorescence lifetimes excited at 420 nm (chlorophyll *a*) and 447 nm (chlorophyll *b*) and detected at 680 nm.

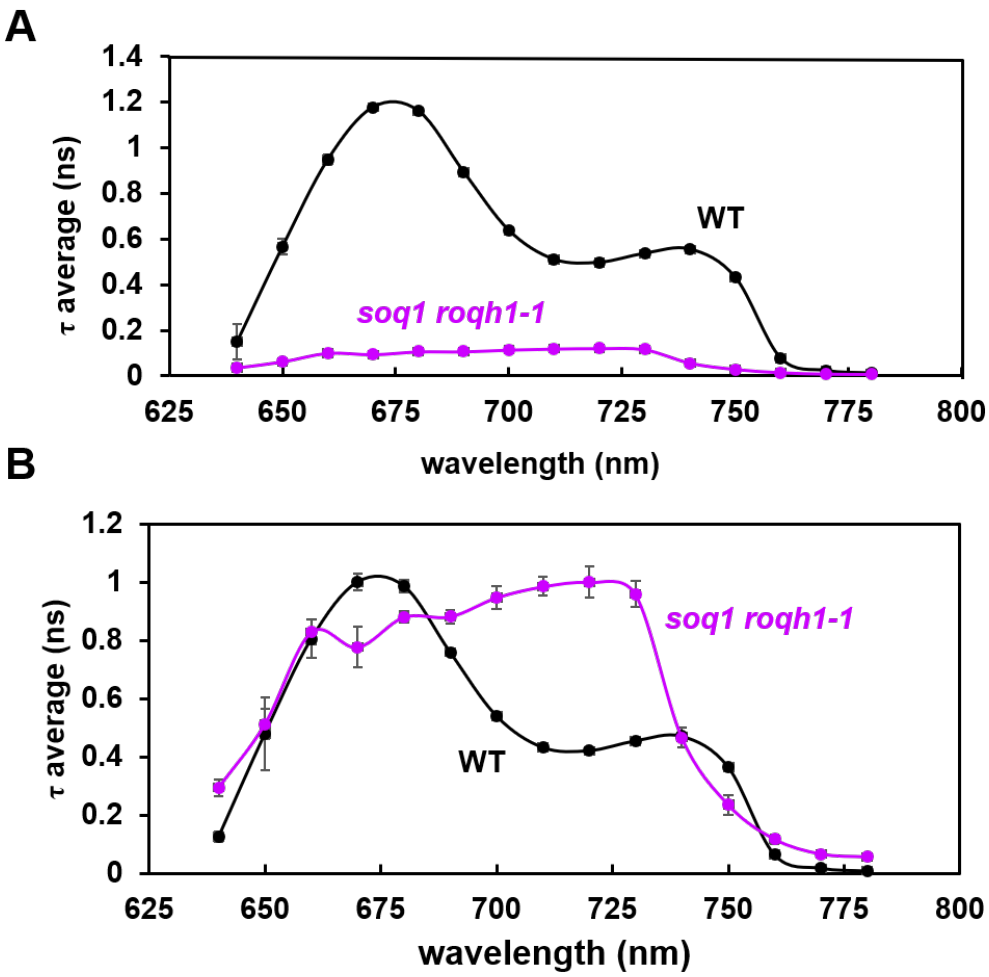

Figure 3-04. Chlorophyll fluorescence lifetimes are shorter across a range of wavelengths in *soq1 roqh1*. Decay associated spectra between 640-780 nm when preferentially exciting chlorophyll *a* at 420 nm.

3.4 Discussion

The chlorophyll fluorescence techniques utilized in this chapter collectively support the hypothesis that the site of qH quenching is the LHCII trimer within the PSII peripheral light-harvesting antenna. However, some questions remain as to whether this is the only quenching site. The 77K fluorescence emission spectrum of *soq1 roqh1* lacks an emission peak corresponding to the proximal antenna of PSII at 685 nm in addition to the LHCII trimer-associated shoulder at 680 nm (Figure 3-03). While it is possible that more than one quenching site may exist, it seems unlikely that the *soq1 roqh1-1 chlorina1* triple mutant would have recovered fluorescence levels similarly to *soq1 chlorina1* if additional quenching sites existed in the PSII core (Figure 3-01). However, disruption of the peripheral antenna in the *chlorina1* mutant leads to additional changes in complex organization including a decrease in PSII dimers and an increase in PSII monomers[52]. It is possible that the dissociation of PSII dimers into monomers disrupts or prevents the formation of quenching sites in the core. Conversely, the quenched proximal antenna peak observed with

77K may be the result of connectivity to the quenched LHCII trimers and not due to additional sites within the core.

Previous work by Alizée Malnoë and Soomin Park indicates that a proportion of qH quenching sites can exist *in vitro*. By isolating thylakoids and separating photosynthetic complexes through fast protein liquid chromatography, Malnoë and Park could measure chlorophyll fluorescence lifetimes from individual eluted fractions. Using this method with wild type and *soq1* thylakoids isolated before and after a cold and high light treatment, they could show that the LHCII trimer fraction remains quenched *in vitro*. While the fluorescence lifetime was not as short as what has been observed *in vivo*, it provides clear evidence for the LHCII trimer as one of the site(s) of quenching. The difference between the *in vitro* and *in vivo* measurements could be due to the existence of other sites in *vivo* which cannot be preserved *in vitro*. However, as previously discussed, this difference could also be due to dissociation of supercomplexes, which would disrupt quenching that occurred through connectivity of the LHCII trimer.

Chapter 4: ROQH1 functions in a complex after cold and high light treatment

4.1 Introduction

The identification and characterization of ROQH1 as an atypical SDR was presented in Chapter 2. The SDR superfamily is one of the largest and oldest protein superfamilies described, containing over 47,000 members and at least 140 different enzymes across all domains of life[80,81,113]. The magnitude of this superfamily requires further subdivision, and thus SDRs are classified into 314 families based on sequence similarities and Hidden Markov Models[113]. This additional nomenclature aims to divide SDRs by type and functional groups. However, a small portion of SDRs (approximately 10% in plants) cannot be classified into an SDR type and are collectively grouped into the 'atypical' or 'unknown' SDR family[81]. Some atypical SDRs have been shown to bind cofactors[82] and ligands[114] and play roles in redox sensing or RNA metabolism, yet currently none have been demonstrated to have enzymatic activity. Due to the limited knowledge and sequence similarity between atypical SDRs, the ROQH1 protein annotation does not provide much insight into the molecular function of ROQH1. Therefore, our efforts have focused on biochemical interactions between ROQH1 and other photosynthetic proteins, specifically the light harvesting antenna of PSII, to investigate the biochemical mechanism of qH relaxation by ROQH1.

The site of qH quenching was demonstrated in Chapter 3 to be the LHCII trimer. Given the proposed function of ROQH1 and site of quenching, it is surprising that ROQH1 is localized to the stroma lamellae membrane rather than the thylakoid grana where the majority of PSII antenna proteins are located. However, light harvesting and NPQ regulation occurs through dynamic changes in thylakoid membrane stacking[70] and organization of the macrostructure of the light-harvesting antenna[115,116]. It is currently unknown how a sustained exposure to cold and high light affects the photosynthetic machinery in Arabidopsis. In the overwintering evergreen, *Pinus sylvestris*, there is a complete loss of PSII-LHCII complexes as well as LHCII trimers and monomers during winter months[40]. In contrast, low temperature fluorescence experiments with the evergreen snow gum, *Eucalyptus pauciflora*, shows a winter-specific chlorophyll protection complex which is likely LHCII oligomers in an aggregated and quenched state[117]. Furthermore, it is unknown whether the induction of qH or the disruption and overexpression of qH proteins

requires or induces specific changes to the photosynthetic complexes. Thus, a second aim of this chapter is to investigate the composition and organization of photosynthetic complexes after cold and high light in different qH mutant backgrounds.

4.2 Materials and Methods

4.2.1 Thylakoid isolation by sucrose cushion

For BN-PAGE and co-immunoprecipitation experiments, thylakoids isolated by sucrose cushion were used. All leaves from 5 5-week-old plants were harvested before and after a cold and high light treatment and ground in a pre-cooled Waring blender with 40 ml cold B1 solution (20 mM tricine-KOH pH 7.8, 400 mM NaCl, 2 mM $MgCl_2$, 0.2 mM Benzamidine, 1 mM aminocaproic acid, 0.2 mM PMSF) for 30 s. The ground solution was filtered through four layers of miracloth and centrifuged for 5 min at 27,000 x g at 4°C. The supernatant was discarded, and the pellet was resuspended with the residual supernatant with a paintbrush and then with 15 ml of B2 solution (20 mM tricine-KOH pH 7.8, 150 mM NaCl, 2 mM $MgCl_2$, 0.2 mM Benzamidine, 1 mM aminocaproic acid, 0.2 mM PMSF). The resuspended solution was overlaid on top of 10 ml 1.3 M sucrose solution (1.3 M sucrose, 20 mM tricine-KOH pH7.8, 1.5 mM NaCl), overlaid on top of 10 ml 1.8 M sucrose solution (1.8 M sucrose, 20 mM tricine-KOH pH7.8, 1.5 mM NaCl) in an ultracentrifuge tube and centrifuged for 30 min at 131,500 x g at 4°C. The entire green precipitate band between 1.3 and 1.8 M sucrose layers (Figure 4-01) was extracted using a glass pipet and bulb and washed with B3 solution (20 mM tricine-KOH pH 7.8, 15 mM NaCl, 5 mM $MgCl_2$). The solution was centrifuged for 15 min at 27,000 x g at 4°C. The pellet was resuspended with storing solution (20 mM tricine-KOH pH 7.8, 0.4 M sucrose, 15 mM NaCl, 5 mM $MgCl_2$) using a paintbrush and centrifuged again for 10 min at 27,000 x g at 4°C. The supernatant was discarded, and the final pellet was resuspended with a paintbrush with residual storing solution and stored at -80°C until further use.

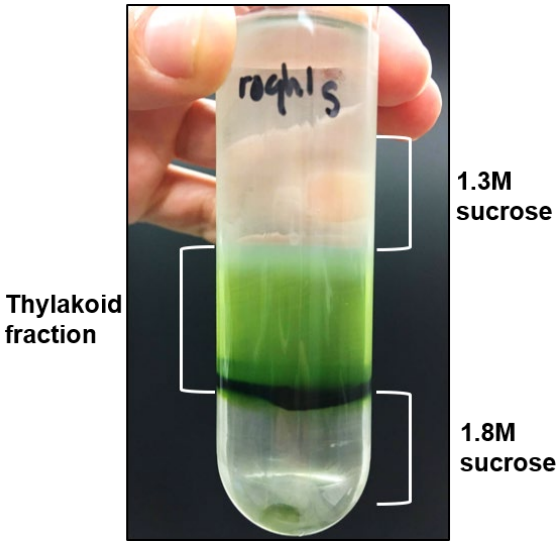

Figure 4-01. Thylakoids isolated by sucrose cushion. After centrifugation, the thylakoid fraction is collected between the 1.3 M and 1.8 M sucrose cushion.

4.2.2 Blue Native PAGE

For BN-PAGE, thylakoids were isolated by sucrose cushion and resuspended in sucrose storage solution (20 mM tricine-KOH pH 7.8, 0.4 M sucrose, 15 mM NaCl, 5 mM $MgCl_2$) to 1.0

mg chlorophyll/mL concentration. An equal volume of storage solution containing 2% n-dodecyl-α-D-maltoside, digitonin, or n-dodecyl-β-D-maltoside was added to solubilize thylakoids at a final concentration of 1% detergent per 0.5 mg chlorophyll/mL. Thylakoids were solubilized on ice in the dark for 15 min. After solubilization, insolubilized material was pelleted by centrifugation at 14,000 x g for 10 min. The supernatant was combined with one-tenth volume of loading buffer (100 mM Bis-Tris-HCl pH 7, 500 mM aminocaproic acid, 30% sucrose, 5% Coomassie G250), and 8 µg total chlorophyll was separated on a 4-16% Bis-Tris Novex NativePAGE gel according to ref[120]. Before immunoblotting the first dimension, the native gel was soaked in denaturing buffer (0.1 M EDTA-NaOH pH 8.0, 0.12 M Tris-HCl pH 6.8, 4% SDS, 12% sucrose, 0.2 M DTT, 0.1 M Na_2CO_3, 8 M urea) for 30 min before transferring. For separation in the second dimension, lanes were cut and soaked in denaturing buffer for 30 min, placed on top of a 10% Bis-Tris 2D Novex NuPAGE gel, sealed with 0.05% agarose and further separated using MES running buffer (50 mM MES, 50 mM Tris, 0.1% SDS, 1 mM EDTA-HCl pH 7.3). The 2D gel was transferred to a 0.45 µm PVDF membrane followed by immunoblotting with antibodies against SOQ1 (1: 200), PsaA (1:10,000), FLAG (1:1,500 dilution), ROQH1 (1: 2,500), D1 (1:10,000 dilution), and Lhcb2 (1:10,000 dilution) antibodies.

4.2.3 Co-Immunoprecipitation

For co-immunoprecipitation experiments, an anti-Flag antibody was covalently coupled to M-270 epoxy dynabeads (Thermo Fischer) at a concentration of 2.8 µg antibody/mg dynabead. The antibody-coupled dynabeads were resuspended in thylakoids isolated before and after a cold and high light treatment and solubilized with 1% β-DM per 0.5 mg/ml total chlorophyll. The beads were incubated at 4°C for 50 min and then washed with phosphate buffered saline (PBS) with 0.5% Triton X-100 for a total of four washes. After washing, the beads were eluted with 0.5 M NH_4OH and 0.5 mM EDTA and concentrated using a SpeedVac and then solubilized for SDS-PAGE and immunoblotted with antibodies against Flag (1:1,500 dilution) and Lhcb1 (1:1,10,000), Lhcb2 (1:5,000), and Lhcb3 (1:5,000).

4.3 Results

4.3.1 qH induction does not affect accumulation or formation of photosynthetic complexes

To shed light on the molecular mechanism of qH, we checked the accumulation and formation of photosynthetic complexes before and after a cold and high light treatment. Blue native PAGE (BN-PAGE) analyses of wild type, *lcnp*, *roqh1-3*, and *soq1 roqh1-1*: ROQH1 OE thylakoids solubilized with either n-dodecyl-β-D-maltoside (β-DM) or 1% digitonin and 1% α-DM showed no difference in photosynthetic complex abundance between genotypes (Figure 4-02, 4-03). As expected,[121] solubilization with digitonin and α-DM preserved the high molecular weight PSII-LHCII supercomplexes better than solubilization with β-DM (Figure 3-02). After 5 h cold and high light, wild type, *lcnp*, *roqh1-3*, and ROQH1 overexpressor similarly showed a decrease in PSII-LHCII supercomplexes and an increase in PSII monomers, RC47 assembly complexes,

and LHCII monomers in both detergent conditions (Figure 4-02 and Figure 4-03). The similar response between wild type and *lcnp* suggests that these changes are independent of qH.

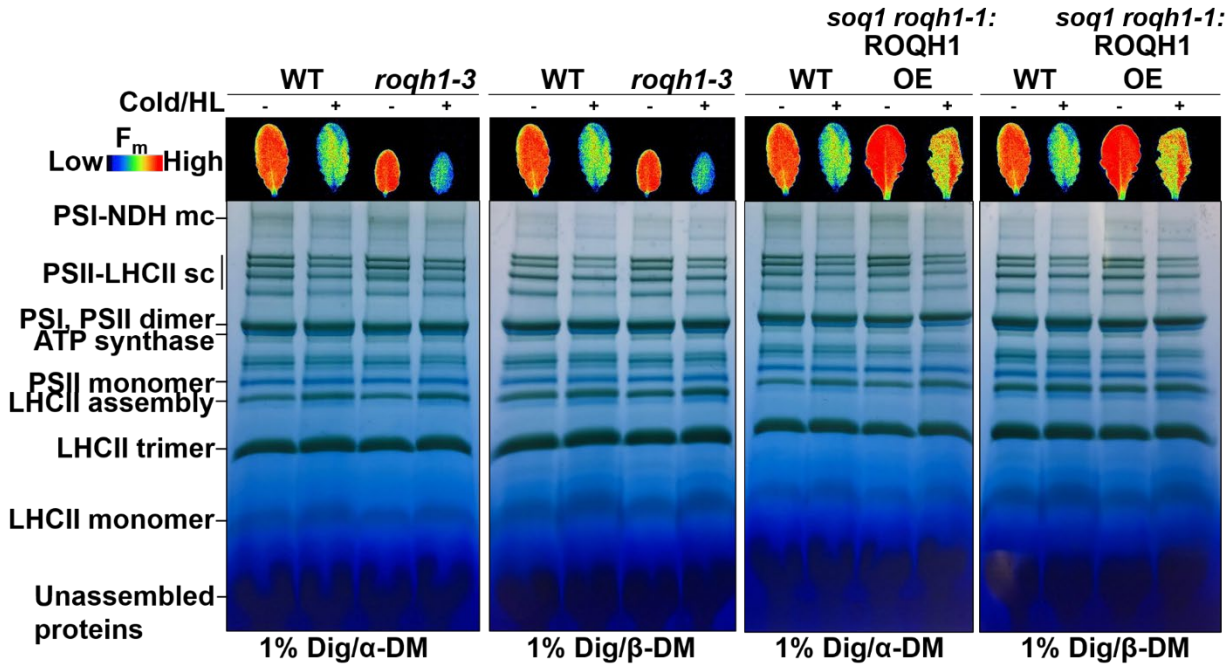

Figure 4-02. Overexpression and disruption of ROQH1 does not affect accumulation or formation of photosynthetic complexes. BN-PAGE of thylakoids isolated from wild-type or *soq1 roqh1-1*: ROQH1 OE plants before or after a cold and high light treatment and solubilized with 1% digitonin and either 1% α-DM or 1% β-DM. Identities of complexes were inferred from ref[59].

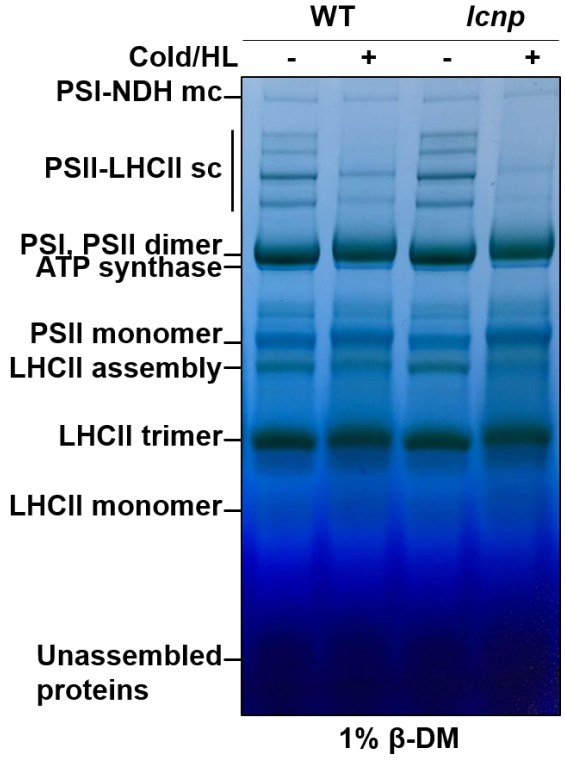

Figure 4-03. Disruption of LCNP does not affect accumulation or formation of photosynthetic complexes. BN-PAGE of thylakoids isolated from plants before or after a cold and high light treatment and solubilized with 1% β-DM.

4.3.2 Overexpression of ROQH1 does not alter the composition of photosynthetic complexes

While the accumulation and formation of photosynthetic complexes appeared unaffected by ROQH1 overexpression, we investigated whether the composition was altered. To assess complex composition, the BN-PAGE of wild type and *soq1 roqh1-1*: ROQH1 OE was run in the second dimension under denaturing conditions and stained with Coomassie and silver stain (Figure 4-04). Complex components were inferred from ref[122] and appeared present in both wild type and overexpressor with similar intensities. This indicated that overexpression of ROQH1 did not affect the composition of photosynthetic complexes.

4.3.3 ROQH1 co-migrates with LHCII trimer and monomer

Because qH requires the peripheral antenna of photosystem II (Figure 3-01), we checked whether ROQH1 or SOQ1 interacts with any photosynthetic complex before and after a cold and high light treatment. Immunoblotting the first dimension of the BN-PAGE with an anti-Flag antibody revealed that under standard growth conditions, ROQH1 migrates with unassembled proteins (Figure 4-5A). However, after the cold and high light treatment, ROQH1 protein level increased, and a small portion migrated slightly above the PSI, PSII dimer band when solubilized with digitonin and α-DM (Figure 4-05A). When solubilized with β-DM, a small portion migrated near the LHCII trimer and monomer band (Figure 4-05B). Immunoblotting with an anti-ROQH1 antibody in either detergent condition in non-tagged lines (wild type and *roqh1-3*) did not provide further information as the antibody only detected non-specific bands (Figure 4-06). This could be due to ROQH1 being a low abundant protein and/or the antibody not recognizing the epitope under native conditions. Immunoblotting with an anti-SOQ1 antibody revealed multiple complexes near the LHCII trimer, PSI and PSII dimer, and PSII-LHCII supercomplexes (Figure 4-07).

To determine whether the ROQH1 and SOQ1 complexes contained photosynthetic chain components, two-dimensional SDS-PAGE immunoblot analysis was performed with photosystem core and antenna subunits D1, PsaA, and Lhcb2 (Figure 4-08 and Figure 4-09). In both detergent conditions, the ROQH1-Flag signal was mainly detected at the expected size of 37 kD as well as 50 kDa, suggesting post-translational covalent modification (Figure 4-08 and Figure 4-09). When solubilized with digitonin and α-DM, SOQ1 co-migrated with LHCII trimer, RC47, PSII monomer, dimer, and PSII-LHCII supercomplexes before and after cold and high light (Figure 4-08). This was consistent with previous reports[95] and suggests that SOQ1 associates with photosynthetic complexes. In contrast, when solubilized with digitonin and α-DM, ROQH1 did not seem to co-migrate with any photosynthetic chain components except potentially D1 at the PSII monomer (Figure 4-08). However, when solubilized with β-DM, ROQH1 co-migrated with Lhcb2 at the LHCII trimer and monomer (Figure 4-08), supporting the hypothesis that ROQH1 may function in a complex with LHCII.

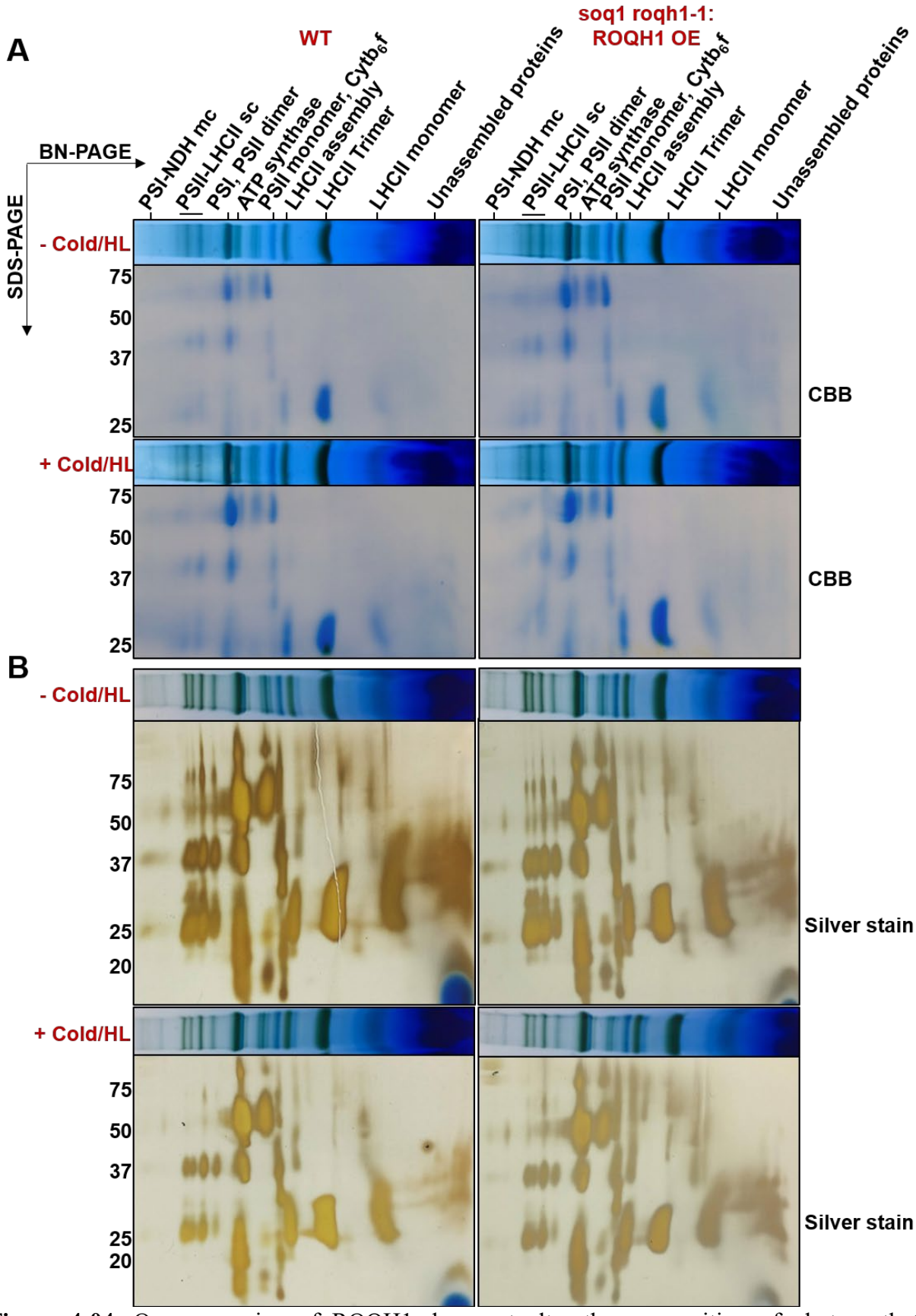

Figure 4-04. Overexpression of ROQH1 does not alter the composition of photosynthetic

complexes. BN-PAGE of thylakoids from wild-type or *soq1 roqh1-1*: ROQH1 OE plants before or after a cold and high light treatment solubilized with **(A)** 1% digitonin and 1% β-DM, separated in the second dimension by SDS-PAGE, and stained with coomassie brilliant blue or **(B)** solubilized with 1% digitonin and 1% α-DM, separated in the second dimension by SDS-PAGE, and stained with silver stain.

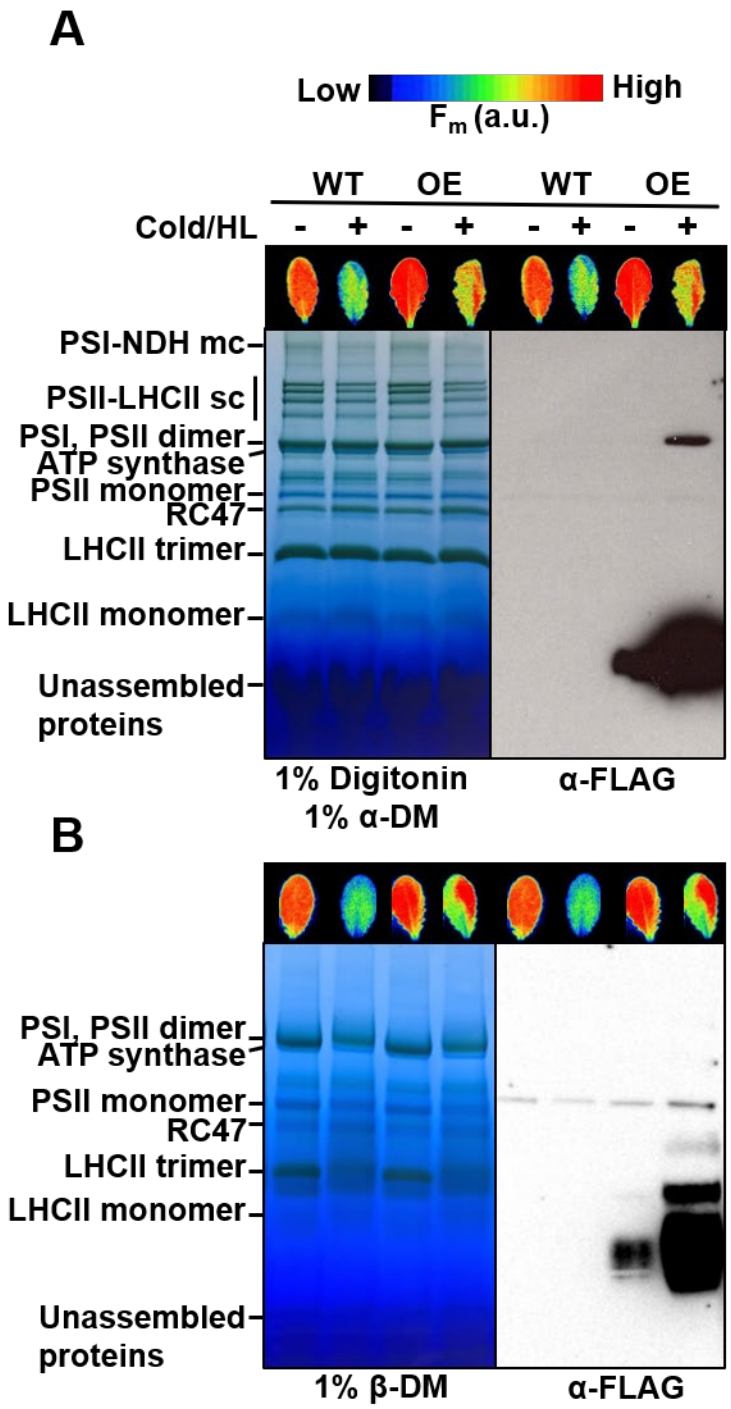

Figure 4-05. ROQH1 functions in a complex after cold and high light. Immunoblot analysis of BN-PAGE from thylakoids isolated from 5-week-old wild type and *soq1 roqh1-1*: ROQH1 OE plants before (-) and after (+) a 5 h cold and high light treatment (1,600 µmol photons m^{-2} s^{-1}) and solubilized with either **(A)** 1% Digitonin and 1% α-DM or **(B)** 1% β-DM and immunoblotted with an anti-Flag antibody.

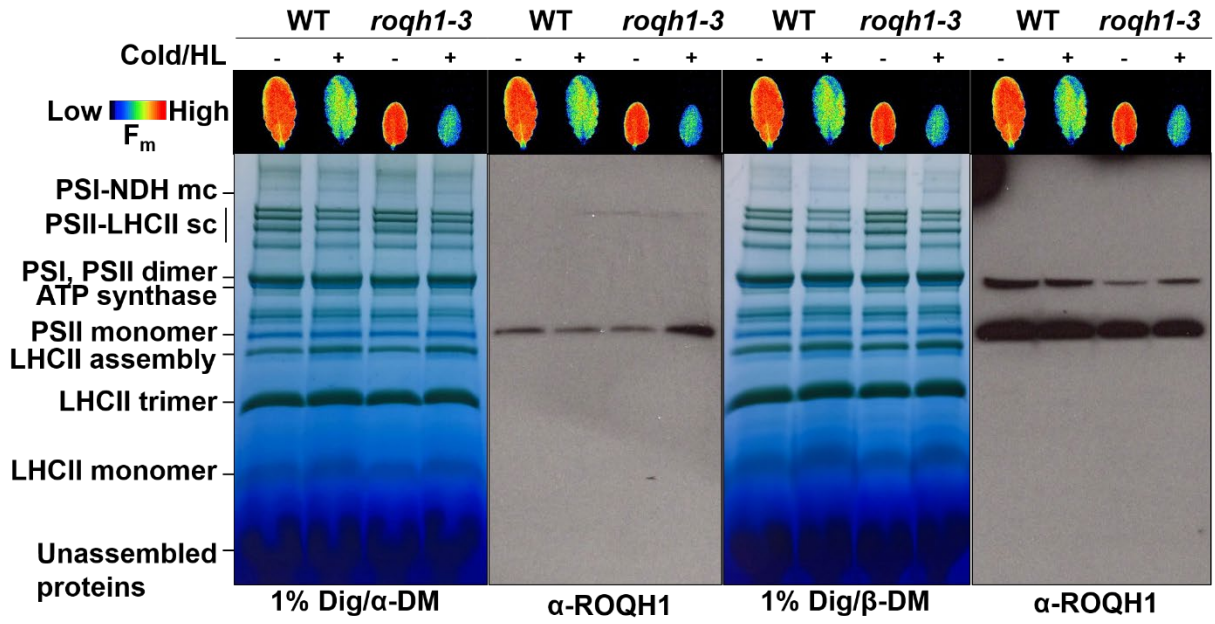

Figure 4-06. The ROQH1 antibody does not detect ROQH1 under native conditions. Immunoblot analysis of BN-PAGE from thylakoids isolated from 5-week-old wild type and *roqh1-3* plants before (-) and after (+) a 5 h cold and high light treatment (1,600 µmol photons m^{-2} s^{-1}) and solubilized with either 1% Digitonin and 1% α-DM or 1% β-DM and immunoblotted with an anti-ROQH1 antibody.

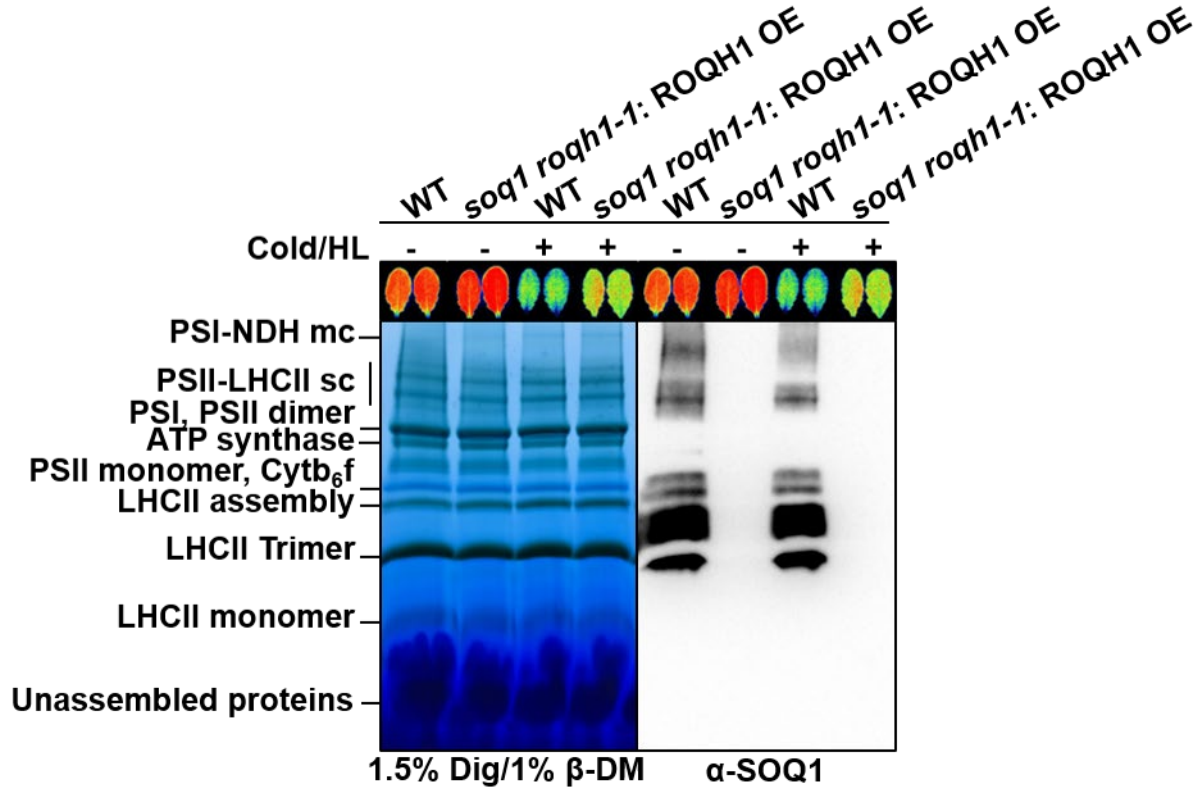

Figure 4-07. SOQ1 co-migrates with multiple photosynthetic complexes. Immunoblot analysis of BN-PAGE from thylakoids isolated from 5-week-old wild type and *soq1 roqh1-1*: ROQH1 OE

plants before (-) and after (+) a 5 h cold and high light treatment (1,600 µmol photons m^{-2} s^{-1}) and solubilized with 1.5% digitonin and 1% β-DM and immunoblotted with an anti-SOQ1 antibody.

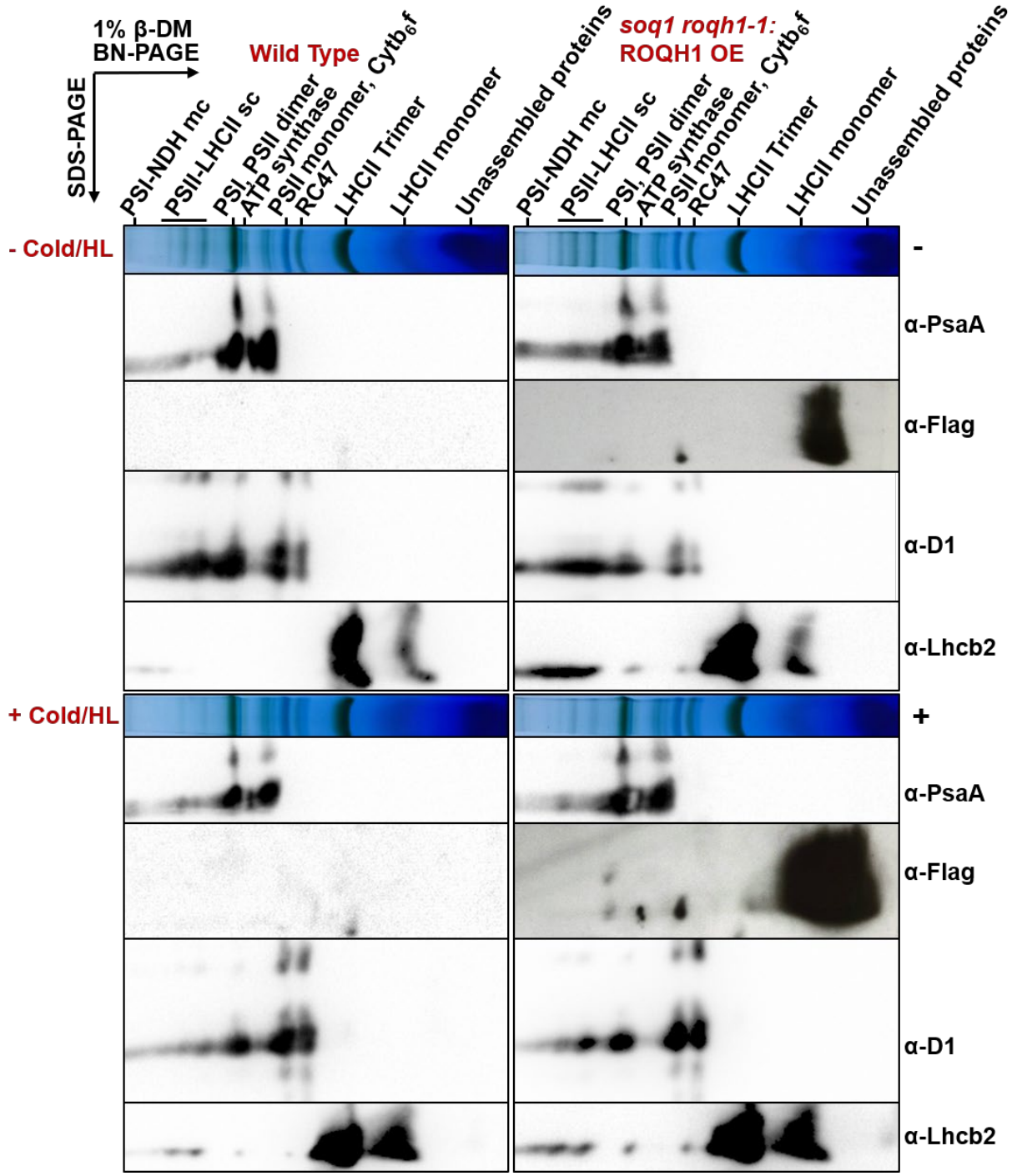

Figure 4-08. ROQH1 has post-translational covalent modification(s) and SOQ1 co-migrates with photosynthetic complexes. Two-dimensional BN/SDS-PAGE analysis from thylakoids isolated from wild type and *soq1 roqh1-1*: ROQH1 OE before (-) and after (+) a 5 h cold and high light treatment (1,600 µmol photons m^{-2} s^{-1}), solubilized with 1% digitonin and 1% α-DM and immunoblotted against SOQ1, Flag, PsaA, D1, and Lhcb2.

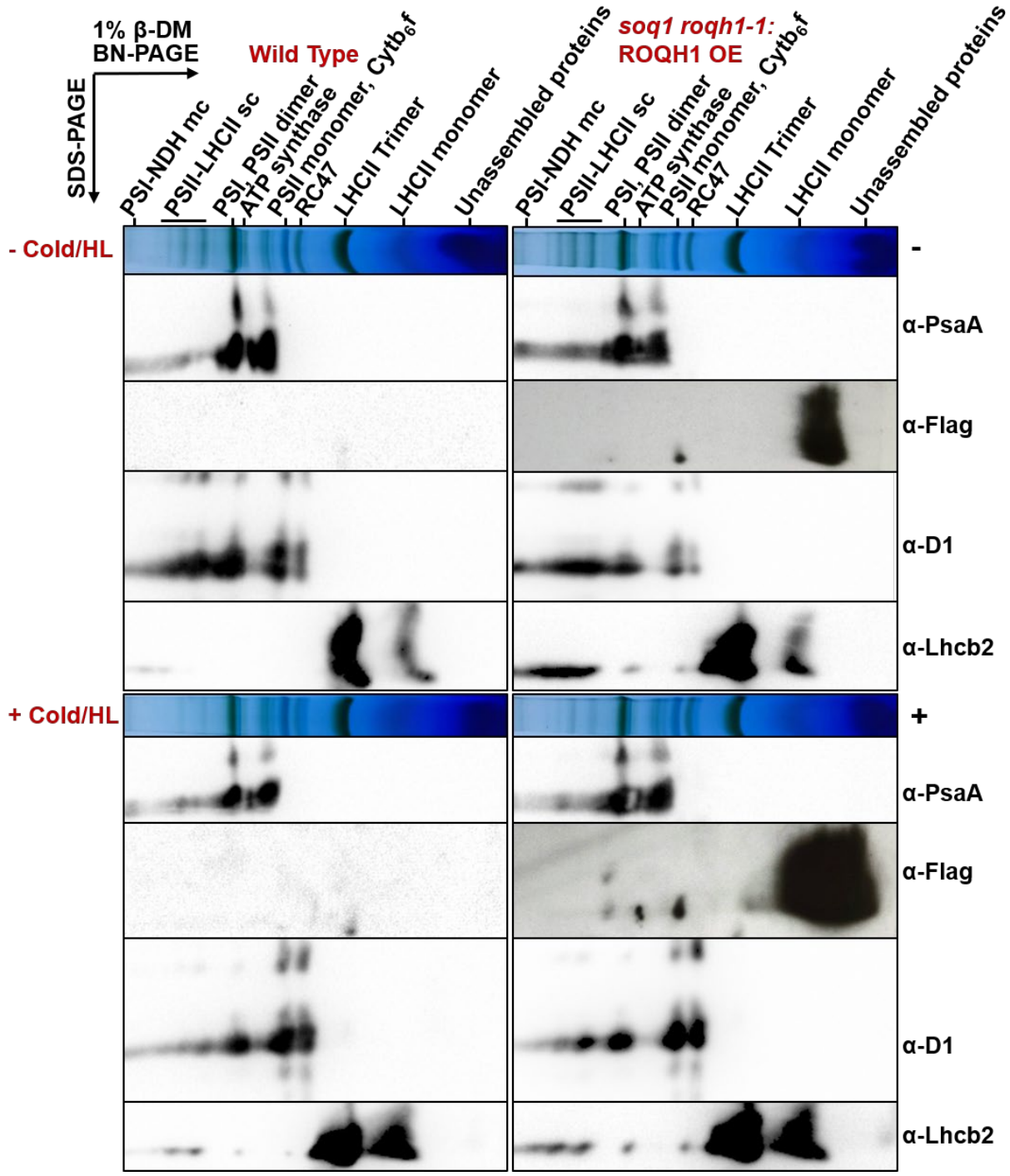

Figure 4-09. ROQH1 co-migrates with LHCII trimer and monomer. Two-dimensional BN/SDS-PAGE analysis from thylakoids isolated from wild type and *soq1 roqh1-1*: ROQH1 OE before (-) and after (+) a 5 h cold and high light treatment (6°C and 1,600 µmol photons m^{-2} s^{-1}), solubilized with 1% β-DM, and immunoblotted with antibodies for Flag, PsaA, D1, and Lhcb2. For an internal loading control, 1 µg total chlorophyll of solubilized *soq1 roqh1-1*: ROQH1 OE thylakoids was loaded in the control lane.

4.3.4 ROQH1 does not co-immunoprecipitate with LHCII trimer proteins

To further investigate the hypothesis that ROQH1 forms a complex with LHCII, we tested whether ROQH1 directly interacts with LHCII through co-immunoprecipitation. Thylakoids isolated from wild type and *soq1 roqh1-1*: ROQH1 OE before and after a cold and high light treatment were solubilized with 1% β-DM and incubated with Dynabeads covalently coupled with an anti-flag antibody. The anti-flag antibody pulled down ROQH1-Flag from both before and after a cold and high light treatment, decreasing the amount of ROQH1 found in the unbound flow-through compared to the initial input (Figure 4-10A). However, when immunoblotted with antibodies against Lhcb1, 2, and 3, the LHCII trimer proteins were detected in the input and unbound flow-through but not in the eluate (Figure 4-10A). To determine if other proteins co-immunoprecipitated with ROQH1-Flag, a portion of the eluate was separated on an SDS-PAGE and silver stained. The stained gel showed multiple bands in each eluate, most likely immunoglobulin G from the anti-Flag antibody and other contaminating proteins (Figure 4-11). The only band that was found in *soq1 roqh1-1*: ROQH1 OE but absent in wild type was approximately 29 kDa, the expected size of ROQH1 (Figure 4-10B).

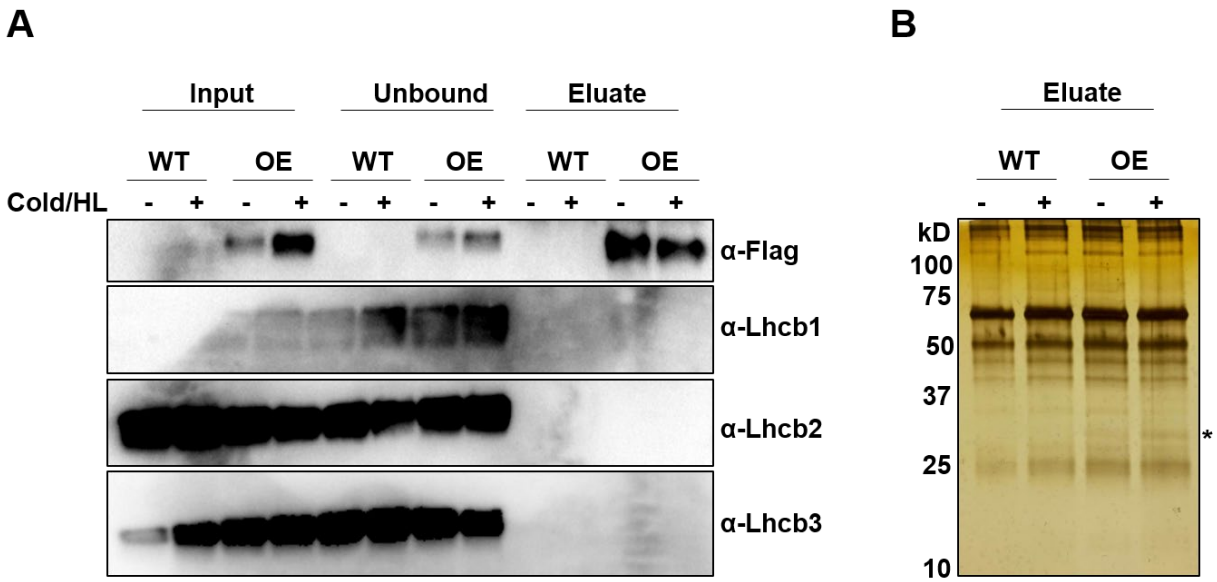

Figure 4-10. ROQH1 does not co-immunoprecipitate with LHCII trimer proteins. **(A)** Co-immunoprecipitation using anti-Flag coupled Dynabeads and thylakoids from wild type and *soq1 roqh1-1*: ROQH1 OE before and after a cold and high light treatment and solubilized with 1% β-DM. The input lanes are solubilized thylakoids never exposed to Dynabeads. The unbound is the thylakoid flow-through after incubation with Dynabeads. The eluate is the immunoprecipitated proteins that remained bound to the antibody-coupled beads after four washes with PBS and 0.5% TritonX 100. **(B)** The eluate separated by SDS-PAGE and silver stained. The asterisk indicates the band presumed to be ROQH1-Flag.

4.4 Discussion

A sustained cold and high light treatment causes dissociation of PSII-LHCII supercomplexes (Figure 4-02 and Figure 4-03), most likely to decrease light absorption and the

functional antenna size of PSII[70]. These changes in complex accumulation after cold and high light are independent of qH induction as similar accumulation is also observed in the *lcnp* mutant (Figure 4-03). However, the similar complex accumulation between wild type and qH mutants does not indicate that these complexes are identical. qH may induce subtle differences that cannot be observed by BN-PAGE including complex composition, conformational states, subunit organization, and pigment orientation.

The site of qH quenching has been demonstrated in Chapter 3 to be the peripheral antenna of PSII (Figure 3-01), specifically the LHCII trimer (Figure 3-04). The majority of LHCII trimers are located within the grana core, yet ROQH1 is peripherally bound to the stroma lamellae membrane. This, however, does not exclude the possibility that ROQH1 could function at a few available LHCII trimers to turn off qH. Our current working hypothesis is that the formation of strong quenchers in the LHCII at the grana margins could quench excitation energy received by LHCII within the grana core. Therefore, access to stroma-exposed LHCII would be sufficient to turn off qH. ROQH1 could interact with antenna located on the outer grana and within the stroma lamellae consistent with its localization. Several stromal lamellae-localized proteins have been shown to have LHCII as their primary substrate, including the STN7 kinase and TAP38 phosphatase involved in state transitions[123]. After a cold and high light treatment, one- and two-dimensional BN/SDS-PAGE indicates that ROQH1-Flag protein level increases and assembles into higher molecular weight complexes (Figure 4-05 and Figure 4-09). The increase in ROQH1-Flag is likely due to the light-regulated I-box element present in the 35S promoter that is driving ROQH1 overexpression[124,125]. Strikingly a possible ROQH1-LHCII complex was observed only upon solubilization with β-DM (Figure 4-09). It may be that with α-DM solubilization, the Flag epitope of ROQH1-Flag is buried into LHCII subcomplexes and cannot be detected by the anti-Flag antibody (Figure 4-08). The β-DM results are consistent with the potential involvement of ROQH1 turning off qH at LHCII. However, co-immunoprecipitation experiments could not demonstrate a direct interaction between LHCII trimer proteins and ROQH1-Flag (Figure 4-10). This could be due to several technical and/or biological reasons. First, any interaction between ROQH1 and LHCII could be weak and easily disrupted by the washes with PBS and 0.5% TritonX-100. Second, the interaction between ROQH1 and LHCII may not be strong enough to extract LHCII proteins embedded in thylakoid membranes. Third, it is possible that the ROQH1-LHCII interaction is indirect such as through an intermediate protein that is also present in the ROQH1-LHCII complex. And finally, our hypothesis suggests that few ROQH1-LHCII interactions are required for quenching to be turned off. It could be that too few LHCII trimers were pulled down to be observed by either western blot or silver stain. Future experiments with more material and sensitive techniques such as mass spectrometry could be used to determine interacting partners and/or substrates of ROQH1.

Chapter 5: Modifying qH to improve NPQ recovery and photosynthetic efficiency in crop plants

5.1 Introduction

Throughout the green revolution, crop performance steadily improved due to fertilizer use, disease and pest control, and traditional breeding methods to improve crop architecture and harvest index. However, over the past 20 years, crop yields have seen little improvement as light interception and partitioning efficiency have reached their maximum potential[124]. Yet food

production needs to double by 2050 to meet the growing population demand in the face of rapidly changing climates and limitations in available arable land. Therefore, agricultural research has focused on energy conversion efficiency, the remaining yield factor that still has potential room for improvement.

The conversion factor is how efficiently light energy can be captured and converted into chemical energy by photosynthesis. In most field environments, periods of light limitation and light excess often fluctuate within the crop canopy due to natural shading events such as passing cloud coverage. While NPQ mechanisms dissipate the excess absorbed energy to protect the photosynthetic apparatus, slow NPQ relaxation kinetics can compete with light harvesting and limit photosynthetic efficiency. Thus, increasing the rate of NPQ relaxation may improve photosynthetic efficiency and crop yield. This was recently demonstrated in tobacco by manipulating qE and qZ by overexpressing photosystem II subunit S (PsbS), violaxanthin de-epoxidase (VDE), and zeaxanthin epoxidase (ZEP). By overexpressing two opposing activities of the xanthophyll cycle, zeaxanthin could be produced and recycled at a faster rate, improving qZ induction and relaxation kinetics under fluctuating light[125]. To ensure that the modified qZ plants could maintain wild type levels of NPQ and photoprotection, PsbS was also overexpressed to enhance qE[125]. As a result, the modified balance between light harvesting and dissipation led to an increase in dry biomass by 15%[125].

Following the success of Kromdijk et al., we focused our efforts on improving other NPQ mechanisms that have longer relaxation kinetics than qE or qZ, namely, qH. To this aim, we utilized the antagonistic functions of LCNP and ROQH1 previously determined in Arabidopsis in Chapter 2 to mitigate or abolish qH in tobacco. We used CRISPR/Cas9 to disrupt both LCNP genes simultaneously and a leaf-specific promoter to overexpress ROQH1, and we tested these constructs transiently in *N. benthamiana* and *N. tabacum*. Stable transgenic *N. tabacum* lines are currently in progress, and we plan to monitor crop performance under greenhouse and field conditions to determine whether qH modification improves photosynthetic efficiency and crop yield.

5.2 Materials and Methods

5.2.1 *In vitro* gRNA activity assay

To disrupt *LCNP* in *N. fabrum*, two guide RNAs were designed to anneal to regions specific to both *LCNP* gene copies within exon 2 and exon 3 (Figure 5-01) using the design tool at www.crispr.mit.edu. The guides were spaced apart so that if cutting occurred at both guides, a 500 bp deletion would occur. To assess gRNA-mediated cutting efficiency, the two *LCNP* genes from *Nicotiana tabacum* cv. Petite Havana and Samsun were amplified by PCR using the forward primer GGTGTGCTACAATTTGGTAG for Petite Havana and TGTCCAACAATCACCTCCTA for Samsun with the reverse primer TGTTGCATTCCTGGCATGGA. The PCR products were gel extracted and combined with assembled ribonucleoproteins (RNPs).

To assemble the RNP complex, the guide RNA duplex was first made with the crRNA and tracrRNA synthesized by Integrated DNA Technologies. An equal volume (1 µl) of 10 µM crRNA and 10 µM tracrRNA were incubated together in a total volume of 10 µl at 98°C for 5 min. Forward and reverse guides were assembled in separate reactions. The assembled guide RNAs were then assembled into the RNP complex. An equal volume (1 µl) of each guide (forward and reverse)

were combined with 1 ul of 10 µM Cas9 enzyme, enzyme reaction buffer (200 mM Hepes, 50 mM $MgCl_2$, 1 M NaCl, 1 mM EDTA, pH 6.5) in a total volume of 7 µl and incubated at RT for 30 min. After 30 min, approximately 500 ng of gel extracted PCR product was added to the reaction for a total volume of 10 µl and incubated at 37°C for 30 min to 2 hours. After incubation, the digestion products were run on a 1% agarose gel.

5.2.2 LCNP CRISPR construct design and assembly

The construct design to disrupt LCNP using CRISPR/Cas9 was based on a previously described approach using the polycistronic T-RNA processing system to multiplex gRNAs[126]. This system uses the endogenous RNase P and RNase Z ribonucleases to cleave the polycistronic transcript into separate and mature tRNA and gRNAs. A tRNA sequence from *N. benthamiana* that was previously tested[127] was spaced in between each guide scaffold and spacer pair and synthesized by IDT as two separate gBlocks with BsaI cut sites on each end. The gBlocks were first assembled via golden gate cloning[128] under the RNA Polymerase III U6 promoter into the pCambia2300 vector that also contained the *Cas9* gene driven by the 35S promoter. From the resulting construct, the polycistronic tRNA-gRNA expression cassette and *Cas9* gene were then amplified as two fragments with BsaI cut sites flanking each end and incorporated into the level 2 vector, pL2V_BAR15325, by golden gate cloning (Figure 5-02).

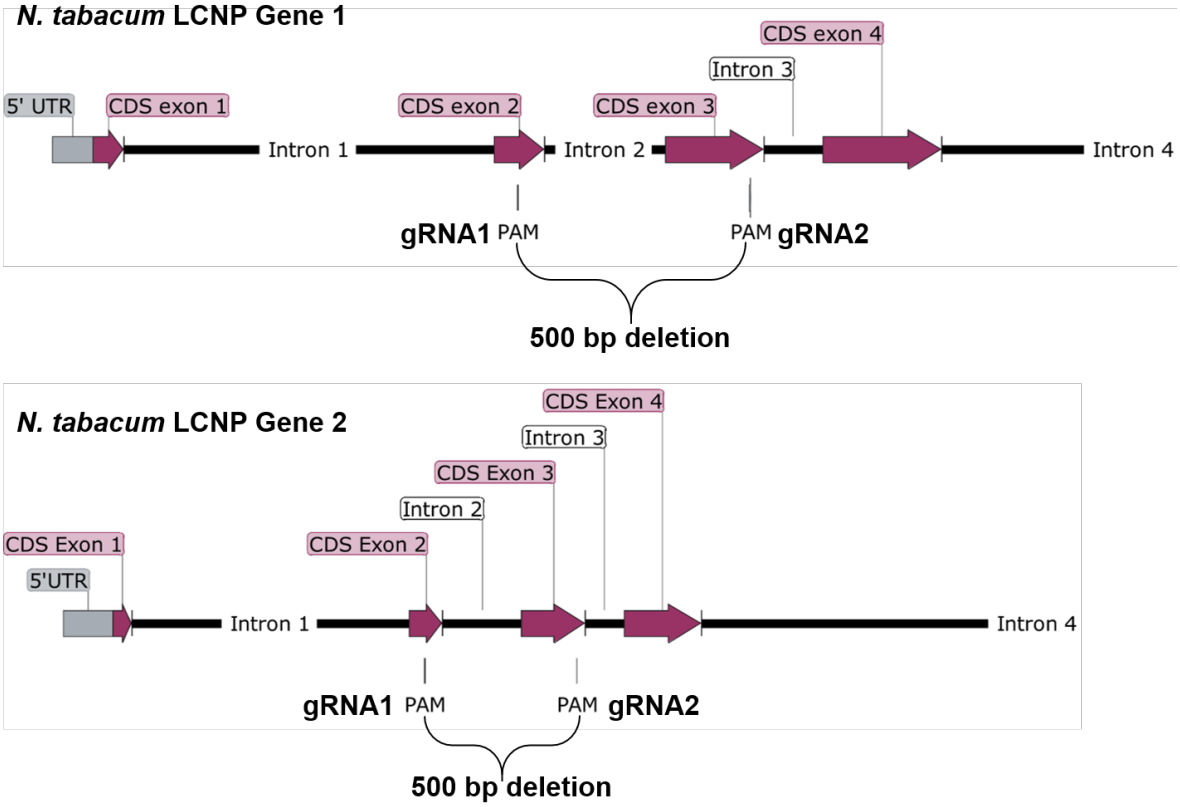

Figure 5-01. Location of gRNAs in LCNP genes in *N. tabacum*. gRNA1 is located within the second exon and gRNA 2 is located within the third exon. When cutting occurs simultaneously with both guides, a 500 bp deletion occurs.

5.2.3 ROQH1 overexpression construct design and assembly

To overexpress ROQH1 under a leaf specific promoter in tobacco, the Arabidopsis coding sequence of ROQH1-Flag previously described and cloned in Chapter 2.3.3 was used. The small subunit of Rubisco (Rbcs1A) promoter and the heat shock protein 18.2 (HSP) terminator from Arabidopsis were chosen for stable overexpression based on previous reports[131,132] and assembled into the level 2 vector, pL2V_BAR15325, by golden gate cloning (Figure 5-03).

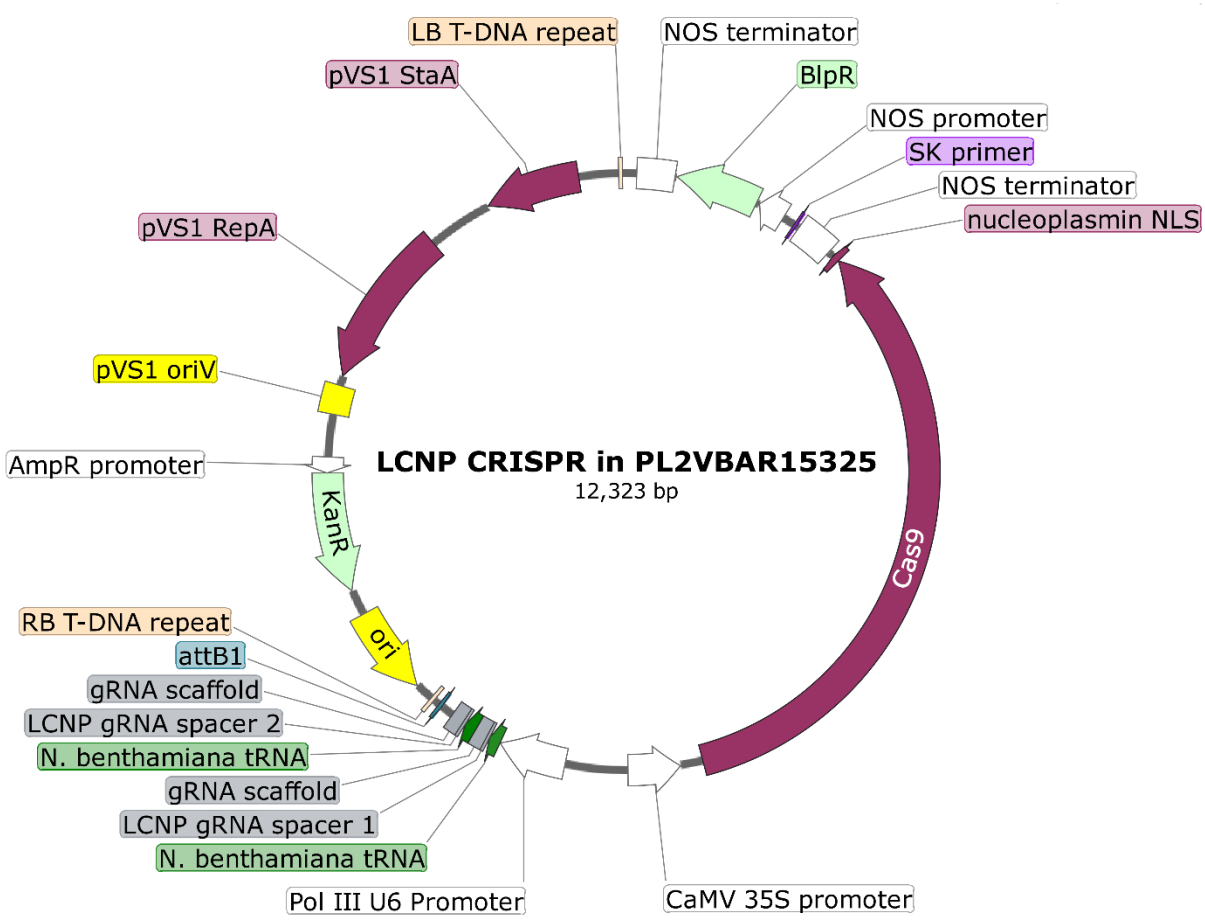

Figure 5-02. Construct map of LCNP CRISPR in pL2V_BAR15325. The polycistronic tRNA-gRNA expression cassette is indicated in green and grey and expressed under the Pol III U6 promoter in white. The *Cas9* gene is indicated in burgundy and expressed under the 35S promoter in white. Construct contains kanamycin resistance for bacteria and Basta resistance for plants.

5.2.4 *Agrobacterium fabrum* transformation

A. fabrum strain GV3101 was transformed with 300-500 ng per construct in a 25 µl volume by snap freezing in liquid nitrogen for 2 min, then thawed at 37°C without shaking for 5 min and resuspended in 200 µl 2X concentrated LB media. The transformants were recovered for 2-3 h at 28°C with shaking and plated on LB agar plates with 50 µg/ml gentamycin, 100 µg/ml rifampicin, and 50 µg/ml kanamycin. Plates were incubated at 28°C for 2 days for single colonies to appear.

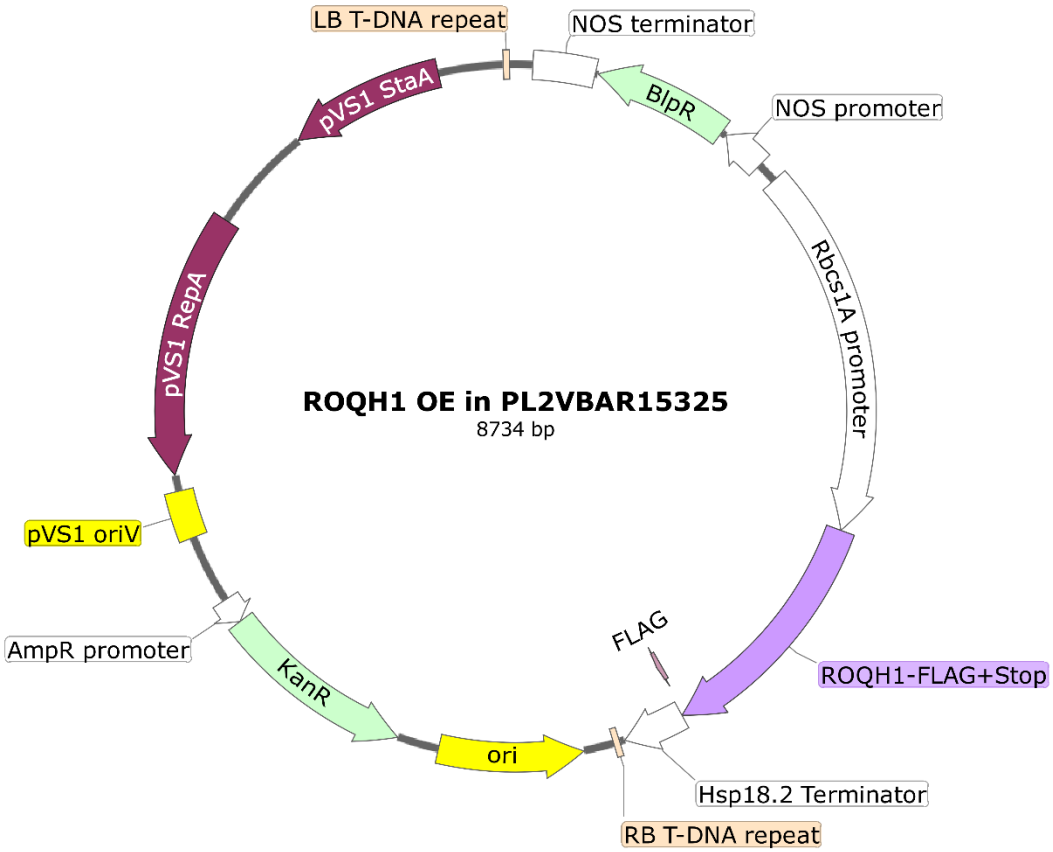

Figure 5-03. Construct map of ROQH1 OE in pL2V_BAR15325. ROQH1 coding sequence in purple is from *Arabidopsis* and contains a C-terminal Flag tag. ROQH1 overexpression is driven by the Rbcs1A promoter and Hsp18.2 terminator in white. Construct contains kanamycin resistance for bacteria and Basta resistance for plants.

5.2.5 Transient Expression in *Nicotiana benthamiana* and *Nicotiana tabacum*

A. fabrum strains containing the construct were grown overnight in 3 ml cultures with antibiotics and pelleted at 8,000 rpm for 10 min. The LB supernatant was removed and the pelleted strains were resuspended in 3 ml of fresh inoculation media (10 mM $MgCl_2$, 10mM MES pH 5.6, 150 µM acetosyringone) and placed on rotator for 3 h at RT to activate virulence. The OD_{600} of each culture was determined at a 1:10 dilution and the culture was diluted in 3 ml volume to reach the desired OD_{600} of 0.375 per construct of interest with 0.125 P19 silencing suppressor construct for a total OD_{600} of 0.5. Using a pipette tip to gently scar the underside of a leaf, 100 µl was infiltrated into the leaf using a 1 ml syringe. Infiltration spots were delineated quickly after infiltration with a marker. Plants recovered for two days under constant low light (70 µmol photons m^{-2} s^{-1}) prior to phenotyping. To induce qH, infiltrated leaves were placed on moist paper towels and placed under 1,600 µmol photons m^{-2} s^{-1}, 6°C for 5 h, and then allowed to recover under low light (20 µmol photons m^{-2} s^{-1}) overnight. Throughout qH induction and relaxation, F_m' was monitored and afterwards, leaf punches for protein samples were collected and snap frozen in liquid nitrogen.

5.3 Results

5.3.1 Ribonucleoprotein (RNP) digestion of *LCNP* genes *in vitro*

To test the efficiency of the designed gRNAs targeted to both *N. tabacum LCNP* genes, both copies were PCR amplified, gel extracted, and digested *in vitro* with ribonucleoprotein (RNP) complexes assembled with each guide. After incubating for 2 h at 37°C, the digestion products were assessed. Each guide cut as predicted, creating digestion products between 1 and 2 kb when only one guide was used (Figure 5-04.) A smaller portion of the digestion was cut by both guides simultaneously, creating a 500 bp product (Figure 5-04). This indicated that the designed gRNAs could target both LCNP genes and digest them *in vitro*.

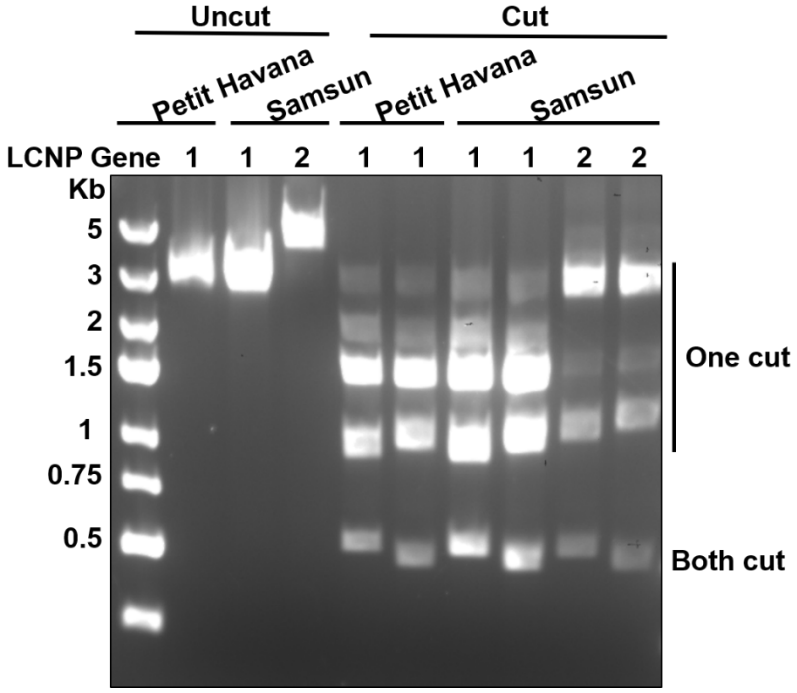

Figure 5-04. Ribonucleoprotein digestion of *LCNP* genes *in vitro*. Both *LCNP* genes (indicated 1 and 2) from *N. tabacum* cv. Samsun and one *LCNP* gene from Petite Havana (we failed to amplify LCNP 2) were PCR amplified, gel extracted, and incubated at 37°C for 2 h with (cut) and without (uncut) RNP complexes assembled with a pair of gRNAs targeted to both *LCNP* genes. Digestion products are run on a 1% agarose gel.

5.3.2 Transient expression of *ROQH1* and disruption of *LCNP* does not alter qH kinetics in *N. benthamiana*

Before producing stable transgenic *N. tabacum* lines with the ROQH1 OE and LCNP CRISPR constructs, we tested their expression transiently in *N. benthamiana*. The gRNAs in the LCNP CRISPR construct were specific for *N. tabacum* and did not align perfectly to the *N. benthamiana* LCNP gene sequence (Figure 5-05), therefore we focused infiltration efforts on ROQH1 expression. Leaves were infiltrated with both constructs along with the empty vector, pL2V_BAR15325, as a control. Leaves were assessed for qH 48 h post infiltration. To examine qH kinetics, infiltrated leaves were treated with 6 h cold and high light (1,600 µmol photons m^{-2} s^{-1}) followed by a 22 h recovery period (20 µmol photons m^{-2} $s^{-}1$). The starting F_m was approximately equal between infiltration areas (Figure 5-06), and leaves were dark-acclimated for 10 min before each fluorescence measurement to ensure qE was relaxed. After 6 h cold and high light, there was a similar decrease in fluorescence across all infiltration spots (Figure 5-06), indicating no difference in qH induction. After 22 h, fluorescence recovered equally between infiltration spots

among most replicates. One leaf showed slightly improved recovery with the ROQH1 OE construct (Figure 5-06), yet this was not reproducible among most leaves. To confirm that ROQH1-Flag was present in the infiltrated leaf tissue, leaf punches were taken following the experiment. Immunoblot analysis confirmed that ROQH1-Flag was transiently expressed in the tissue infiltrated with the ROQH1 OE construct and was absent in the tissue infiltrated with the empty vector (Figure 5-05). Thus, the lack of significant difference in qH induction and relaxation kinetics was not attributed to unsuccessful infiltration or expression.

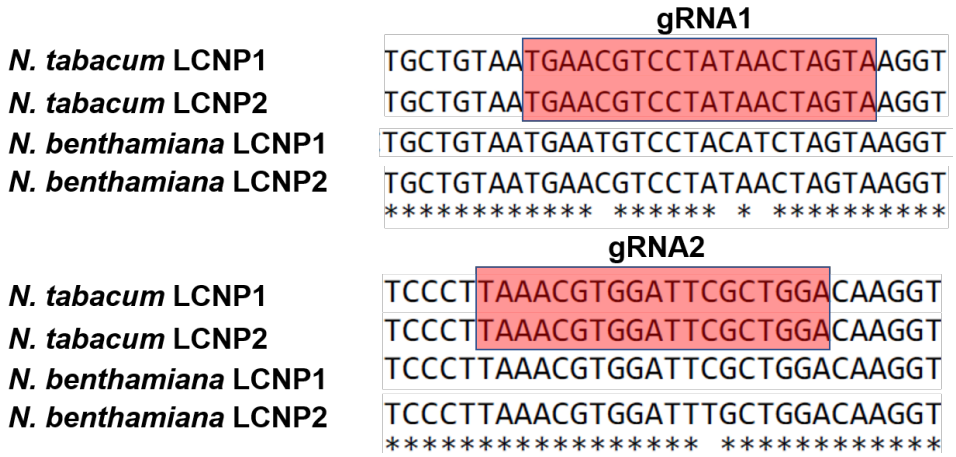

Figure 5-05. The LCNP gRNAs are specific for *N. tabacum*. Clustal multiple sequence alignment for the region around gRNA1 within the second exon and gRNA2 within the third exon. The *N. tabacum* sequence matches the guide sequence yet the *N. benthamiana* sequence contains mismatches.

5.3.3 *N. benthamiana* ROQH1 proteins lack key residues

To investigate possible reasons as to why transient expression of ROQH1 did not alter qH induction or relaxation we compared the ROQH1 protein sequence from Arabidopsis and tobacco. Using the Arabidopsis protein sequence and tBLASTn, we identified two ROQH1 homologs in *N. benthamiana* and *N. tabacum*. The multiple sequence alignment revealed that the co-factor binding motif (GGXGXXG) was completely conserved among both genes in each species (Figure 5-07). However, both sequences from *N. benthamiana* lacked at least 25 consecutive residues within the first 200 residues, including key amino acids that form the partial catalytic tetrad, D-S-VXXK (Figure 5-07). The D and S residues were conserved yet the VXXK motif was entirely absent. This may be due to incorrect gene models in tobacco and should be confirmed through PCR amplification and sequence analysis. In Arabidopsis, it is unclear how critical these residues are for protein function and whether ROQH1 has catalytic activity at all. Yet the entire D-S-VXXXK motif is present in ROQH1 homologs in *Phaedactylum tricornutum*, *Chlamydomonas reinhardtii*, *Physomitrella patens*, and *Oryza sativa*, suggesting that this sequence is important for either protein folding, stability, or function (Figure 2-25). In addition to the 25 residues, all four sequences from *N. benthamiana* and *N. tabacum* lacked 14 residues near the C-terminus (Figure 5-07), which also may be necessary for protein function in tobacco.

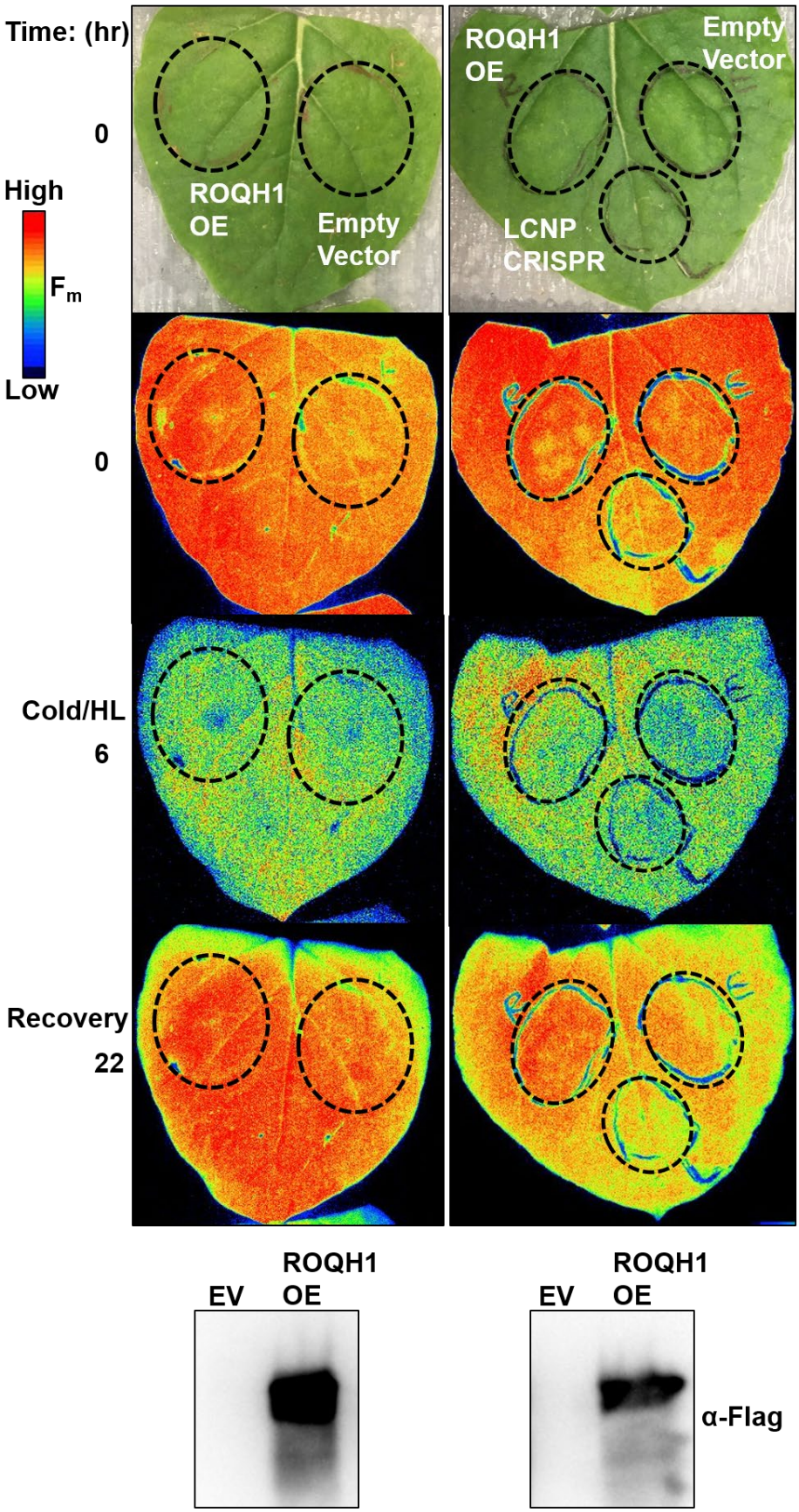

Figure 5-06. Transient expression of *ROQH1* does not alter qH in *N. benthamiana*. Fluorescence kinetics of leaves throughout a cold and high light stress and recovery treatment. Detached leaves 48 h post infiltration were placed on moist paper towel and dark adapted for 10 min before each fluorescence measurement to relax qE. The same leaves were used for immunoblot analysis after the experiment for detection of ROQH1-Flag.

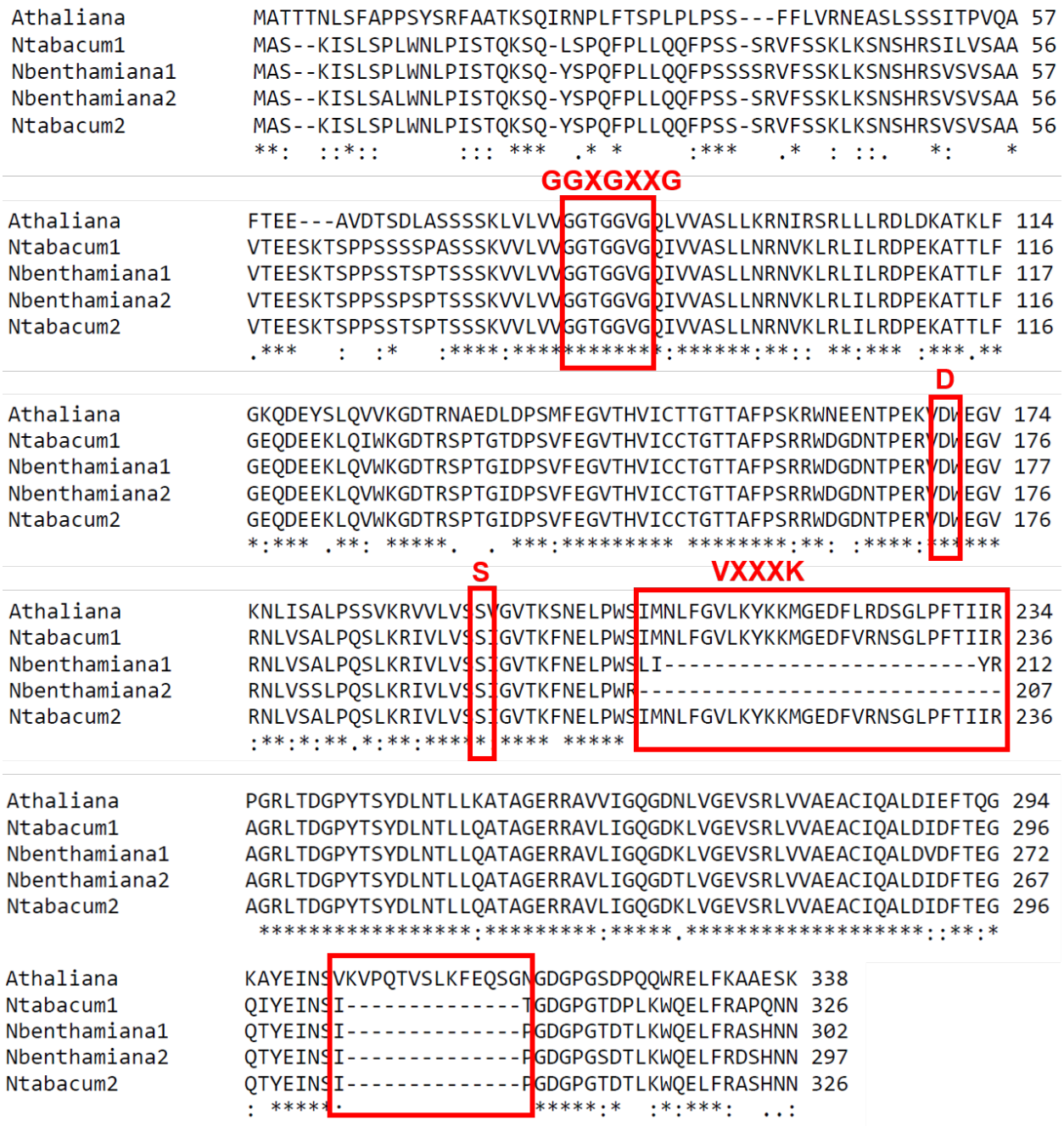

Figure 5-07. *N. benthamiana* ROQH1 proteins lack key residues. Multiple sequence alignment of ROQH1 protein sequences from Arabidopsis, *N. benthamiana*, and *N. tabacum*. The amino acid sequences were aligned using Clustal Omega (https://www.ebi.ac.uk/Tools/msa/clustalo/). The conserved Gly-rich cofactor-binding motif (GGXGXXG), partial catalytic tetrad (D-S-VXXXK), and missing residues are outlined in red.

5.3.4 Transient expression of *ROQH1* and disruption of *LCNP* in *N. tabacum*

As the gRNAs were specific to the *N. tabacum LCNP* gene sequences, we also infiltrated *N. tabacum* with the LCNP CRISPR and ROQH1 constructs alongside *N. benthamiana*. While a similar volume was used for both tobacco species, the media infiltrated the *N. tabacum* leaves with less resistance and in a more sectored area compared to *N. benthamiana*. Since the *N. tabacum* leaves were larger than the *N. benthamiana* leaves, they were cut in half in order to lie flat under the high light panel and video imaging PAM. Before starting the cold and high light treatment, the initial F_m was measured and found to be lower for areas infiltrated with the LCNP CRISPR and ROQH1 constructs than the areas infiltrated with the empty vector (Figure 5-08), indicating that qH induction would be difficult to compare between leaf spots. However, after a 6 h cold and high light treatment, the LCNP CRISPR and ROQH1 leaf spots photobleached, and the fluorescence was undetectable and did not improve after a recovery period (Figure 5-08). Immunoblot analysis after the time course showed that the ROQH1-Flag protein was present in the photobleached leaf spots (Figure 5-08), although not to the same level as the infiltrated *N. benthamiana* leaves (Figure 5-06).

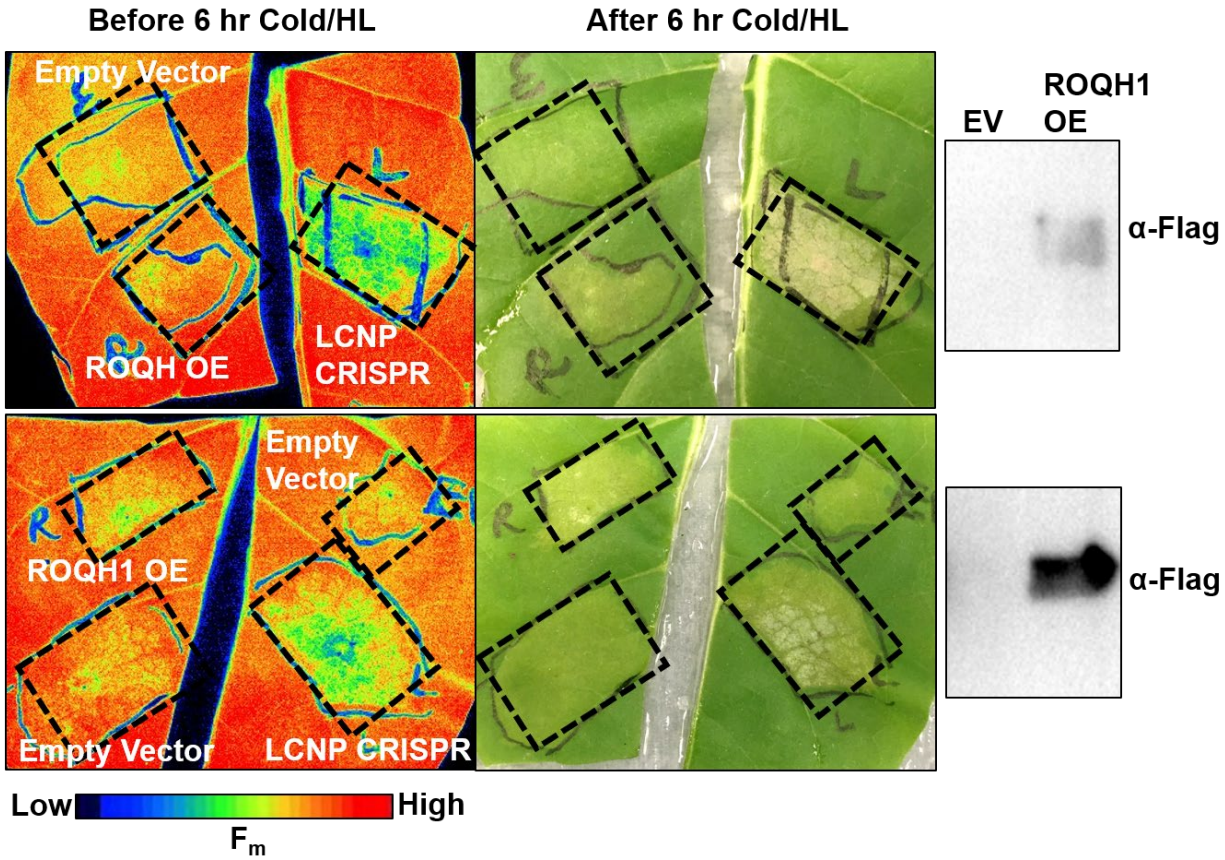

Figure 5-08. Transient expression of *ROQH1* and disruption of *LCNP* results in photobleaching in *N. tabacum*. False-colored dark-adapted fluorescence (F_m) and images of leaves before and after a 6 h cold and high light treatment. Detached leaves 48 h post infiltration were cut in half and placed on moist paper towel and dark adapted for 10 min before the fluorescence measurement. The same leaves were used for immunoblot analysis after the experiment for detection of ROQH1-Flag.

5.4 Discussion

Transient expression of ROQH1 and disruption of LCNP did not alter qH kinetics in *N. benthamiana,* yet this could be due to several reasons. For ROQH1 overexpression, the Arabidopsis coding sequence could produce a version of ROQH1 that does not function in tobacco. While there are two ROQH1 homologs present in *N. benthamiana*, both are missing two sequence motifs that are present in Arabidopsis. These deletions may be critical to relax qH in *N. benthamiana* and this could be tested by transiently overexpressing the native ROQH1 coding sequence in *N. benthamiana*. However, it may also indicate that other relaxation factor(s) are involved in addition to or instead of ROQH1. Furthermore, it has not been confirmed whether qH even occurs in tobacco. This should be verified using stable transgenic lines overexpressing ROQH1 and disrupted in SOQ1 or LCNP. For LCNP disruption, the gRNAs were designed for *N. tabacum* and did not align perfectly to the *N. benthamiana LCNP* gene sequences (Figure 5-05). Thus, Cas9-mediated cutting may not have occurred. For this reason, we infiltrated the LCNP CRISPR construct into *N. tabacum* in addition to *N. benthamiana*. However, the infiltrated area photobleached during the cold and high light treatment and could not recover. While the loss of a photoprotective mechanism such as qH can result in bleaching after stress[36], more likely this was due to foreign protein toxicity[131], as the starting F_m was already decreased before the cold and high light treatment in comparison to the empty vector (Figure 5-08). To confirm foreign protein toxicity, the GUS marker protein should be expressed under the 35S or Rbcs promoter in the pL2V_BAR15325 vector in addition to the empty vector control. However, if cutting did occur, the resulting phenotype could still be hard to distinguish for two reasons. First, in Arabidopsis, the fluorescence phenotype between wild type and *lcnp* is hard to distinguish if the cold and high light treatment is not long enough to induce a significant amount of qH in wild type. While 5-6 h is sufficient for Arabidopsis, 6 h may not be the appropriate length of time for *N. benthamiana*. Second, it is likely that only a small portion of infiltrated cells would express Cas9, gRNAs, and have simultaneous cutting events at both *LCNP* genes, resulting in a mosaic phenotype within the infiltrated area. Therefore, the best way to assess qH and LCNP disruption is through the production of stable transgenic *N. tabacum* lines.

Stable transformation of *N. tabacum* is currently underway in the lab of Stephen Long at the University of Illinois. While there is still a risk that the Arabidopsis ROQH1 protein will not function in qH relaxation in *N. tabacum*, the gRNAs should perfectly anneal and disrupt LCNP. The LCNP construct is the first CRISPR construct to be in the Illinois tobacco transformation pipeline, and therefore 30 independent lines are being generated in comparison to 15 lines for the ROQH1 OE construct. Once enough mature plants are produced, greenhouse trials in Illinois and cold and high light experiments in Berkeley can occur with the transgenic plants. For the greenhouse trials, biomass, water use efficiency, and photosynthetic parameters such as the quantum efficiency of photosystem II can be monitored. However, no phenotype may be observed among the different lines if the plants do not experience cold mornings or similar abiotic stresses. For this reason, it will be important to check for ROQH1-Flag and Cas9 protein accumulation and similarly perform cold and high light experiments to ensure a phenotype is present. With promising results of either limited or abolished qH, the best lines will move forward for field trials in Illinois. Following field trials, optimized constructs can be integrated into staple crops such as corn and cowpea for improved crop yield and food production.

Chapter 6: Conclusions

Photosynthesis is a process of primary importance and occurs in numerous environments, some of which include severe abiotic stress. For the photosynthetic machinery to operate under these conditions such as low temperatures, high light, drought, or high salinity, plants must regulate light harvesting and photoprotection accordingly. Under sustained stress, such as harsh cold winters, plants downregulate their photosynthetic capacity[38] and employ sustained quenching mechanisms that last throughout the winter season and only begin to relax when the warmth of spring arrives. Currently two phases of sustained quenching have been described in overwintering evergreens[37]. The rapid phase that is due to qE, and the slow phase that is due to either qZ and/or qI[37]. However, this does not exclude the possibility that the slow phase is also due to other sustained quenching mechanisms such as qH.

It is difficult to assess whether qH occurs in non-model plant species as it is not correlated with the formation of a transthylakoid ΔpH, pigment accumulation or de-epoxidation state, or loss of abundant photosynthetic proteins like D1. Instead it involves proteins that are low abundant and just recently identified and characterized in Arabidopsis within the last six years[35,36]. Under non-stress conditions, qH is prevented through a thioredoxin domain within the SOQ1 protein[35]. Further research is required to determine whether the thioredoxin domain acts on cysteine residues within LCNP or within another intermediate protein. Induction of qH under cold and high light requires the lipocalin, LCNP[36], which is hypothesized to migrate to the thylakoid membrane surrounding the embedded LHCII trimer proteins and alter the lipid environment. As a result, a conformational change is induced producing strong quenching sites within the LHCII trimer. Through connectivity to the LHCII trimer, these quenching sites can also quench the energy transferred through parts of the PSII and PSI antenna. This type of quenching is distinct from other well characterized mechanisms as it is sustained, taking hours to days to turn off, even when the LHCII trimers are isolated *in vitro*.

The ROQH1 protein isolated and characterized in this work is an atypical short chain dehydrogenase/reductase that functions in a complex with LHCII trimers located in the grana margins. While the exact molecular mechanism of relaxation by ROQH1 is unknown, genetic characterization provides insight into important residues and possible domains critical for function. Both *roqh1-1* and *roqh1-2* point mutations affect protein accumulation and/or stability to varying degrees, yet the *roqh1-1* mutation near the partial catalytic tetrad clearly has a severe effect on protein function. Since atypical SDRs are currently known to be catalytically inactive, it is possible that ROQH1 functions around or within the LHCII trimer without performing catalysis or requires additional protein partners to relax quenching. Future studies with additional mutants from the suppressor screen or biochemical experiments using purified recombinant ROQH1 protein may advance our understanding of ROQH1 function and the molecular mechanism of qH relaxation.

In addition to qH, only two other quenching mechanisms are known to currently have molecular factors involved in relaxation. State transitions, or qT, is a mechanism that does not result in thermal dissipation but rather energy distribution. It relies on a kinase to phosphorylate light-harvesting proteins and initiate their migration within the membrane from PSII to PSI. Under light conditions that favors PSI, a phosphatase removes the phosphate and reverses the migration back to PSII, effectively turning off qT. However, it is the activity of the kinase that is redox regulated[43,44] while the phosphatase is redox-independent and constitutively active at low levels[45]. The second mechanism, OCP-mediated quenching, occurs in cyanobacteria and requires the FRP protein to turn quenching off. Similar to qH, the ratio of the activating protein, OCP to FRP is

critical to achieve the necessary level of photoprotection and their respective synthesis is thus regulated accordingly[132]. Comparing what we know about these two mechanisms may improve our limited knowledge on the mechanism and regulation of qH.

Improving NPQ relaxation has been shown to be a promising way to improve photosynthetic efficiency and crop yield[127]. Having a dosage-dependent relaxation factor makes modifying qH relaxation a potentially straightforward task. In this work, ROQH1 overexpression was found to limit qH in Arabidopsis to similar levels as the *lcnp* mutant. If qH is an overprotective mechanism that can be induced under certain crop field conditions, then abolishing qH by either overexpressing *ROQH1* or disrupting *LCNP* would be beneficial. However, if crop plants do experience conditions where qH is protective and critical for survival, then overexpressing ROQH1 may have negative effects on crop yield. Future studies on stable tobacco lines overexpressing ROQH1 or disrupted in LCNP will provide insight on the necessity of qH. If qH is required, one strategy to improve qH relaxation while maintaining necessary qH levels would be to overexpress *LCNP* in addition to *ROQH1*. The ideal ratio of LCNP to ROQH1 would be important similarly to OCP-mediated photoprotection and this would require further investigation, possibly by trial and error. However, other engineering routes for improving light capture and conversion may contain more obstacles and be less feasible, such as modifying the antenna size within a crop canopy to improve light capture of the lower-most leaves or replacing PSI with a type 2 reaction center from purple bacteria[135]. With an increasing population, changing climate, and dependence on plants for food and energy, modifying qH may be a necessary and simpler way to improve photosynthesis and meet our global food and fuel demands.

References

1. Niyogi, K. K. Photoprotection revisited: Genetic and molecular approaches. *Annual Review of Plant Physiology and Plant Molecular Biology* **50**, 333–359 (1999).
2. Demmig-Adams, B. & Adams III, W. W. Photoprotection and other responses of plants to high light stress. *Annu. Rev. Plant Phvsiol. Plant Mol. Bioi.* **43**, 599–626 (1992).
3. Wada, M. Chloroplast movement. **210**, 177–182 (2013).
4. Pribil, M., Labs, M. & Leister, D. Structure and dynamics of thylakoids in land plants. *Journal of Experimental Botany* **65**, 1955–1972 (2014).
5. Bielczynski, L. W., Schansker, G. & Croce, R. Effect of Light Acclimation on the Organization of Photosystem II Super- and Sub-Complexes in *Arabidopsis thaliana*. *Front. Plant Sci.* **7**, (2016).
6. Telfer, A., Bishop, S. M., Phillips, D. & Barber, J. Isolated photosynthetic reaction center of photosystem II as a sensitizer for the formation of singlet oxygen. Detection and quantum yield determination using a chemical trapping technique. *J. Biol. Chem.* **269**, 13244–13253 (1994).
7. Krieger-Liszkay, A., Fufezan, C. & Trebst, A. Singlet oxygen production in photosystem II and related protection mechanism. *Photosynthesis Research* 551–564 (2008).
8. Ramel, F. *et al.* Chemical Quenching of Singlet Oxygen by Carotenoids in Plants1[C][W]. *Plant Physiol* **158**, 1267–1278 (2012).
9. Mehler, A. H. Studies on reactions of illuminated chloroplasts. I. Mechanism of the reduction of oxygen and other Hill reagents. *Arch. Biochem. Biophys.* **33**, 65–77 (1951).
10. Baker, N. R. Chlorophyll fluorescence: a probe of photosynthesis in vivo. *Annual review of plant biology* **59**, 89–113 (2008).
11. Schreiber, U. Pulse-amplitude modulation (PAM) fluorometry and saturation pulse method: an overview. in *Chlorophyll a fluorescence: a signature of photosynthesis* 279–319 (2004). doi:10.1007/978-1-4020-3218-9.
12. Kautsky H, Apel W, A. H. Chlorophyllfluoreszenz und kohlensäureassimilation. XIII. Die fluoreszenkurve und die photochemie der pflanze. *Biochem. Zeit* **322**, 277–292 (1960).
13. Genty, B., Briantais, J.-M. & Baker, N. R. The relationship between the quantum yield of photosynthetic electron transport and quenching of chlorophyll fluorescence. *Biochimica et Biophysica Acta (BBA) - General Subjects* **990**, 87–92 (1989).
14. Öquist, G. & Huner, N. P. A. Photosynthesis of Overwintering Evergreen Plants. *Annual Review of Plant Biology* **54**, 329–355 (2003).
15. Walters, R. G. & Horton, P. Resolution of components of non-photochemical chlorophyll fluorescence quenching in barley leaves. *Photosynth. Res.* **27**, 121–133 (1991).
16. Malnoë, A. Photoinhibition or photoprotection of photosynthesis? Update on the (newly termed) sustained quenching component qH. *Environmental and Experimental Botany* **154**, 123–133 (2018).
17. Müller, P., Li, X.-P. & Niyogi, K. K. Non-photochemical quenching: a response to excess light energy. *Plant Physiology* 1558–1566 (2001).
18. Li, X.-P. *et al.* Regulation of photosynthetic light harvesting involves intrathylakoid lumen pH sensing by the PsbS protein. *Journal of Biological Chemistry* **279**, 22866–22874 (2004).
19. Hager, A. Light dependent decrease of the pH-value in a chloroplast compartment causing the enzymatic interconversion of violaxanthin to zeaxanthin; relations to photophosphorylation. *Planta* **89**, 224–243 (1969).
20. Yamamoto, H. Y., Kamite, L. & Wang, Y.-Y. An ascorbate-induced absorbance change in chloroplasts from violaxanthin de-epoxidation. *Plant physiology* **49**, 224–228 (1972).

21. Demmig, B., Winter, K., Krüger, A. & Czygan, F.-C. Photoinhibition and zeaxanthin formation in intact leaves. A possible role of the xanthophyll cycle in the dissipation of excess light energy. *Plant Physiology* **84**, 218–224 (1987).
22. Niyogi, K. K., Grossman, A. R. & Björkman, O. Arabidopsis Mutants Define a Central Role for the Xanthophyll Cycle in the Regulation of Photosynthetic Energy Conversion. *The Plant cell* **10**, 1121–1134 (1998).
23. Havaux, M., Bonfils, J.-P., Lütz, C. & Niyogi, K. K. Photodamage of the Photosynthetic Apparatus and its Dependence on the Leaf Developmental Stage in the *npq1* Arabidopsis Mutant Deficient in the Xanthophyll Cycle Enzyme Violaxanthin de-epoxidase. *Plant physiology* **124**, 273–284 (2000).
24. Dominici, P. *et al.* Biochemical properties of the PsbS subunit of photosystem II either purified from chloroplast or recombinant. *Journal of Biological Chemistry* **277**, 2250–22758 (2002).
25. Enrico, T. *et al.* Evidence for interaction of PsbS with photosynthetic complexes in maize thylakoids. *Biochim. Biophys. Acta* 703–722 (2007).
26. Daskalakis, V. Protein-protein interactions within photosystem II under photoprotection: the synergy between CP29 minor antenna, subunit S (PsbS) and zeaxanthin at all-atom resolution. *Physical Chemistry Chemical Physics* (2018).
27. Townsend, A. J. *et al.* The causes of altered chlorophyll fluorescence quenching induction in the *Arabidopsis* mutant lacking all minor antenna complexes. *Biochim. Biophys. Acta* 666–675 (2018).
28. Dall'Osto, L., Caffarri, S. & Bassi, R. A mechanism of nonphotochemical energy dissipation, independent from PsbS, revealed by a conformational change in the antenna protein CP26. *The Plant cell* **17**, 1217–1232 (2005).
29. Betterle, N., Ballottari, M., Hienerwadel, R., Dall'Osto, L. & Bassi, R. Dynamics of zeaxanthin binding to the photosystem II monomeric antenna protein Lhcb6 (CP24) and modulation of its photoprotection properties. *Archives of Biochemistry and Biophysics* **504**, 67–77 (2010).
30. Nilkens, M. *et al.* Identification of a slowly inducible zeaxanthin-dependent component of non-photochemical quenching of chlorophyll fluorescence generated under steady-state conditions in Arabidopsis. *Biochimica et Biophysica Acta - Bioenergetics* **1797**, 466–475 (2010).
31. Aro, E. M., Virgin, I. & Andersson, B. Photoinhibition of Photosystem II. Inactivation, protein damage and turnover. *Biochim. Biophys. Acta* **1143**, 113–134 (1993).
32. Melis, null. Photosystem-II damage and repair cycle in chloroplasts: what modulates the rate of photodamage ? *Trends Plant Sci.* **4**, 130–135 (1999).
33. Krause, G. H. Photoinhibition of photosynthesis. An evaluation of damaging and protective mechanisms **74**, 566–574 (1988).
34. Demmig, B. & Björkman, O. Comparison of the effect of excessive light on chlorophyll fluorescence (77K) and photon yield of O_2 evolution in leaves of higher plants. *Planta* **171**, 171–184 (1987).
35. Brooks, M. D., Sylak-Glassman, E. J., Fleming, G. R. & Niyogi, K. K. A thioredoxin-like/β-propeller protein maintains the efficiency of light harvesting in Arabidopsis. *Proceedings of the National Academy of Sciences of the United States of America* **110**, E2733-40 (2013).
36. Malnoë, A. *et al.* The Plastid Lipocalin LCNP is Required for Sustained Photoprotective Energy Dissipation in Arabidopsis. *The Plant Cell* **30**, 196–208 (2017).

37. Verhoeven, A. Sustained energy dissipation in winter evergreens. *New Phytol* **201**, 57–65 (2014).
38. Adams, W. W., Zarter, C. R., Ebbert, V. & Demmig-Adams, B. Photoprotective Strategies of Overwintering Evergreens. *BioScience* **54**, 41 (2004).
39. Adams III, W. W., Demmig-Adams, B., Rosenstiel, T. N., Brightwell, A. K. & Ebbert, V. Photosynthesis and Photoprotection in Overwintering Evergreen Plants. *Plant biol* **4**, 545–557 (2002).
40. Ottander, C., Campbell, D. & Oquist, G. Seasonal changes in photosystem II organisation and pigment composition in *Pinus syivestris*. 8.
41. Cazzaniga, S., Dall' Osto, L., Kong, S.-G., Wada, M. & Bassi, R. Interaction between avoidance of photon absorption, excess energy dissipation and zeaxanthin synthesis against photooxidative stress in *Arabidopsis*. *Plant J* **76**, 568–579 (2013).
42. Murata, N. I. LIGHT-INDUCED CHANGE OF CHLOROPHYLL *a* FLUORESCENCE IN *PORPHYRIDIUM CRUENTUM*. *Biochim. Biophys. Acta* 10 (1969).
43. Bellafiore, S., Barneche, F., Peltier, G. & Rochaix, J.-D. State transitions and light adaptation require chloroplast thylakoid protein kinase STN7. *Nature* **433**, 892–895 (2005).
44. Wunder, T. *et al.* Control of STN7 transcript abundance and transient STN7 dimerisation are involved in the regulation of STN7 activity. *Planta* **237**, 541–558 (2013).
45. Pribil, M., Pesaresi, P., Hertle, A., Barbato, R. & Leister, D. Role of Plastid Protein Phosphatase TAP38 in LHCII Dephosphorylation and Thylakoid Electron Flow. *PLoS Biol* **8**, (2010).
46. Walters, R. G. & Horton, P. Resolution of components of non-photochemical chlorophyll fluorescence quenching in barley leaves. *Photosynth Res* **27**, 121–133 (1991).
47. Trotta, A., Suorsa, M., Rantala, M., Lundin, B. & Aro, E.-M. Serine and threonine residues of plant STN7 kinase are differentially phosphorylated upon changing light conditions and specifically influence the activity and stability of the kinase. *Plant J* **87**, 484–494 (2016).
48. Dekker, J. P. & Boekema, E. J. Supramolecular organization of thylakoid membrane proteins in green plants. *Biochimica et biophysica acta* **1706**, 12–39 (2005).
49. Kowalczyk, N. *et al.* Photosynthesis in Chondrus crispus: the contribution of energy spill-over in the regulation of excitonic flux. *Biochim. Biophys. Acta* **1827**, 834–842 (2013).
50. Levesque-Tremblay, G., Havaux, M. & Ouellet, F. The chloroplastic lipocalin AtCHL prevents lipid peroxidation and protects Arabidopsis against oxidative stress. *The Plant Journal* **60**, 691–702 (2009).
51. Grzyb, J., Latowski, D. & Strzalka, K. Lipocalins – a family portrait. *Journal of Plant Physiology* **163**, 895—915 (2006).
52. Kim, E.-H. *et al.* The multiple roles of light-harvesting chlorophyll *a*/*b*-protein complexes define structure and optimize function of Arabidopsis chloroplasts: A study using two chlorophyll *b*-less mutants. *Biochimica et Biophysica Acta* **1787**, 973–984 (2009).
53. Glazebrook, D. W. and J. Setting Up Arabidopsis Crosses. *Cold Spring Harbor Protocols* pdb.prot4623 (2006) doi:10.1101/pdb.prot4623.
54. Earley, K. W. *et al.* Gateway-compatible vectors for plant functional genomics and proteomics. *The Plant Journal* **45**, 616–629 (2006).
55. Zhang, X., Henriques, R., Lin, S.-S., Niu, Q.-W. & Chua, N.-H. *Agrobacterium*-mediated transformation of *Arabidopsis thaliana* using the floral dip method. *Nature Protocols* **1**, 1–6 (2006).

56. Müller-Moulé, P., Conklin, P. L. & Niyogi, K. K. Ascorbate deficiency can limit violaxanthin de-epoxidase activity in vivo. *Plant Physiology* **128**, 970–977 (2002).
57. McDonald, K. L. Rapid Embedding Methods into Epoxy and LR White Resins for Morphological and Immunological Analysis of Cryofixed Biological Specimens. *Microsc Microanal* **20**, 152–163 (2014).
58. Pradhan Mitra, P. & Loqué, D. Histochemical Staining of Arabidopsis thaliana Secondary Cell Wall Elements. *JoVE* 51381 (2014) doi:10.3791/51381.
59. Järvi, S., Suorsa, M., Paakkarinen, V. & Aro, E.-M. Optimized native gel systems for separation of thylakoid protein complexes: novel super- and mega-complexes. *Biochem. J.* **439**, 207–214 (2011).
60. Emanuelsson, O., Nielsen, H., Brunak, S. & von Heijne, G. Predicting subcellular localization of proteins based on their N-terminal amino acid sequence. *J. Mol. Biol.* **300**, 1005–1016 (2000).
61. Tomizioli, M. *et al.* Deciphering thylakoid sub-compartments using a mass spectrometry-based approach. *Mol & Cellular Proteomics* **13**, 2147–2167 (2014).
62. Schwacke, R. *et al.* ARAMEMNON, a Novel Database for Arabidopsis Integral Membrane Proteins. *Plant Physiol.* **131**, 16–26 (2003).
63. Omasits, U., Ahrens, C. H., Müller, S. & Wollscheid, B. Protter: interactive protein feature visualization and integration with experimental proteomic data. *Bioinformatics* **30**, 884–886 (2014).
64. Björkman, O. Responses to different quantum flux densities. in *Physiological Plant Ecology I. Responses to the Physical Environment* (eds. Lange, O. L., Nobel, P. S., Osmond, C. B. & Ziegler, H.) 57–108 (Springer-Verlag Berlin Heidelberg, 1981).
65. Lichtenthaler, H. K. *et al.* Photosynthetic activity, chloroplast ultrastructure, and leaf characteristics of high-light and low-light plants and of sun and shade leaves. *Photosynth. Res.* **2**, 115–141 (1981).
66. Eskins, K., Duysen, M. E. & Olson, L. Pigment Analysis of Chloroplast Pigment-Protein Complexes in Wheat. *Plant physiology* **71**, 777–779 (1983).
67. Bailey, S., Walters, R. G., Jansson, S. & Horton, P. Acclimation of *Arabidopsis thaliana* to the light environment: the existence of separate low light and high light responses. *Planta* **213**, 794–801 (2001).
68. Bielczynski, L. W., Schansker, G. & Croce, R. Effect of light acclimation on the organization of photosystem II super- and sub-complexes in *Arabidopsis thaliana*. *Frontiers in plant science* **7**, 105 (2016).
69. Anderson, J. M., Chow, W. S. & De Las Rivas, J. Dynamic flexibility in the structure and function of photosystem II in higher plant thylakoid membranes: the grana enigma. *Photosynthesis Research* vol. 98 575–587 (2008).
70. Pribil, M., Labs, M. & Leister, D. Structure and dynamics of thylakoids in land plants. *Journal of Experimental Botany* **65**, 1955–1972 (2014).
71. Anderson, J. M., Horton, P., Kim, E.-H. & Chow, W. S. Towards elucidation of dynamic structural changes of plant thylakoid architecture. *Phil. Trans. R. Soc. B* **367**, 3515–24 (2012).
72. Casal, J. J. Photoreceptor signaling networks in plant responses to shade. *Annu. Rev. Plant Biol.* **64**, 403–427 (2013).
73. Keller, M. M. *et al.* Cryptochrome 1 and phytochrome B control shade-avoidance responses in Arabidopsis via partially independent hormonal cascades. *The Plant Journal* **67**, 195–207 (2011).

74. Fey, V. *et al.* Retrograde plastid redox signals in the expression of nuclear genes for chloroplast proteins of *Arabidopsis thaliana*. *THE JOURNAL OF BIOLOGICAL CHEMISTRY* **280**, 5318–5328 (2005).
75. Pfalz, J. *et al.* Environmental control of plant nuclear gene expression by chloroplast redox signals. *Frontiers in plant science* **3**, 257 (2012).
76. Walters, R. G., Rogers, J. J. M., Shephard, F. & Horton, P. Acclimation of *Arabidopsis thaliana* to the light environment: the role of photoreceptors. *Planta* **209**, 517–527 (1999).
77. Dall'Osto, L., Ünlü, C., Cazzaniga, S. & Van Amerongen, H. Disturbed excitation energy transfer in *Arabidopsis thaliana* mutants lacking minor antenna complexes of photosystem II. *Biochimica et Biophysica Acta* **1837**, 1981–1988 (2014).
78. Naranjo, B. *et al.* The chloroplast NADPH thioredoxin reductase C, NTRC, controls non-photochemical quenching of light energy and photosynthetic electron transport in Arabidopsis. *Plant, Cell & Environment* **39**, 804–822 (2016).
79. Oppermann, U. C. T., Filling, C. & Jörnvall, H. Forms and functions of human SDR enzymes. *Chemico-Biological Interactions* **130–132**, 699–705 (2001).
80. Kavanagh, K. L., Jörnvall, H., Persson, B. & Oppermann, U. The SDR superfamily: functional and structural diversity within a family of metabolic and regulatory enzymes. *Cell. Mol. Life Sci.* **65**, 3895–3906 (2008).
81. Moummou, H., Kallberg, Y., Tonfack, L. B., Persson, B. & Van Der Rest, B. The plant short-chain dehydrogenase (SDR) superfamily: genome-wide inventory and diversification patterns. *BMC Plant Biology* **12**, 219–236 (2012).
82. Buysschaert, G., Verstraete, K., Savvides, S. N. & Vergauwen, B. Structural and biochemical characterization of an atypical short-chain dehydrogenase/reductase reveals an unusual cofactor preference. *FEBS Journal* **280**, 1358–1370 (2013).
83. Bollenbach, T. J. & Stern, D. B. Divalent metal-dependent catalysis and cleavage specificity of CSP41, a chloroplast endoribonuclease belonging to the short chain dehydrogenase/ reductase superfamily. *Nucleic Acids Research* **31**, 4317–4325 (2003).
84. Link, S., Engelmann, K., Meierhoff, K. & Westhoff, P. The Atypical Short-Chain Dehydrogenases HCF173 and HCF244 Are Jointly Involved in Translational Initiation of the psbA mRNA of Arabidopsis. *Plant Physiol* **160**, 2202–2218 (2012).
85. Lamb, H. K. *et al.* The negative transcriptional regulator NmrA discriminates between oxidized and reduced dinucleotides. *Journal of Biological Chemistry* **278**, 32107–32114 (2003).
86. Andrianopoulos, A., Kourambas, S., Sharp, J. A., Davis, M. A. & Hynes, M. J. Characterization of the *Aspergillus nidulans nmrA* gene involved in nitrogen metabolite repression. *Journal of Bacteriology* **180**, 1973–1977 (1998).
87. Karpowicz, S. J., Prochnik, S. E., Grossman, A. R. & Merchant, S. S. The GreenCut2 resource, a phylogenomically derived inventory of proteins specific to the plant lineage. *Journal of Biological Chemistry* **286**, 21427–21439 (2011).
88. Fristedt, R. Chloroplast function revealed through analysis of GreenCut2 genes. *Journal of Experimental Botany* **68**, 2111–2120 (2017).
89. Kallberg, Y., Oppermann, U., Jörnvall, H. & Persson, B. Short-chain dehydrogenases/reductases (SDRs). Coenzyme-based functional assignments in completed genomes. *Eur. J. Biochem.* **269**, 4409–4417 (2002).

90. Ermakova-Gerdes, S. & Vermaas, W. Inactivation of the open reading frame *slr*0399 in *Synechocystis* sp. PCC 6803 functionally complements mutations near the Q_A niche of photosystem II. *THE JOURNAL OF BIOLOGICAL CHEMISTRY* **274**, 30540–30549 (1999).
91. Knoppová, J. *et al.* Discovery of a chlorophyll binding protein complex involved in the early steps of photosystem II assembly in *Synechocystis*. *The Plant cell* **26**, 1200–1212 (2014).
92. Staleva, H. *et al.* Mechanism of photoprotection in the cyanobacterial ancestor of plant antenna proteins. *Nature Chemical Biology* **11**, 287–292 (2015).
93. Komenda, J. & Sobotka, R. Cyanobacterial high-light-inducible proteins — protectors of chlorophyll – protein synthesis and assembly. *Biochimica et Biophysica Acta* **1857**, 288–295 (2016).
94. Duc, C., Sherstnev, A., Cole, C., Barton, G. J. & Simpson, G. G. Transcription termination and chimeric RNA formation controlled by *Arabidopsis thaliana* FPA. *PLoS Genetics* **9**, e1003867 (2013).
95. Brooks, M. D. A Suppressor of Quenching Regulates Photosynthetic Light Harvesting. *Dissertation* (2012).
96. Lakshmi, B., Mishra, M., Srinivasan, N. & Archunan, G. Structure-based phylogenetic analysis of the lipocalin superfamily. *PLoS ONE* **10**, e0135507 (2015).
97. Kirilovsky, D. & Kerfeld, C. A. The orange carotenoid protein in photoprotection of photosystem II in cyanobacteria. *Biochimica et Biophysica Acta* **1817**, 158–166 (2012).
98. Wilson, A. *et al.* A photoactive carotenoid protein acting as light intensity sensor. *Proc. Natl. Acad. Sci. USA* **105**, 12075–12080 (2008).
99. Boulay, C., Wilson, A., D'Haene, S. & Kirilovsky, D. Identification of a protein required for recovery of full antenna capacity in OCP-related photoprotective mechanism in cyanobacteria. *Proc. Natl. Acad. Sci. USA* **107**, 11620–11625 (2010).
100. Thurotte, A. *et al.* The cyanobacterial fluorescence recovery protein has two distinct activities: orange carotenoid protein amino acids involved in FRP interaction. *Biochimica et Biophysica Acta* **1858**, 308–317 (2017).
101. Sutter, M. *et al.* Crystal structure of the FRP and identification of the active site for modulation of OCP-mediated photoprotection in cyanobacteria. *Proc. Natl. Acad. Sci. USA* **110**, 10022–10027 (2013).
102. Bricker, T. M. & Frankel, L. K. The structure and function of CP47 and CP43 in Photosystem II. *Photosynthesis Research* vol. 72 131–146 (2002).
103. Green, B. R. & Durnford, D. G. the Chlorophyll-Carotenoid Proteins of Oxygenic Photosynthesis. *Annual Review of Plant Physiology and Plant Molecular Biology* **47**, 685–714 (1996).
104. Jansson, S. A guide to the Lhc genes and their relatives in Arabidopsis. *Trends in Plant Science* **4**, 236–240 (1999).
105. Stirbet, A. & Govindjee. On the relation between the Kautsky effect (chlorophyll a fluorescence induction) and Photosystem II: Basics and applications of the OJIP fluorescence transient. *Journal of Photochemistry and Photobiology B: Biology* **104**, 236–257 (2011).
106. Küpper, H. *et al.* Analysis of OJIP Chlorophyll Fluorescence Kinetics and Q_A Reoxidation Kinetics by Direct Fast Imaging. *Plant Physiol.* **179**, 369–381 (2019).
107. Lamb, J. J., Røkke, G. & Hohmann-Marriott, M. F. Chlorophyll fluorescence emission spectroscopy of oxygenic organisms at 77 K. *Photosynthetica* **56**, 105–124 (2018).
108. Pinnola, A. *et al.* Light-Harvesting Complex Stress-Related Proteins Catalyze Excess Energy Dissipation in Both Photosystems of *Physcomitrella patens*. *Plant Cell* **27**, 3213–3227 (2015).

109. Leuenberger, M. L. Exploration of Nonphotochemical Quenching Mechanisms in *A. thaliana* via Time Correlated Single Photon Counting Snapshots. 129.
110. Espineda, C. E., Linford, A. S., Devine, D. & Brusslan, J. A. The *AtCAO* gene, encoding chlorophyll *a* oxygenase, is required for chlorophyll *b* synthesis in *Arabidopsis thaliana*. *Proc. Natl. Acad. Sci. USA* **96**, 10507–10511 (1999).
111. de Marchin, T., Ghysels, B., Nicolay, S. & Franck, F. Analysis of PSII antenna size heterogeneity of Chlamydomonas reinhardtii during state transitions. doi:10.1016/j.bbabio.2013.07.009.
112. Chukhutsina, V. U., Holzwarth, A. R. & Croce, R. Time-resolved fluorescence measurements on leaves: principles and recent developments. *Photosynth Res* **140**, 355–369 (2019).
113. Kallberg, Y., Oppermann, U. & Persson, B. Classification of the short-chain dehydrogenase/reductase superfamily using hidden Markov models. *The FEBS Journal* **277**, 2375–2386 (2010).
114. Bhatia, C. *et al.* Towards a systematic analysis of human short-chain dehydrogenases/reductases (SDR): Ligand identification and structure-activity relationships. doi:10.1016/j.cbi.2014.12.013.
115. Kiss, A. Z., Ruban, A. V. & Horton, P. The PsbS Protein Controls the Organization of the Photosystem II Antenna in Higher Plant Thylakoid Membranes. *J. Biol. Chem.* **283**, 3972–3978 (2008).
116. Horton, P. Optimization of light harvesting and photoprotection: molecular mechanisms and physiological consequences. *Phil. Trans. R. Soc. B* **367**, 3455–3465 (2012).
117. Gilmore, A. M. & Ball, M. C. Protection and storage of chlorophyll in overwintering evergreens. *Proc Natl Acad Sci U S A* **97**, 11098–11101 (2000).
118. Berthold, D. A., Babcock, G. T. & Yocum, C. F. A highly resolved, oxygen-evolving photosystem II preparation from spinach thylakoid membranes: EPR and electron-transport properties. *FEBS Letters* **134**, 231–234 (1981).
119. Iwai, M., Takahashi, Y. & Minagawa, J. Molecular Remodeling of Photosystem II during State Transitions in Chlamydomonas reinhardtii. *The Plant Cell* (2008) doi:10.1105/tpc.108.059352.
120. Wittig, I., Braun, H. & Scha, H. Blue native PAGE. (2006) doi:10.1038/nprot.2006.62.
121. Pagliano, C., Barera, S., Chimirri, F., Saracco, G. & Barber, J. Comparison of the α and β isomeric forms of the detergent n-dodecyl-D-maltoside for solubilizing photosynthetic complexes from pea thylakoid membranes. *Biochimica et Biophysica Acta - Bioenergetics* **1817**, 1506–1515 (2012).
122. Fu, A. *et al.* A chloroplast cyclophilin functions in the assembly and maintenance of photosystem II in Arabidopsis thaliana. *Proceedings of the National Academy of Sciences* **104**, 15947–15952 (2007).
123. Wunder, T. *et al.* The major thylakoid protein kinases STN7 and STN8 revisited : effects of altered STN8 levels and regulatory specificities of the STN kinases. *Frontiers in plant science* **4**, 1–15 (2013).
124. Bhullar, S. *et al.* Functional analysis of cauliflower mosaic virus 35S promoter: re-evaluation of the role of subdomains B5, B4 and B2 in promoter activity. *Plant Biotechnology Journal* **5**, 696–708 (2007).
125. Borello, U., Ceccarelli, E. & Giuliano, G. Constitutive, light-responsive and circadian clock-responsive factors compete for the different *I* box elements in plant light-regulated promoters. *The Plant Journal* **4**, 611–619 (1993).

126.Zhu, X.-G., Long, S. P. & Ort, D. R. Improving Photosynthetic Efficiency for Greater Yield. *Annu. Rev. Plant Biol.* **61**, 235–261 (2010).
127.Kromdijk, J. *et al.* Improving photosynthesis and crop productivity by accelerating recovery from photoprotection. *Science* **354**, 857–861 (2016).
128.Xie, K., Minkenberg, B. & Yang, Y. Boosting CRISPR/Cas9 multiplex editing capability with the endogenous tRNA-processing system. *Proc Natl Acad Sci USA* **112**, 3570–3575 (2015).
129.Vazquez-Vilar, M. *et al.* A modular toolbox for gRNA–Cas9 genome engineering in plants based on the GoldenBraid standard. *Plant Methods* **12**, 10 (2016).
130.Engler, C., Kandzia, R. & Marillonnet, S. A One Pot, One Step, Precision Cloning Method with High Throughput Capability. *PLoS ONE* **3**, e3647 (2008).
131.Nagaya, S., Kawamura, K., Shinmyo, A. & Kato, K. The HSP Terminator of Arabidopsis thaliana Increases Gene Expression in Plant Cells. *Plant Cell Physiol* **51**, 328–332 (2010).
132.Leonelli, L., Erickson, E., Lyska, D. & Niyogi, K. K. Transient expression in Nicotiana benthamiana for rapid functional analysis of genes involved in non-photochemical quenching and carotenoid biosynthesis. *Plant J* **88**, 375–386 (2016).
133.Wagner, B. *et al.* Plant virus expression systems for transient production of recombinant allergens in Nicotiana benthamiana. *Methods* **32**, 227–234 (2004).
134.Gwizdala, M., Wilson, A., Omairi-Nasser, A. & Kirilovsky, D. Characterization of the Synechocystis PCC 6803 Fluorescence Recovery Protein involved in photoprotection. *Biochim. Biophys. Acta* **1827**, 348–354 (2013).
135.Ort, D. R. *et al.* Redesigning photosynthesis to sustainably meet global food and bioenergy demand. *Proc Natl Acad Sci U S A* **112**, 8529–8536 (2015).